Journal of Paleontology, page 1 of 62

0022-3360/22/1937-2337
doi: 10.1017/jpa.2022.7

JOURNAL OF PALEONTOLOGY
A PUBLICATION OF THE Paleontological SOCIETY

Systematic paleontology, acritarch biostratigraphy, and $\delta^{13}C$ chemostratigraphy of the early Ediacaran Krol A Formation, Lesser Himalaya, northern India

Shuhai Xiao,[1]* Ganqing Jiang,[2] Qin Ye,[3] Qing Ouyang,[4] Dhiraj M. Banerjee,[5] Birendra P. Singh,[6] A. D. Muscente,[7] Chuanming Zhou,[4] and Nigel C. Hughes[8]

[1]Department of Geosciences, Virginia Tech, Blacksburg, VA 24061, USA <xiao@vt.edu>
[2]Department of Geoscience, University of Nevada, Las Vegas, NV 89154, USA <ganqing.jiang@unlv.edu>
[3]State Key Laboratory of Biogeology and Environmental Geology, School of Earth Sciences, China University of Geosciences, Wuhan 430074, China <yeqin@cug.edu.cn >
[4]State Key Laboratory of Palaeobiology and Stratigraphy, Nanjing Institute of Geology and Palaeontology, and Center for Excellence in Life and Palaeoenvironment, Chinese Academy of Sciences, Nanjing 210008, China <qouyang@nigpas.ac.cn><cmzhou@nigpas.ac.cn>
[5]Department of Geology, Chhatra Marg, University of Delhi, Delhi 110007, India <dhirajmohanbanerjee@gmail.com>
[6]Department of Geology, Panjab University, Chandigarh 160014, India <bpsinghpu@gmail.com>
[7]Department of Geology, Cornell College, Mount Vernon, IA 52314, USA <dmuscente@cornellcollege.edu>
[8]Department of Earth and Planetary Sciences, University of California, Riverside, CA 92521, USA <nigel.hughes@ucr.edu>

Abstract.—Acritarch biostratigraphic and $\delta^{13}C$ chemostratigraphic data from the Krol A Formation in the Solan area (Lesser Himalaya, northern India) are integrated to aid inter-basinal correlation of early–middle Ediacaran strata. We identified a prominent negative $\delta^{13}C$ excursion (likely equivalent to EN2 in the lower Doushantuo Formation in the Yangtze Gorges area of South China), over a dozen species of acanthomorphs (including two new species—*Cavaspina tiwariae* Xiao n. sp., *Dictyotidium grazhdankinii* Xiao n. sp.), and numerous other microfossils from an interval in the Krol A Formation. Most microfossil taxa from the Krol A and the underlying Infra-Krol formations are also present in the Doushantuo Formation. Infra-Krol acanthomorphs support a correlation with the earliest Doushantuo biozone: the *Appendisphaera grandis-Weissiella grandistella-Tianzhushania spinosa* Assemblage Zone. Krol A microfossils indicate a correlation with the second or (more likely, when $\delta^{13}C$ data are considered) the third biozone in the lower Doushantuo Formation (i.e., the *Tanarium tuberosum-Schizofusa zangwenlongii* or *Tanarium conoideum-Cavaspina basiconica* Assemblage Zone). The association of acanthomorphs with EN2 in the Krol Formation fills a critical gap in South China where chert nodules, and thus acanthomorphs, are rare in the EN2 interval. Like many other Ediacaran acanthomorphs assemblages, Krol A and Doushantuo acanthomorphs are distributed in low paleolatitudes, and they may represent a distinct paleobiogeographic province in east Gondwana. The Indian data affirm the stratigraphic significance of acanthomorphs and $\delta^{13}C$, clarify key issues of lower Ediacaran bio- and chemostratigraphic correlation, and strengthen the basis for the study of Ediacaran eukaryote evolution and paleobiogeography.

UUID: http://zoobank.org/5289fdb2-0e49-4b3b-880f-f5b21acab371.

Introduction

The Ediacaran Period (635–539 Ma) represents a critical transition in the evolutionary path of the Earth-life system. To better understand the tempo, mode, and mechanisms of Ediacaran evolution, a solid chronostratigraphic framework is needed. In the past two decades, considerable progress has been made toward global chronostratigraphic correlation of Ediacaran strata (Xiao and Narbonne, 2020). However, key obstacles have yet to be overcome to achieve Phanerozoic-style chronostratigraphic division and correlation based on biostratigraphic data. Importantly, although there has been increasing evidence for a first-order subdivision and correlation of upper Ediacaran strata (ca. 580–539 Ma) on the basis of Ediacara-type macrofossils (Waggoner, 2003; Boag et al., 2016; Muscente et al., 2019), biostratigraphic subdivision and correlation of lower Ediacaran strata (ca. 635–580 Ma) on the basis of microfossils has not been achieved on a global scale. This is a major weakness in Ediacaran evolution and biostratigraphy, not only because microfossils are the foundation to understand early Ediacaran biodiversity and evolution, but also because they have potential as an effective tool for global biostratigraphic correlation (just as they do in Phanerozoic biostratigraphy).

*Corresponding author.

One group of Ediacaran microfossils—variously known as giant acanthomorph acritarchs (Vidal, 1990), Doushantuo-Pertatataka acanthomorphs or DPAs (Zhou et al., 2001, 2007), Ediacaran complex acanthomorph palynoflora or ECAP (Grey, 2005), and large ornamented Ediacaran microfossils or LOEMs (Cohen et al., 2009)—is particularly useful in biostratigraphic correlation of lower Ediacaran strata. These acanthomorphic acritarchs or spinose organic-walled microfossils are characterized by large spherical vesicles (typically >200 μm in diameter; Xiao et al., 2014) ornamented with morphologically complex processes or spines. They are taxonomically diverse, particularly in the lower Ediacaran system, although large acanthomorphs are sparsely known from older strata (Agić et al., 2015) and smaller acanthomorphs (<100 μm in diameter) are also present in the Ediacaran (Yin et al., 2011).

Earlier work treated Ediacaran acanthomorphs as a coherent group of microfossils that diversified after the ca. 635 Ma Marinoan glaciation and largely disappeared before the ca. 580 Ma Gaskiers glaciation and the Shuram negative $\delta^{13}C$ excursion or its equivalent EN3 in South China (Xiao, 2004a; Zhou et al., 2007; McFadden et al., 2008). More recent work, however, demonstrated that some acanthomorphs taxa that were thought to be restricted in the lower Ediacaran may range into upper Ediacaran and pre-Ediacaran strata. For example, Ouyang et al. (2017) argued that some DPA taxa extend into the Shuram (EN3) interval at the Liujiayuanzi section in Hunan Province, South China. Grazhdankin et al. (2020) reported DPA taxa from the lower Cambrian Oppokun Formation at the Khastakhskaya borehole, Lena-Anabar Basin, north-central Siberia, although the Cambrian age interpretation was based on small shelly fossils such as *Cambrotubulus* Missarzhevsky in Rozanov et al., 1969, and *Anabarites* Missarzhevsky in Voronova and Missarzhevsky, 1969, which have also been found in terminal Ediacaran strata (Knoll et al., 1995; Zhu et al., 2017; Cai et al., 2019), and hence these DPAs are best regarded as terminal Ediacaran–lower Cambrian in age. Golubkova et al. (2015) reported DPAs from upper Ediacaran strata at the Keltmen-1 Borehole in the Timan Ridge of the East European Platform, although Vorob'Eva et al. (2009) considered these strata middle Ediacaran in age. Anderson et al. (2017, 2019) described a few DPA taxa from the upper Khesen Formation in the Khuvsgul terrane of northern Mongolia, which is considered terminal Ediacaran but may well be early Cambrian in age (Anttila et al., 2021). Perhaps the most contentious is the report of numerous DPA taxa, including several eponymous taxa used to define Ediacaran acanthomorph assemblage biozones, from the Semri Group of the Lower Vindhyan Supergroup in the Chambal Valley of eastern Rajasthan of central-western India (Prasad and Asher, 2016) because the Semri Group in the Son Valley of central India is widely regarded as Paleo-/Mesoproterozoic in age (Rasmussen et al., 2002; Ray et al., 2002), although Prasad and Asher (2016, 2021) argued this unit is Ediacaran in age. The potential occurrence of DPA taxa in Paleo-/Mesoproterozoic strata would greatly complicate and compromise our attempt to use them to divide and correlate Ediacaran strata, and thus the age and taxonomic identification of these Semri DPA taxa warrant close scrutiny.

On the bright side, there has been success in regional biostratigraphic correlation of lower Ediacaran strata based on acanthomorphic acritarchs. Grey (2005), for example, building upon an earlier study by Zang and Walter (1992), systematically investigated acanthomorphs from early Ediacaran shales and fine-grained siltstones using the hydrofluoric (HF) extraction method. She established four acanthomorph biozones that can be used to correlate lower Ediacaran strata across the Officer Basin, Amadeus Basin, and Stuart Shelf in Australia. Other paleontologists have applied the HF extraction method to analyze acanthomorphs from lower Ediacaran shales and siltstones in Siberia (Kolosova, 1991; Moczydłowska, Vidal, and Rudavskaya, 1993; Golubkova et al., 2010; Sergeev et al., 2011; Moczydłowska and Nagovitsin, 2012) and Baltica (Vorob'Eva et al., 2009; Golubkova et al., 2015), although a regional biostratigraphic zonation has not been established.

Silicified and phosphatized acanthomorphs also feature prominently in early Ediacaran biostratigraphy. The preservation of these acanthomorphs involve early diagenetic silica or phosphate precipitation on organic substrates, thus encasing organic substrates (e.g., cell walls) and essentially forming three-dimensional casts and molds of organic structures (e.g., cells) (Xiao and Tang, 2022). Acanthomorphs preserved in cherts and phosphorites are often studied in thin sections (e.g., Yin and Li, 1978) and phosphatized microfossils preserved in a carbonate matrix also can be extracted using the acetic acid maceration method (e.g., Xiao and Knoll, 2000). In several studies of silicified acanthomorphs from the lower Ediacaran Doushantuo Formation in the Yangtze Gorges area of South China (McFadden et al., 2009; Yin et al., 2009; Liu et al., 2014a; Liu and Moczydłowska, 2019), different schemes of acanthomorph-based biostratigraphic zonation have been proposed. Although the application of these biozones in regional biostratigraphic correlation remains a challenge, preliminary data indicate that numerous acanthomorphs have robust biostratigraphic significance in the Yangtze Gorges area (Ouyang et al., 2021). The encouraging success from the Yangtze Gorges area gives us hope that intra- and inter-basinal correlation of lower Ediacaran strata using silicified and phosphatized acanthomorphs is achievable. This optimism is strengthened by a multiplicity of acanthomorphs from Ediacaran cherts and phosphorites in South China (e.g., Xiao et al., 2014; Liu and Moczydłowska, 2019), northern India (e.g., Shukla and Tiwari, 2014; Joshi and Tiwari, 2016; Sharma et al., 2021), Baltica (Vidal, 1990), Svalbard (Knoll, 1992), Greenland (Willman et al., 2021), and Mongolia (Anderson et al., 2017, 2019).

A necessary step toward a global acanthomorph-based biostratigraphic framework is to test the biozonations from Australia and the Yangtze Gorges area in other sedimentary basins. There are, however, several major obstacles. First, acanthomorphs preserved in shales versus cherts/phosphorites are studied using different methods, may have different taphonomic histories, and may represent different depositional environments. These differences unavoidably make it difficult for a direct comparison between these taphonomic windows; indeed, taxonomic criteria are not practically the same for acanthomorphs preserved in shales versus cherts and phosphorites (Xiao et al., 2014). Second, there is considerable variation from basin to basin in terms of sampling intensity. Among silicified acanthomorph assemblages, for example, those in the Doushantuo Formation in the Yangtze Gorges area have been much more extensively investigated than those in other early Ediacaran basins, with data accumulated over several decades by multiple research groups who sampled dozens of easily accessible localities,

examined tens of thousands of thin sections, and detailed their results in numerous monographs (e.g., Yin and Li, 1978; Yin, 1987; Zhang et al., 1998; McFadden et al., 2009; Liu et al., 2014a; Liu and Moczydłowska, 2019; Ouyang et al., 2021). In comparison, silicified Ediacaran acanthomorphs from the Scotia Group in Svalbard (Knoll, 1992) and the Biskopås Conglomerate in southern Norway (Spjeldnaes, 1963, 1967; Vidal, 1990) are less extensively surveyed, although those from the Infra-Krol and Krol A formations in the Krol Belt of northern India have gained more research attention in recent years (Shukla and Tiwari, 2014; Joshi and Tiwari, 2016; Sharma et al., 2021). This disparity in sampling and research intensity makes it difficult to carry out detailed interbasinal correlation. Third, other than the Doushantuo Formation in South China (e.g., McFadden et al., 2008; Xiao et al., 2012; Liu et al., 2014a; Ouyang et al., 2019), few Ediacaran successions have been assessed using an integrative approach to calibrate and test acanthomorph biostratigraphy versus $\delta^{13}C$ chemostratigraphy.

To address these problems and to achieve a global chronostratigraphic framework for the early Ediacaran Period, we envision the steps outlined below. First, it is imperative to substantially improve the sampling intensity of under-studied successions. Second, to isolate taphonomic factors as a potential source of bias, it is necessary to carry out comparative studies of acanthomorph assemblages preserved in similar taphonomic mode. Third, after biozonation has been established and tested among assemblages of similar taphonomic mode, we need to bridge the gap between the silicification/phosphatization and carbonaceous-compression modes by comparing acanthomorphs from chert/phosphorite and shale facies. It is important to emphasize that acanthomorph biostratigraphic data, whenever possible, must be integrated with other chronostratigraphic tools such as $\delta^{13}C$, $^{87}Sr/^{87}Sr$, and geochronometric dates (Xiao et al., 2016), as has been done in the Doushantuo Formation in South China (e.g., McFadden et al., 2008; Liu et al., 2014a; Ouyang et al., 2017, 2019; Liu and Moczydłowska, 2019).

As an effort to implement this campaign, we carried out an integrative study of the Krol A Formation in the Solan area of the Krol Belt, Lesser Himalaya, northern India (Fig. 1). The Krol A Formation was chosen as a target of this study for several reasons. First, previous investigations have shown that the Krol A and the underlying Infra-Krol formations contain microfossils whose preservation mode is similar to those in the Doushantuo Formation in the Yangtze Gorges area. Earlier studies revealed silicified filamentous and coccoidal microfossils from chert nodules in the Infra-Krol Formation of the Nainital area (Acharyya et al., 1989; Venkatachala et al., 1990) and the Krol A Formation of the Solan area (Kumar and Rai, 1992). Subsequent investigations recovered various silicified acanthomorphs and multicellular algae from the Infra-Krol Formation in both the Solan and Nainital areas (Tiwari and Azmi, 1992; Tiwari and Knoll, 1994; Tiwari and Pant, 2004; Shukla et al., 2005b; Joshi and Tiwari, 2016), as well as the Krol A Formation in the Solan area (Shukla et al., 2008; Shukla and Tiwari, 2014; Sharma et al., 2021) (Table 1). In particular, the report of *Tianzhushania spinosa* Yin and Li, 1978, and *T. polysiphonia* Yin in Yin and Liu, 1988, from the Infra-Krol Formation on the Nainital area (Joshi and Tiwari, 2016) bolsters a direct biostratigraphic correlation with the lower Doushantuo Formation in the Yangtze Gorges area, where these two taxa are characteristically abundant (McFadden et al., 2009; Yin et al., 2009). Second, the correlation between Ediacaran successions in South China and northern India is facilitated by their paleogeographic proximity during the Ediacaran Period (Jiang et al., 2003a; Merdith et al., 2021). Finally, the Krol A Formation consists of interbedded shale and dolostone with fossiliferous chert nodules, offering an opportunity for integrative investigation of acanthomorph biostratigraphy and $\delta^{13}C$ chemostratigraphy, given that previous studies of Krol A acanthomorphs (see references above) were decoupled from sequence stratigraphic and $\delta^{13}C$ chemostratigraphic investigations (Jiang et al., 2002, 2003b; Kaufman et al., 2006). Thus, the Krol A Formation is an ideal test ground for the bio- and chemostratigraphic framework derived from the Doushantuo Formation South China, particularly the Yangtze Gorges area, because of the lithostratigraphic similarity, paleogeographic proximity, and taphonomic comparability between these two successions. No other Ediacaran succession, to our knowledge, offers such a great opportunity. To take full advantage of this opportunity, we carried out a systematic and integrative paleontological and geochemical analysis of the Krol A Formation in the Solan area.

Geological setting

Neoproterozoic strata of the Krol Belt, Lesser Himalaya, northern India crop out in a series of doubly plunging synclines from Solan in the northwest to Nainital in the southeast (Fig. 1) (Auden, 1934; Singh and Rai, 1983; Shanker et al., 1993). Following the stratigraphic scheme of Jain et al. (2020), these strata consist of three parts: (1) Tonian siliciclastic-dominated rocks of the Jaunsar/Simla groups; (2) Cryogenian diamictite, siltstone, and sandstone of the Blaini Group; and (3) Ediacaran shale/siltstone and carbonates of the Krol Group, which includes the Infra-Krol Formation (Jain et al., 2020). There are no precise radioisotopic dates from syndepositional ash beds to constrain the depositional age of these units, but detrital zircon ages indicate that the Jaunsar/Simla groups are likely of Tonian age (≤850 Ma; Frank et al., 2001; McKenzie et al., 2011; Webb et al., 2011), and the glaciogenic rocks of the Blaini Group are of Cryogenian age (≤ 692 ± 18 Ma, Etienne et al., 2011; ≤ 678 ± 10 Ma, Hofmann et al., 2011). The Ediacaran age of the Krol Group is inferred from the occurrence at the top of the Blaini Group of a thin (<10 m) carbonate unit characteristic of the basal Ediacaran cap dolostone (Jiang et al., 2002; Etienne et al., 2011), sequence and $\delta^{13}C$ chemostratigraphic correlation with other Ediacaran successions—particularly the Doushantuo and Dengying formations in South China (Jiang et al., 2002, 2003a; Kaufman et al., 2006), the presence of Ediacaran microfossils in the Infra-Krol and Krol A formations (e.g., Tiwari and Knoll, 1994; Tiwari and Pant, 2004; Shukla et al., 2008; Shukla and Tiwari, 2014; Joshi and Tiwari, 2016; Sharma et al., 2021), the presence in the overlying Tal Group of early Cambrian acritarchs (Tiwari, 1999), small shelly fossils (Bhatt et al., 1985; Bhatt, 1991), and trilobites (Hughes et al., 2005), as well as the report of the terminal Ediacaran fossil *Shaanxilithes ningqiangensis* Xing, Yue, and Zhang in Xing et al., 1984, from the uppermost Krol and basalmost Tal groups (Tarhan et al., 2014; Bhargava et al., 2021).

Ediacaran strata in the Krol Belt were traditionally mapped as Infra-Krol, Krol Sandstone, Krol A, B, C, D, and E units

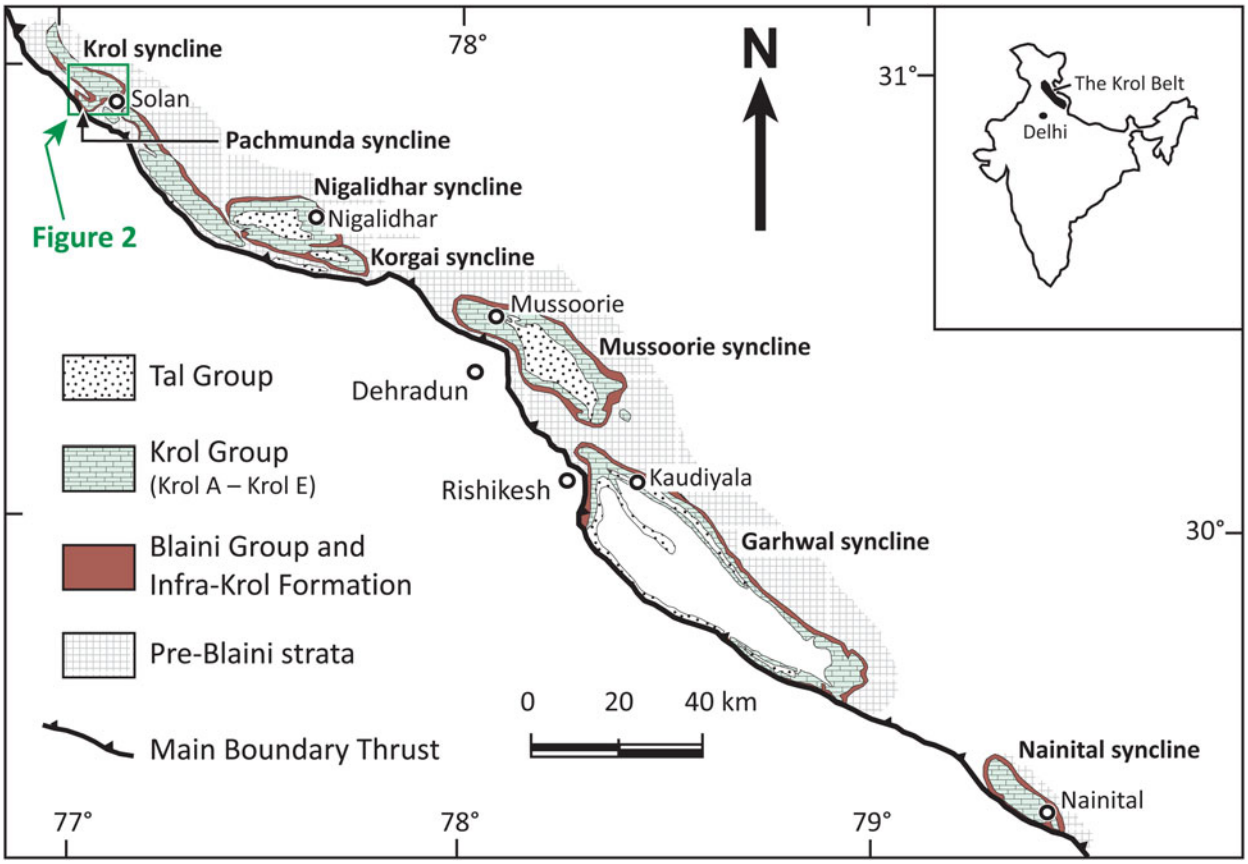

Figure 1. Simplified geological map showing the exposure of late Neoproterozoic strata (Blaini, Krol, and Tal groups) along the Krol Belt of the Lesser Himalaya, northern India. Modified from Singh and Rai (1983). Inset map shows location of the Krol Belt in northern India. The geology of the Krol and Pachmunda synclines in the Solan area is provided in Figure 2.

(Figs. 2, 3.1) (Auden, 1934; Bhattacharya and Niyogi, 1971). Shanker et al. (1993, 1997) recommended raising the Krol to group status and formalized the internal subdivisions of the Krol Group as the Chambaghat Formation (Krol Sandstone), Mahi Formation (Krol A), Jarashi Formation (Krol B), and Kauriyala Formation (Krol C, D, and E). These formation names, however, have not been widely accepted in India. Because the traditional nomenclature (i.e., Krol A, B, C, D, E) has been widely used in geological maps, Jain et al. (2020) suggested raising the informal letter names to formation status and including the Infra-Krol Formation in the Krol Group (Fig. 3.1). In this paper, we follow the stratigraphic nomenclature of Jain et al. (2020), who also placed the basal Ediacaran cap carbonate in the uppermost the Blaini Group, although some authors placed it in the basal Infra-Krol Formation (Jiang et al., 2003a). A particular point that needs to be clarified is the relationship between the Krol Sandstone and Infra-Krol Formation. Because the Krol Sandstone is present only in the Solan and Nainital areas and its immediate overlying strata vary from shale (the definition of the Infra-Krol Formation) to interbedded shaly dolostone and shale (the definition of Krol A Formation), lithostratigraphically the Infra-Krol Formation may extend above the Krol Sandstone in some places (Jiang et al., 2002). With this consideration, the Krol Sandstone may be better defined as a member or an informal lithostratigraphic unit within the Infra-Krol Formation (Fig. 3.1).

The measured and sampled sections for this study cover the uppermost Infra-Krol Formation through the lower part of Krol C Formation in the southeastern corner of the Pachmunda syncline in the Solan area (Figs. 2, 3.2). Section DH-14 (N30°53′57.8″, E77°05′14.0″; Fig. 2) was measured through an excavated quarry that covers the top of the Infra-Krol Formation, Krol Sandstone, and Krol A Formation. Section DH2-14 (N30°53′41.3″, E77°05′29.5″; Fig. 2) was measured from the Solan-Barog road towards north along a construction roadcut, and covers the uppermost Krol A, Krol B, and lower Krol C formations.

The Infra-Krol Formation consists of black shales with an up-section increase in siltstone and fine-grained sandstone beds towards the Krol Sandstone. The Krol Sandstone in the measured section (DH-14 in Fig. 2) is ~33 m thick and contains cross stratification in the middle part. At this section, interbedded silty shale and shaly dolostone of the Krol A Formation directly overlie the Krol Sandstone (Fig. 4.1). Black to dark, spherical chert nodules of 0.3–2 cm in diameter (Fig. 4.2, 4.4) and thin (<2 cm), laterally discontinuous chert bands (Fig. 4.3) are found at multiple horizons from the lower to middle Krol A Formation (Fig. 3.2). Towards the upper Krol A Formation (Fig. 4.5), chert nodules become larger in size (up to 7 cm in diameter) and are often flattened along the bedding (Fig. 4.6). The Krol B Formation in the measured section (DH2-14 in Fig. 2) is only 10 m thick and consists of reddish siltstone/mudstone with silty dolostone interbeds. A 0.4-m-thick calcareous

Table 1. Summary of previous reports of acanthomorphic acritarchs from the Infra-Krol and Krol A formations in Lesser Himalaya.

Author	Stratigraphic unit	Locality	Taxa	Note
Tiwari and Azmi, 1992	Infra-Krol	Solan	Form B	Same specimen as *Ericiasphaera spjeldnaesii* (Tiwari and Knoll, 1994, pl. 1, fig. 1); here considered to be *Cymatiosphaeroides forabilatus*.
Tiwari and Knoll, 1994	Infra-Krol	Solan	*Asterocapsoides* sp.	Probably *Asterocapsoides wenganensis*.
		Solan	*Ericiasphaera spjeldnaesii*	One of the two specimens (pl. 1, fig. 1) is here considered to be *C. forabilatus*; the other specimen (pl. 1, fig. 5) has been assigned to *Gyalosphaeridium pulchrum* by Liu and Moczydłowska (2019).
		Nainital	*Echinosphaeridium maximum*	= *Knollisphaeridium maximum*.
		Unspecified	Unnamed taxon (pl. 1, fig. 6)	Considered to be *Tianzhushania spinosa* by Zhang et al. (1998); here considered to be *C. forabilatus*.
Tiwari and Pant, 2004	Infra-Krol	Unspecified	*Asterocapsoides sinensis*	Also illustrated in Sharma et al. (2012); acutely conical processes, probably *A. robustus*.
		Solan	*Asterocapsoides* sp.	Previously illustrated as *Asterocapsoides* sp. (Tiwari and Knoll, 1994, pl. 1, fig. 2); probably *A. wenganensis*.
		Unspecified	*Cymatiosphaeroides yinii*	
		Unspecified	*Echinosphaeridium maximum*	Needs further examination.
		Unspecified	*Ericiasphaera spjeldnaesii*	Specimens in fig. 6A, B and fig. 6C, D appear to have been previously illustrated (Tiwari and Knoll, 1994, pl. 1, figs. 1 & 5, respectively). Specimens in fig. 6E–G appear to have hollow processes and, if confirmed, should be transferred to a species of *Appendisphaera*.
		Unspecified	Undefined acritarch	Described as "a single process emerging from the interior."
		Unspecified	Unnamed specimen	Described as "compressed large acanthomorphic acritarch."
Shukla et al., 2008	Infra-Krol & Krol A (unspecified)	Solan & Nigalidhar	*Cymatiosphaeroides kullingii*	Needs further examination.
		Solan	*Echinosphaeridium maximum*	Needs further examination; one of the two specimens (pl. 2, figs. 13, 14) may be *Cymatiosphaeroides forabilatus*.
		Solan	*Ericiasphaera rigida* Zhang et al., 1998	Needs further examination.
		Solan	*Filisphaeridium* sp.	Needs further examination.
		Solan	*Goniosphaeridium conoideum* (Kolosova, 1991) Zhang et al., 1998	Needs further examination.
		Solan & Nainital	*Gorgonisphaeridium maximum* (Yin, 1987) Knoll, 1991	Needs further examination.
		Solan	*Meghystrichosphaeridium perfectum* (Kolosova, 1991) Zhang et al., 1998	Needs further examination.
		Solan	*Papillomembrana compta*	Needs further examination.
		Solan	*Tianzhushania spinosa*	Not *T. spinosa*; possibly *Cymatiosphaeroides forabilatus*.
		Solan	*Trachyhystrichosphaera aimika* Hermann in Timofeev et al., 1976	Needs further examination.
Shukla and Tiwari, 2014	Krol A	Solan	*Appendisphaera fragilis*	
			Appendisphaera grandis	Considered to be *A. tenuis* by Liu and Moczydłowska, 2019.
			Asterocapsoides sp. A	Two specimens (fig. 4F, H) seem to have biform processes; perhaps a species of *Mengeopsphaera*.
			Asterocapsoides sp. B	Specimens have acutely conical processes; either *A. robustus* or *A. wenganensis*.
			Cavaspina acuminata	
			Cavaspina basiconica	
			Eotylotopalla dactylos Zhang et al., 1998	Conical processes are different from the slightly tapering and distally rounded processes of *E. dactylos*; some processes are somewhat similar to those of *Tanarium capitatum* Liu and Moczydłowska, 2019.
			Knollisphaeridium sp.	Possibly *Knollisphaeridium coniformum* Liu and Moczydłowska, 2019.
			Papillomembrana sp.	Possibly a species of *Appendisphaera*.
			Weissiella cf. *grandistella*	Here considered to be *W. brevis*.
			Unnamed Form A	= *Cavaspina tiwariae* Xiao n. sp.
			Unnamed Form B	
			Unnamed Form C	Process morphology is somewhat similar to *Briareus borealis* Knoll, 1992.
			Unnamed Form D	
			Unnamed Form E	*Cymatiosphaeroides forabilatus*.
Joshi and Tiwari, 2016	Infra-Krol	Nainital	*Papillomembrana compta*	
			Tianzhushania polysiphonia	
			Tianzhushania spinosa	
			Unnamed Form 'A'	Somewhat similar to *Tianzhushania spinosa*, as noted by original authors.
			Unnamed Form 'B'	Poorly preserved specimens of *Tianzhushania* or *Crassimembrana* Ouyang et al., 2021.
Sharma et al., 2021	Krol A	Solan	*Asterocapsoides sinensis*	One of the two specimens (fig. 9B) has acutely conical processes and may be *A. robustus*; the other specimen (fig. 9C) is poorly preserved and lacks diagnostic features of *A. sinensis*.
			Tianzhushania spinosa	Not *T. spinosa*, possibly *Knollisphaeridium coniformum*.

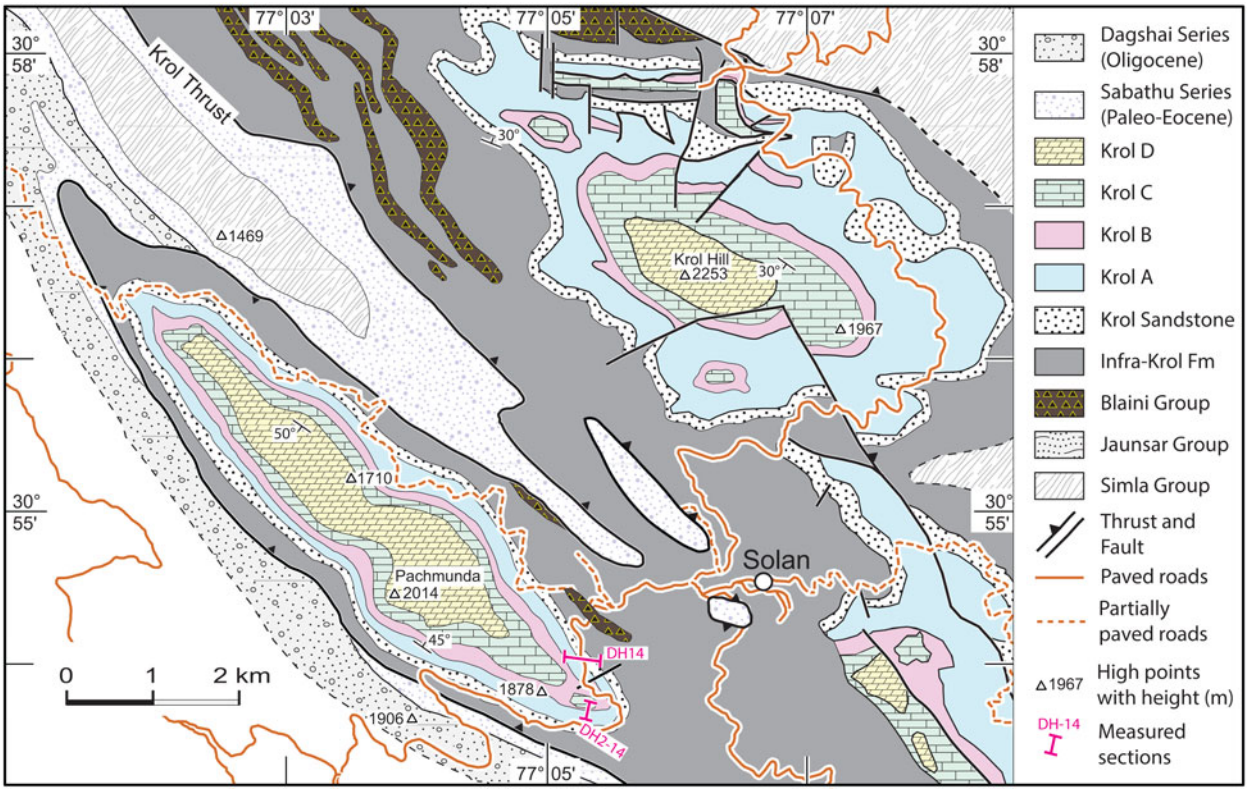

Figure 2. Geological map of the Solan area (Krol and Pachmunda synclines) showing the location of measured sections DH-14 and DH2-14. Modified from Auden (1934) and Bhattacharya and Niyogi (1971).

sandstone layer marks the top of the Krol B Formation, which is overlain by a 15-m-thick, thinly bedded, calcareous shale and lime mudstone of the lowermost Krol C Formation. The rest of the Krol C Formation consists of black to dark-gray bituminous limestone (Fig. 3.2).

Materials and methods

One hundred eighty rock samples at 0.2–1.0 m stratigraphic spacing were collected from the Krol A–C formations at the study sections for petrographic and geochemical ($\delta^{13}C$ and $\delta^{18}O$) analyses. Samples were washed and cut in the laboratory to exposure fresh surfaces for petrographic thin section preparation and geochemical microsampling. Carbonate powders were drilled from fresh surfaces of the samples. For isotope analyses, ~50–200 µg of carbonate powders were allowed to react with orthophosphoric acid for 10 minutes at 70°C, using a Kiel IV carbonate device connected to a Finnigan Delta V Plus mass spectrometer via dual-inlet at the University of Nevada Las Vegas. Isotope values are reported in δ notation relative to Vienna Pee Dee Belemnite standard (VPDB). Analytical uncertainty monitored by NBS-19 and an internal standard was <0.08‰ for both $\delta^{13}C$ and $\delta^{18}O$.

Chert nodule samples were collected, along with the geochemical samples, from 13 horizons of the Krol A Formation for micropaleontological study (Fig. 3.2). They were cleaned and embedded in epoxy for the preparation of standard petrographic thin sections. Nodules were not cut with controlled stratigraphic orientations because most were loosened from friable host rock. Thin sections were systematically examined under an Olympus BX-51 and a Zeiss Axioscope A1 transmitted light microscope. Microfossils were positioned using built-in coordinate systems and illustrated microfossils were additionally positioned using an England Finder slide. Selected microfossils were photographed using digital cameras attached to the microscopes. Ninety-four petrographic slides were examined and 274 ornamented acritarch specimens were photographed. The ornamented acritarch taxa are described in Systematic Paleontology because of their biostratigraphic significance. Representative sphaeromorphs, filaments, coccoids, and multicellular algae are illustrated, but not described in detail.

Repositories and institutional abbreviations.—All illustrated microfossils are deposited in the Virginia Polytechnic Institute Geosciences Museum (VPIGM). For each illustrated specimen, the thin section number (which contains the sample number, e.g., thin section DH-14-65.0-B comes from sample DH-14-65.0), Olympus BX-51 coordinates (e.g., 14.3 × 134.6), and England Finder coordinates (e.g., EF-Q28-4) are given. Descriptive terminology is adopted from Xiao et al. (2014). Taxonomic nomenclature follows the International Code of Nomenclature for Algae, Fungi, and Plants (Turland et al., 2018).

Systematic paleontology

Group Acritarcha Evitt, 1963

Genus *Appendisphaera* Moczydłowska, Vidal, and Rudavskaya, 1993, emend. Moczydłowska, 2005

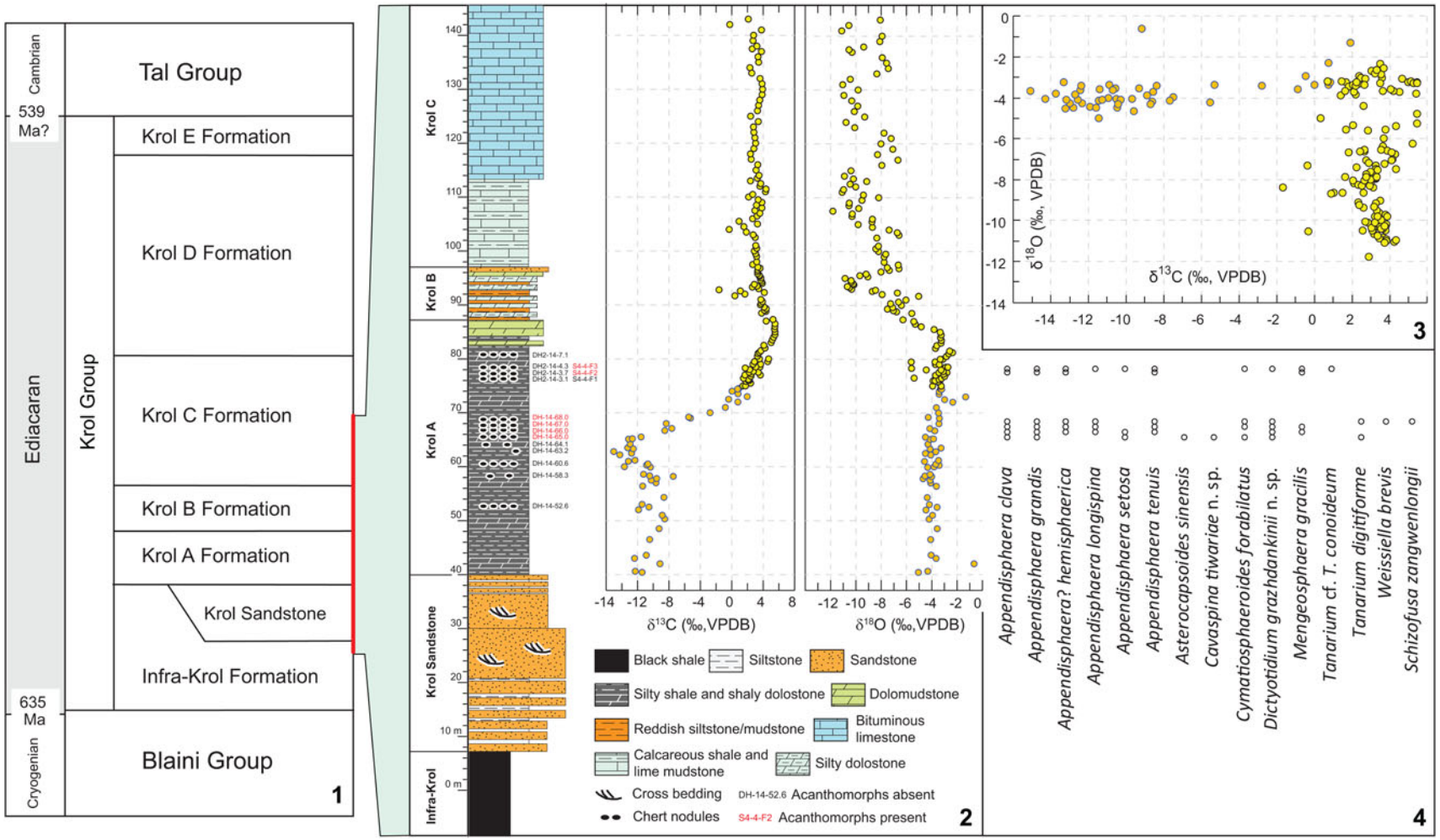

Figure 3. Litho-, chemo-, and biostratigraphy of the measured sections in the southeastern corner of the Pachmunda syncline (see Fig. 2 for location). (**1**) Stratigraphic nomenclature of the Ediacaran units in the Krol Belt. (**2**) Composite stratigraphic log of the measured sections from the topmost Infra-Krol Formation to the Krol C Formation. The stratigraphic position of chert nodule samples is marked, along with carbonate $\delta^{13}C$ and $\delta^{18}O$ data from Krol A to Krol C. Sample numbers in black contains no acanthomorphs, but are not necessarily non-fossiliferous. (**3**) $\delta^{13}C$–$\delta^{18}O$ cross-plot. The lower–middle Krol A Formation (~40–75 m) has negative $\delta^{13}C$ values but consistent $\delta^{18}O$ values around −4‰ (brown symbols). The rest of the $\delta^{13}C$ and $\delta^{18}O$ data are shown in yellow symbols. (**4**) Stratigraphic occurrence of the leiosphere *Schizofusa zangwenlongii*, the herkomorph *Dictyotidium grazhdankinii* Xiao n. sp., and all acanthomorph species recovered from the Krol A Formation. Stratigraphic heights are aligned to the stratigraphic column in (**2**). Note the occurrence of *Appendisphaera grandis*, *Schizofusa zangwenlongii*, and *Tanarium* cf. *T. conoideum*. These are either eponymous or morphologically similar species of the three assemblage zones recognized by Liu and Moczydłowska (2019) from member II of the Doushantuo Formation in the Yangtze Gorges area (i.e., the *Appendisphaera grandis-Weissiella grandistella-Tianzhushania spinosa*, the *Tanarium tuberosum-Schizofusa zangwenlongii*, and the *Tanarium conoideum-Cavaspina basiconica* assemblage zones). Also note that Liu and Moczydłowska (2019) regarded *Weissiella brevis*, which occurs in the Krol A Formation, as synonymous with *W. grandistella*.

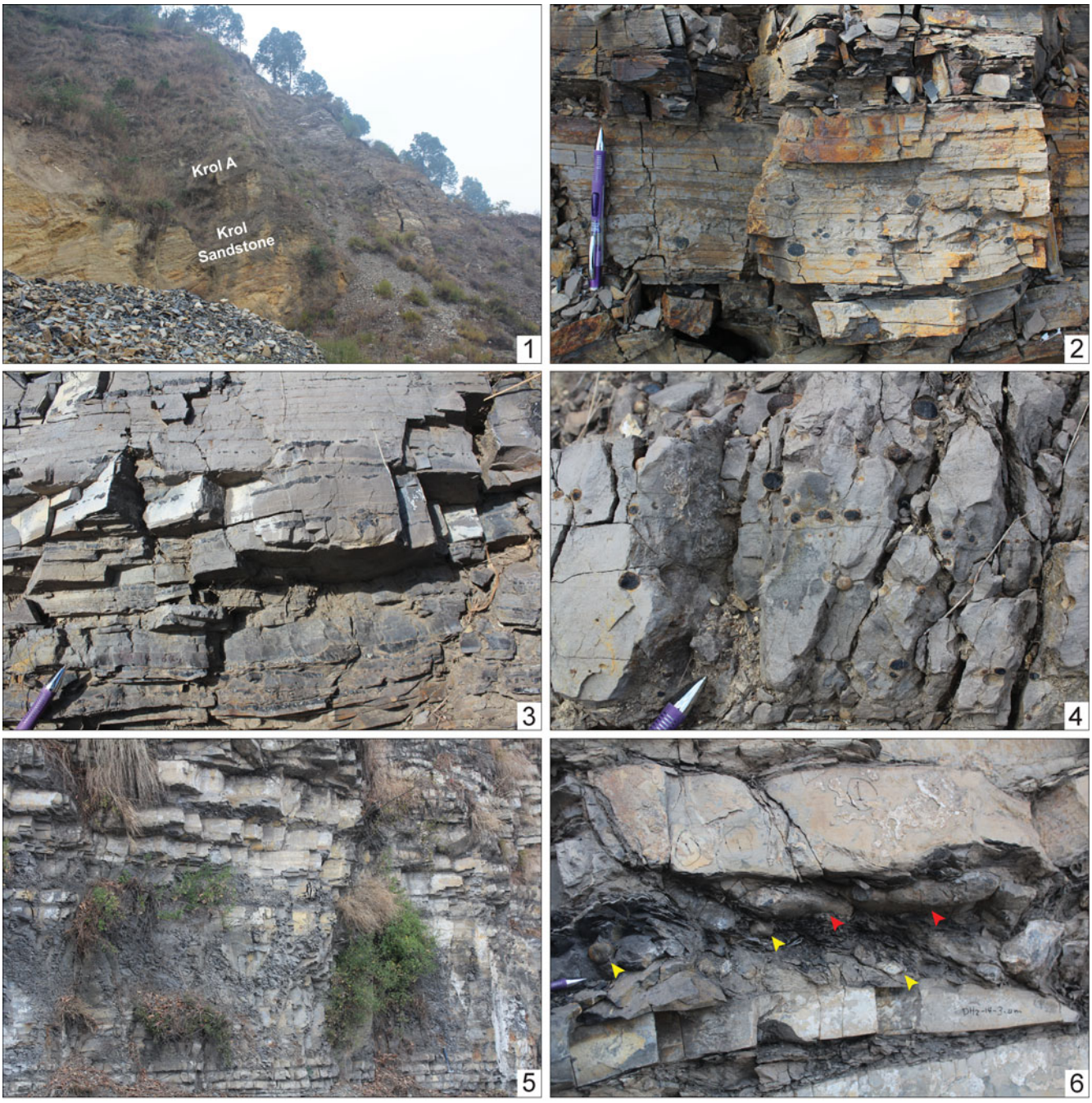

Figure 4. Field photos of the measured sections. (**1**) Overview of the Krol Sandstone and Krol A Formation in a newly excavated quarry (section DH-14). Outcrop shown here is ~60 m thick (40 m of Krol A and 20 m of Krol Sandstone). (**2**) Chert nodules in silty dolostone of Krol A (sample DH-14-52.6 in Fig. 3.2). (**3**) Chert nodules and bands in dolomitic shale and microcrystalline dolostone of Krol A (sample DH-14-64.1 in Fig. 3.2). (**4**) Chert nodules in silty dolostone of Krol A (sample DH-14-66.0 in Fig. 3.2). (**5**) Interbedded shale and dolostone of Krol A along the road in section DH2-14 (0.0–3.2 m). (**6**) Chert nodules in dolomitic shales of Krol A (samples DH2-14-3.1 and S4-4-F1 in Fig. 3.2). There are small (yellow arrows) and large (red arrows) chert nodules in the upper part of Krol A. Large chert nodules typically do not contain fossils. Pencil (14 cm) and pencil head (1.8 cm) for scale in (2–4, 6). Rock hammer (30 cm) for scale in (5) (lower right).

Type species.—Appendisphaera grandis Moczydłowska, Vidal, and Rudavskaya, 1993, emend. Moczydłowska, 2005.

Other species.—Appendisphaera anguina Grey, 2005; *A.*? *brevispina* Liu et al., 2014; *A. clava* Liu et al., 2014; *A. clustera* Liu and Moczydłowska, 2019; *A. fragilis* Moczydłowska, Vidal, and Rudavskaya, 1993; *A. heliaca* (Liu and Moczydłowska, 2019) Ouyang et al., 2021; *A.*? *hemisphaerica* Liu et al., 2014; *A. lemniscata* Liu and Moczydłowska, 2019; *A. longispina* Liu et al., 2014; *A. longitubularis* (Liu et al., 2014) Liu and Moczydłowska, 2019, an orthographic correction of *A. longitubulare* as published in Liu and Moczydłowska (2019); *A. magnifica* (Zhang et al., 1998) Liu et al., 2014; *A. setosa* Liu et al., 2014; *A. tabifica* Moczydłowska, Vidal, and Rudavskaya, 1993; *A. tenuis* Moczydłowska, Vidal, and Rudavskaya, 1993.

Remarks.—Several *Appendisphaera* species published in the literature have been synonymized with existing species or transferred to other genera, hence they are not listed above. Liu and Moczydłowska (2019, p. 61) considered *Appendisphaera barbata* Grey, 2005, *A. centoreticulata* Grey, 2005, *A. dilutopila* (Zang in Zang and Walter, 1992) Grey, 2005, and *A. minutiforma* Grey, 2005, as junior synonyms of *A. tabifica*. They also regarded *A. minima* Nagovitsin and Faizullin in Nagovitsin et al., 2004, as a junior synonym of *A. tenuis*, and excluded *A. crebra* (Zang in Zang and Walter, 1992) Liu et al., 2014, from the genus *Appendisphaera*. Liu and Moczydłowska (2019) indicated that *A. magnifica* is synonymous with *A. grandis*, but did not provide any justification; in this paper we follow Liu et al. (2014a) and Ouyang et al. (2021) and regard *A. magnifica* as a distinct species of *Appendisphaera* (see discussion under the species *A. grandis*).

A Doushantuo specimen illustrated in Liu et al. (2021) as *Ericiasphaera magna* seems to have hollow rather than solid process (see Liu et al., 2021, fig. 4.5, 4.6), and thus may belong to the genus *Appendisphaera*. It is somewhat similar to *A. setosa* or *A. tenuis* in process density and morphology, particularly the extremely thin processes (~1.0–1.5 µm wide at the base and ~0.3 µm wide above the base).

Appendisphaera clava Liu et al., 2014
Figures 5, 6

2013 Unnamed (E); Liu et al., fig. 12A, B.
2014a *Appendisphaera clava* Liu et al., p. 12, figs. 5.4, 8.1–8.5, 9.1–9.7.
2015 *Appendisphaera clava*; Muscente et al., fig. 5D.
2019 *Appendisphaera clava*; Ouyang et al., fig. 8G, H (part).
2020 *Appendisphaera clava*; Grazhdankin et al., fig. 3C.
2021 *Appendisphaera clava*; Ouyang et al., fig. 10K, L.

Holotype.—IGCAGS–WFG–676, reposited at Institute of Geology, Chinese Academy of Geological Sciences, from the lower member III of the Ediacaran Doushantuo Formation at Wangfenggang section in the Yangtze Gorges area, Hubei Province, South China (Liu et al., 2014a, fig. 8.1, 8.2).

Occurrence.—Ediacaran of South China and northern India, and lower Cambrian of Siberia. South China: member II and equivalent strata of the Doushantuo Formation at Jinguadun (Ouyang et al., 2021) and Wuzhishan (Ouyang et al., 2021) in the Yangtze Gorges and surrounding areas; member III of the Doushantuo Formation at Wangfenggang and Niuping in the Yangtze Gorges area (Liu et al., 2014a). Northern India: Ediacaran Krol A Formation in the Solan area of northern India (this paper). Siberia: upper Ediacaran or lower Cambrian Oppokun Formation, Khastakhskaya borehole, Lena-Anabar Basin, north-central Siberia (Grazhdankin et al., 2020).

Description and measurements.—Medium-sized to large spherical vesicles with evenly spaced processes that are short, hollow, slightly expanded at base, basally separate, distally pointed, and open to vesicle interior. Vesicle diameter difficult to measure with precision, but likely >200 µm (see Figs. 5.1, 6.1). Approximately 19–34 processes per 100 µm of vesicle periphery, process spacing 1–3 µm at base, process width 2–3 µm at base, and process length 4–11 µm. Basal expansions conical in shape and 1–2 µm in height. Apical spines of processes 2–10 µm in length and ~0.5 µm in maximum width.

Materials.—Six illustrated specimens (Figs. 5, 6) and 53 additional specimens.

Remarks.—The Krol A specimens are similar to the holotype of *Appendisphaera clava* in vesicle size, process density, process morphology, and the size and shape of the basal expansion. The specimens are somewhat similar to *A. tenuis* in process length and density, but they better conform to the diagnosis of *A. clava* in its larger vesicle and processes with a more notable basal expansion. For comparison, the holotype of *A. clava* is 420 µm in vesicle diameter (vs. 87–147 µm in specimens identified as *A. tenuis*), and its processes have a visible basal expansion and are 12 µm in length (vs. 7–16 µm in *A. tenuis*) and ~1 µm in process basal width (measurements not reported for *A. tenuis*); as a result, process length is only 2.9% of vesicle diameter in *A. clava* (vs. 8–11% in *A. tenuis*) (Moczydłowska, 2005; Liu et al., 2014a).

Ouyang et al. (2019) illustrated two specimens of *Appendisphaera clava*, but one of them (their fig. 8E, F) seems to have long processes (>20 µm in length) and may belong to *A. grandis*.

Appendisphaera grandis Moczydłowska, Vidal, and Rudavskaya, 1993, emend. Moczydłowska, 2005
Figure 7

1993 *Appendisphaera grandis* Moczydłowska et al., p. 503, text-fig. 5, pl. 1, figs. 1, 2.
2005 *Appendisphaera grandis*; Moczydłowska, p. 294, figs. 3, 4.
non 2014 *Appendisphaera grandis*; Shukla and Tiwari, p. 215, fig. 4D, E.
2016 *Appendisphaera grandis*; Prasad and Asher, p. 42, pl. 2, figs. 3, 4.
non 2016 *Appendisphaera grandis*; Sharma et al., fig. 4B.
2017 *Appendisphaera fragilis* Moczydłowska, Vidal, and Rudavskaya; Ouyang et al., fig. 8D–F.
2019 *Appendisphaera grandis*; Anderson et al., p. 507, fig. 6A–D.
2019 *Appendisphaera grandis*; Liu and Moczydłowska, p. 48, figs. 21–23, and synonyms therein (except *Appendisphaera*? *hemisphaerica* illustrated in Hawkins et al., 2017, fig. 9C, D; *Meghystrichosphaeridium magnificum* illustrated in Zhang et al., 1998, fig. 10.5, 10.6; and Liu et al., 2013, fig. 11I, J; and *Appendisphaera magnifica* illustrated in Liu et al., 2014a, figs. 19, 20; and in Hawkins et al., 2017, fig. 9A, B).
2019 *Appendisphaera grandis*; Shang et al., p. 7, fig. 3, and synonyms therein (except *Appendisphaera*? *hemisphaerica* illustrated in fig. 9C, D of Hawkins et al., 2017).
2019 *Appendisphaera grandis*; Ouyang et al., fig. 8I–K.
2020 *Appendisphaera grandis*; Shang and Liu, p. 156, fig. 4.

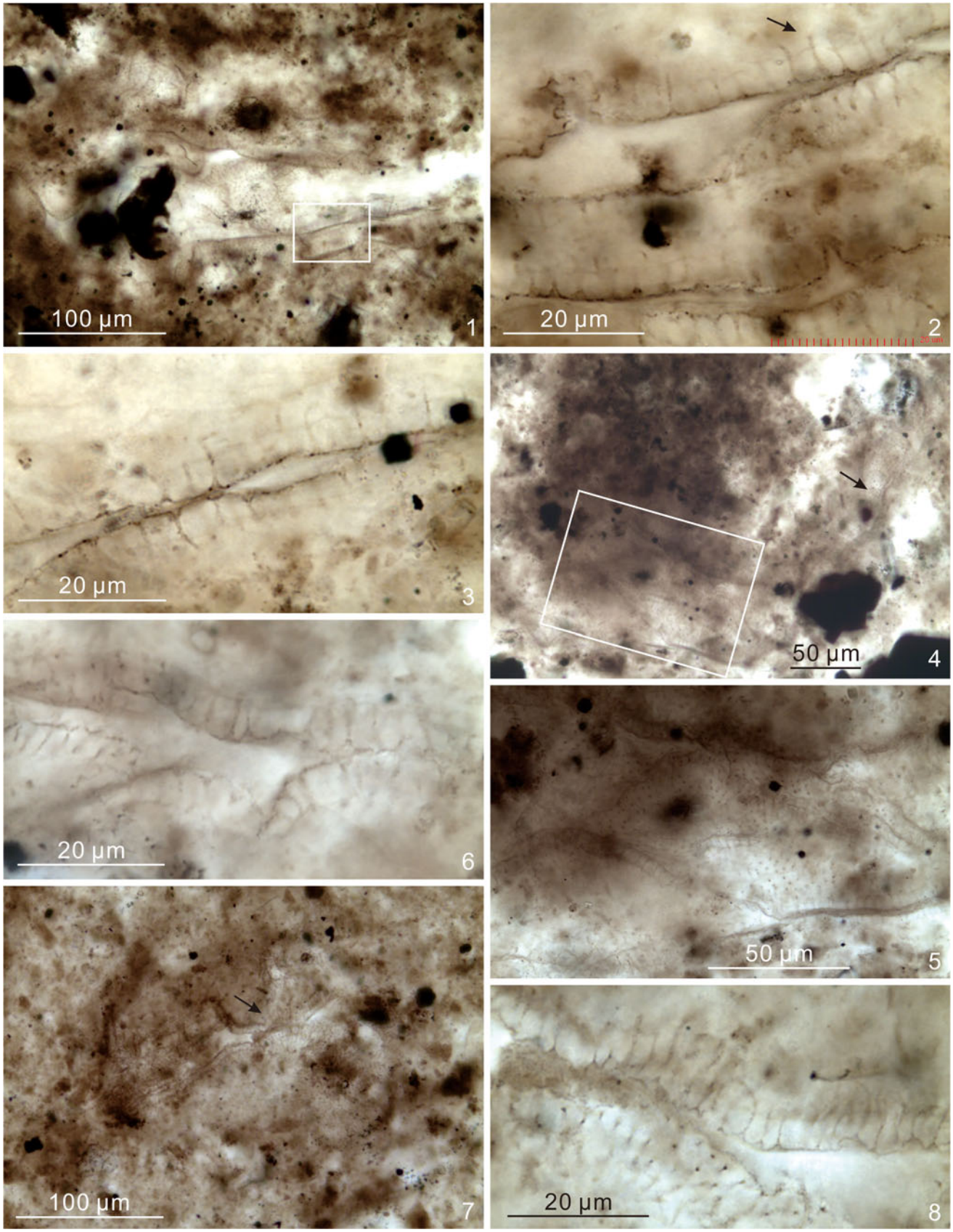

Figure 5. *Appendisphaera clava*. (**1–3**) DH-14-67.0-B-2, 20.8 × 111.6, EF-H11-2, VPIGM-4847, rectangle in (**1**) marks area shown in (**2**) at a different focal level, arrow in (**2**) marks area shown in (**3**) at a different focal level; (**4–6**) S4-4-F2-7, 3.0 × 139.5, EF-AA39-1, VPIGM-4889, rectangle in (**4**) marks area shown in (**5**) at a different focal level and with a slight rotation, arrow in (**4**) marks area shown in (**6**) at a different focal level and with a slight rotation; (**7, 8**) S4-4-F2-5, 23.0 × 107.0, EF-E7-1, VPIGM-4878, arrow in (**7**) marks area shown in (**8**) at a different focal level and with a slight rotation. All specimens illustrated in this paper are from the Krol A Formation, Solan, northern India. For each illustrated specimen, the following information is given: thin section number (which is the sample number with a differentiating suffix if multiple thin sections were made from the sample), Olympus BX-51 coordinates, England Finder coordinates, and VPIGM catalog number.

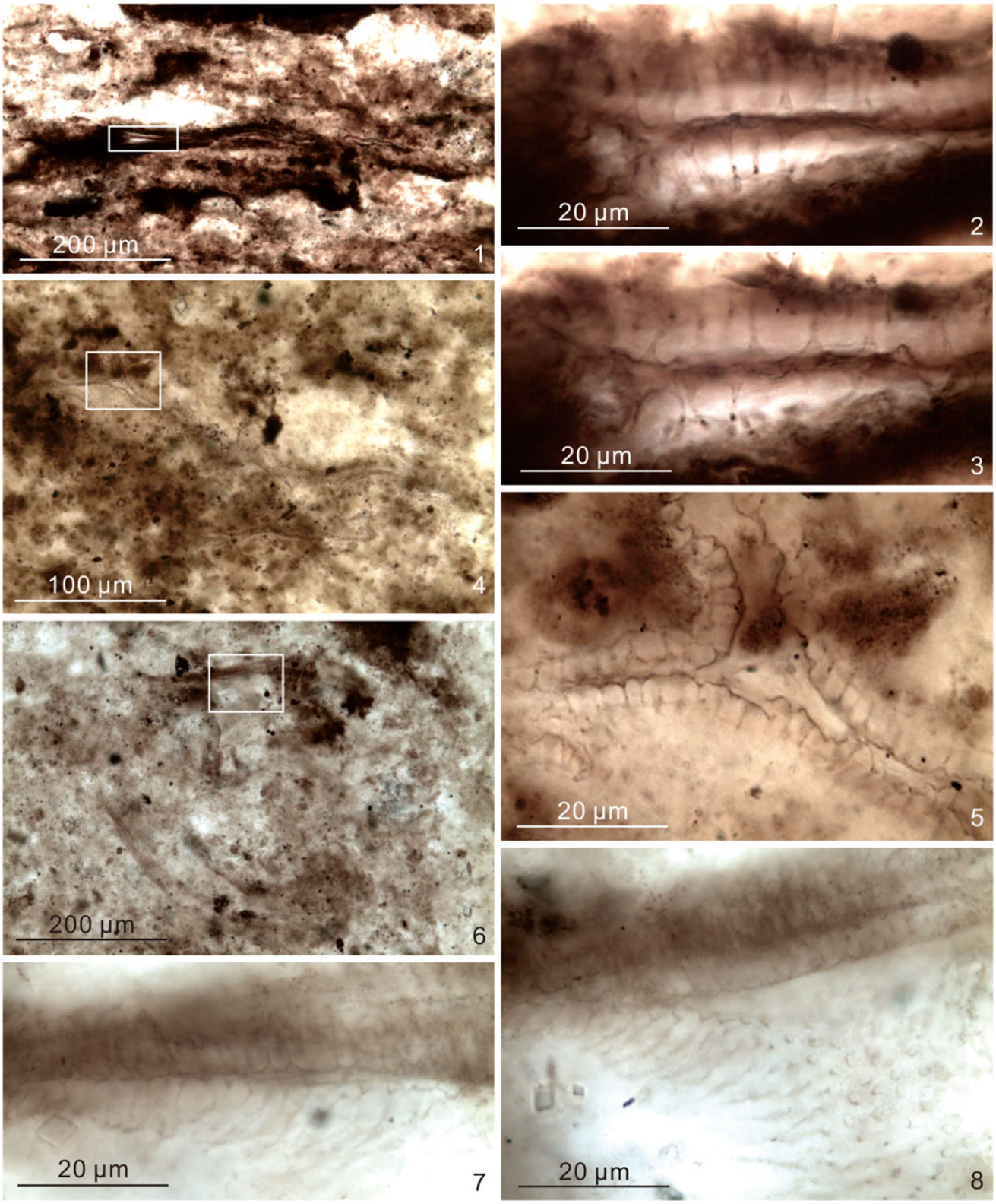

Figure 6. *Appendisphaera clava*. (**1–3**) S4-4-F1-4, 17.0 × 124.5, EF-L24-4, VPIGM-4871, rectangle in (**1**) marks area shown in (**2**) and (**3**) at different focal levels; (**4, 5**) DH-14-67.0-C-2, 13.6 × 134.3, EF-P34-1, VPIGM-4853, rectangle in (**4**) marks area shown in (**5**); (**6–8**) S4-4-F2-7, 6.8 × 139.3, EF-V39-3, VPIGM-4890, rectangle in (**6**) marks area shown in (**7**) and (**8**) at different focal levels.

2021 *Appendisphaera grandis*; Ouyang et al., fig. 10M–P.
2021 *Appendisphaera grandis*; Liu et al., fig. 5.4.

Holotype.—PMU-Sib.1-R/63/2, reposited at Uppsala University, from the Ediacaran Khamaka Formation, Zapad

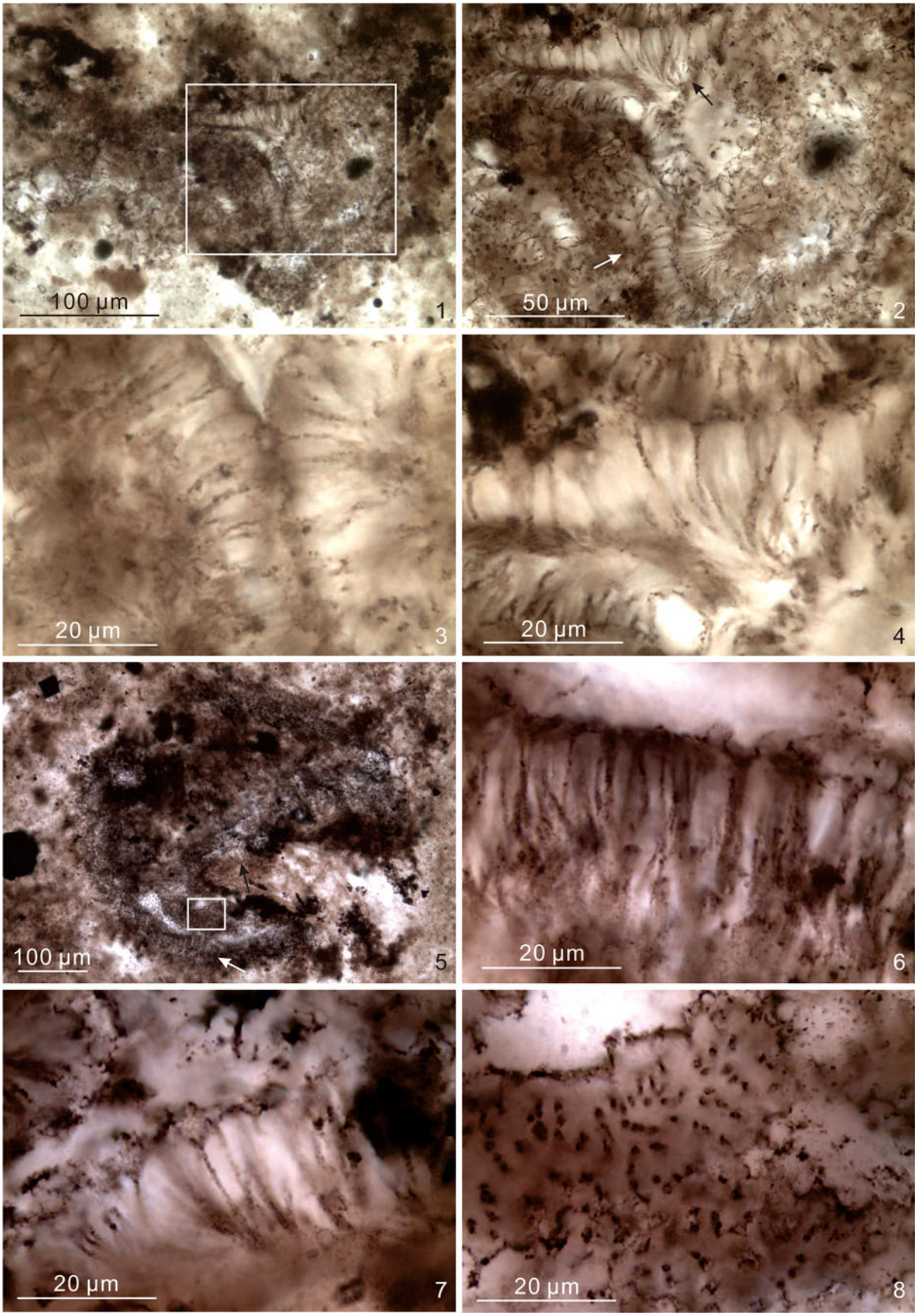

Figure 7. *Appendisphaera grandis*. (**1–4**) S4-4-F2-5, 10.5 × 132.3, EF-S32-2, VPIGM-4873, rectangle in (**1**) marks area shown in (**2**), white and black arrows in (**2**) mark areas shown in (**3**) (different focal level) and (**4**), respectively; (**5–8**) DH-14-66.0-B-2, 9.8 × 120.8, EF-S21-1, VPIGM-4840, white arrow, black arrow, and rectangle in (**5**) mark areas shown in (**6–8**), respectively.

742 borehole at a depth of 1887.0–1894.0 m, Nepa-Botuoba region, Yakutia, Siberian (Moczydłowska, Vidal, and Rudavskaya, 1993, p. 503, text-fig. 5A–D).

Occurrence.—Ediacaran of South China, Siberia, Australia (see Liu and Moczydłowska, 2019, and Shang et al., 2019, for detailed occurrence information), and India (this paper). This species also has been reported from the upper Khesen Formation at Urandush Uul in northern Mongolia (Anderson et al., 2017, 2019), which is considered terminal Ediacaran in age, although the uppermost Khesen Formation contains Cambrian-age detrital zircons (Anttila and Macdonald, 2020). The occurrence of *Appendisphaera grandis* in the Semri Group of the Lower Vindhyan Supergroup in the Chambal Valley of eastern Rajasthan of central-western India (Prasad and Asher, 2016) is intriguing because the Semri Group in central India is widely regarded as Paleo-/Mesoproterozoic in age, ca. 1600 Ma (Rasmussen et al., 2002; Ray et al., 2002); this record and its age warrants further confirmation because of its profound biostratigraphic implications (Hughes, 2017) and because *Appendisphaera grandis* is the eponymous species of the early Ediacaran *Appendisphaera grandis-Weissiella grandistella-Tianzhushania spinosa* Assemblage Zone of Liu and Moczydłowska (2019).

Description and measurements.—Medium-sized to large spherical vesicles with closely and evenly spaced processes that are long, hollow, cylindrical or slightly expanded at base, distally tapering, and open to vesicle interior. Vesicle diameter difficult to measure with precision due to deformation, but one specimen is ~440 µm in diameter (Fig. 7.5). Approximately 15–50 processes per 100 µm of vesicle periphery, process spacing up to 1.4 µm at base, although many processes are in basal contact with each other, process length 17–21 µm. Most processes are cylindrical (~0.5 µm in width; Fig. 7.6), although some appear to have a basal expansion supporting an apical spine (Fig. 7.3, 7.4, 7.7). We cannot exclude the possibility that the basal expansion is a diagenetic artifact; nonetheless, the apparent basal expansion measures up to 3–4 µm in width and 3–4 µm in height, and the apical spine is 12–17 µm in length and ~0.5 µm in maximum width.

Materials.—Two illustrated specimens (Fig. 7) and 18 additional specimens.

Remarks.—The Krol A specimens are identified as *Appendisphaera grandis* based on their relatively long and densely distributed processes. Some, but not all, processes in the Krol A specimens have a slightly expanded base (e.g., Fig. 7.3, 7.4), but they are otherwise similar to the holotype (Moczydłowska et al., 1993) and other specimens identified as *Appendisphaera grandis* (Liu and Moczydłowska, 2019).

Meghystrichosphaeridium magnificum Zhang et al., 1998, is somewhat similar to *Appendisphaera grandis* in vesicle size, process density, and process morphology. Liu et al. (2014a) acknowledged these similarities, but emphasized that the processes of *M. magnificum* are more regularly and evenly distributed, and that they taper toward a more sharply pointed distal end than those of *A. grandis*. Thus, they transferred this species to the genus *Appendisphaera*, but maintained it as a distinct species, *A. magnifica*. Subsequently, without providing explanation or justification, Liu and Moczydłowska (2019) marked *M. magnificum* as an invalid species and listed it as a junior synonym of *A. grandis*. As far as we can tell, *M. magnificum* is an effectively and validly published species (Zhang et al., 1998). Not knowing the basis for the synonymization proposed by Liu and Moczydłowska (2019), we follow Liu et al. (2014a), Hawkins et al. (2017), and Ouyang et al. (2021) and treat *A. magnifica* and *A. grandis* as distinct taxa.

Liu and Moczydłowska (2019) included specimens identified by Hawkins et al. (2017) as *Appendisphaera*? *hemisphaerica* and *A. crebra* (Zang in Zang and Walter, 1992) Liu et al., 2014 in the synonym list of *A. grandis*, but no justification was provided. Similarly, Shang et al. (2019) included the *Appendisphaera*? *hemisphaerica* specimen illustrated by Hawkins et al. (2017) in the synonym list of *A. grandis*, again without explanation or justification. We re-examined Hawkins et al.'s (2017) specimens under a transmitted light microscope by adjusting the focal level, and were able to confirm that the *A.*? *hemisphaerica* specimen in Hawkins et al. (2017) has basally separate biform processes with a clearly defined basal expansion (~4 µm in diameter) and a thin apical spine (~1 µm in diameter), features that are compatible with *A.*? *hemisphaerica*. Although some processes of *A. grandis* can have a slightly widened base (Moczydłowska, 2005), they are not biform and typically are narrower in basal width (e.g., 1–2 µm, Shang et al., 2019; 1–3 µm, Liu and Moczydłowska, 2019; 2–3 µm, Liu et al., 2021). Thus, the specimen illustrated in Hawkins et al. (2017) better fits the diagnosis of *A.*? *hemisphaerica* than that of *A. grandis*. The *A. crebra* specimen of Hawkins et al. (2017) is poorly preserved, and may be assigned to *A. grandis* given that the holotype of *A. crebra* may not belong to the genus *Appendisphaera* (Liu and Moczydłowska, 2019).

A specimen illustrated as *Appendisphaera fragilis* in Ouyang et al. (2017) has longer and more densely arranged processes than the holotype of *A. fragilis*, but better fits the diagnosis of *A. grandis*; this specimen is also listed as a synonym of *A. grandis* in Liu and Moczydłowska (2019), Shang et al. (2019), and Shang and Liu (2020), but only the latter authors offered an explanation.

Specimens identified as *Appendisphaera grandis* from the Semri Group of the Lower Vindhyan Supergroup in the Chambal Valley of eastern Rajasthan of India (Prasad and Asher, 2016) do have thin and densely distributed processes, but their vesicles (50–80 µm in diameter) are smaller than the holotype of *A. grandis* (105–108 µm in diameter; Moczydłowska et al., 1993). As mentioned above, the occurrence of *A. grandis* in the Semri Group needs to be verified, considering its profound biostratigraphic implications (Hughes, 2017).

We agree with Liu and Moczydłowska (2019) that the two specimens illustrated as *A. grandis* in Shukla and Tiwari (2014), one of which was also illustrated in Sharma et al. (2016), are better assigned to *A. tenuis*, because their processes are proportionally shorter than those in *A. grandis*.

Appendisphaera? *hemisphaerica* Liu et al., 2014
Figures 8–12

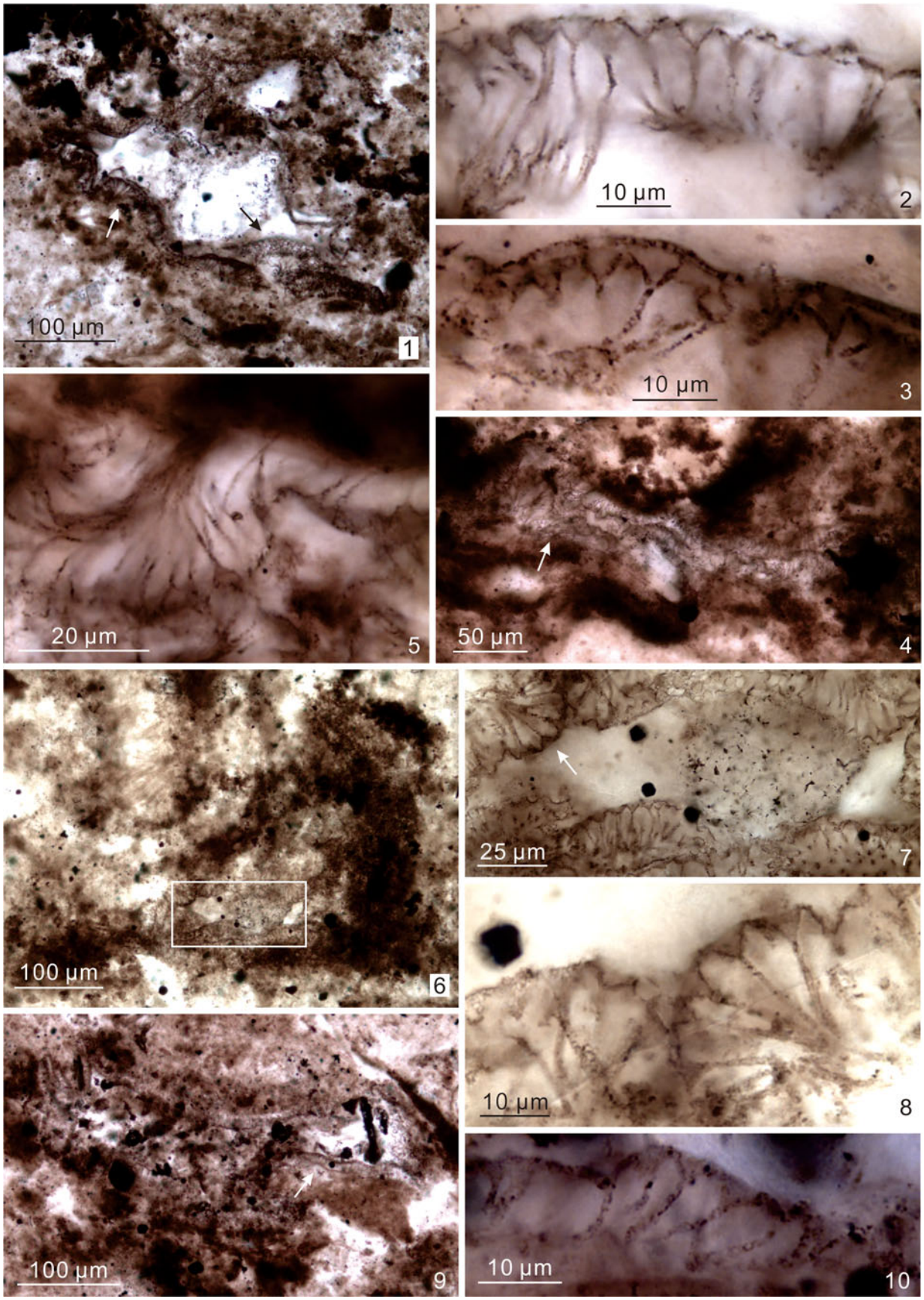

Figure 8. *Appendisphaera*? *hemisphaerica*. (**1–3**) DH-14-67.0-A-2, 15.8 × 111.7, EF-M11-4, VPIGM-4842, black and white arrows in (**1**) mark areas shown in (**2, 3**), respectively, at different focal levels; (**4, 5**) DH-14-67.0-A-2, 18.8 × 117.9, EF-J17-4, VPIGM-4843, arrow in (**4**) marks area shown in (**5**) at a different focal level; (**6–8**) S4-4-F2-7, 17.0 × 125.9, EF-L26-3, VPIGM-4887, rectangle in (**6**) marks area shown in (**7**), arrow in (**7**) marks area shown in (**8**) with a 180° rotation; (**9, 10**) DH-14-66.0-B-2, 11.4 × 107.4, EF-Q7-4, VPIGM-4839, arrow in (**9**) marks area shown in (**10**) at a different focal level.

2014a *Appendisphaera*? *hemisphaerica* Liu et al., p. 17, figs. 13–15.
non *Appendisphaera*? *hemisphaerica*; Ouyang et al., 2015 p. 215, pl. I, figs. 3, 5.
2017 *Appendisphaera*? *hemisphaerica*; Hawkins et al., fig. 9C, D.
2018 *Appendisphaera*? *hemisphaerica*; Shang et al., fig. 4B.
2019 *Appendisphaera*? *hemisphaerica*; Shang et al., p. 7, fig. 4A, B.

Holotype.—IGCAGS–WFG–248, reposited at Institute of Geology, Chinese Academy of Geological Sciences, from the lower member III of the Ediacaran Doushantuo Formation at Wangfenggang section in the Yangtze Gorges area, Hubei Province, South China (Liu et al., 2014a, fig. 13.1–13.3).

Occurrence.—Ediacaran of South China and northern India. South China: member II of the Doushantuo Formation at Siduping section in the Zhangjiajie area, Hunan Province (Hawkins et al., 2017); member III of the Doushantuo Formation at Wangfenggang and Niuping sections in the Yangtze Gorges area of Hubei Province (Liu et al., 2014a); Doushantuo Formation at Liujing section in Guizhou Province (Shang et al., 2019). Northern India: Krol A Formation at Solan of northern India (this paper).

Description and measurements.—Medium-sized to large spherical vesicles with closely and evenly spaced biform processes that are characterized by an easily recognizable basal expansion subtending a thin and long apical spine. Processes open to vesicle interior. Vesicle diameter ~300 µm, as estimated from three specimens (Figs. 8.1, 8.9, 9.3). Approximately 13–21 processes per 100 µm of vesicle periphery, process spacing 1–3 µm at base, but many processes are in basal contact, and process length 12–29 µm. Basal expansion conical and often inflated (Fig. 9.2, 9.5, 9.7), 3–6 µm in width, and 2–4 µm in height. Apical spine thin and cylindrical in shape, ~1 µm in width, and 7–25 µm in length.

Materials.—Eighteen illustrated specimens (Figs. 8–12) and six additional specimens.

Remarks.—*Appendisphaera*? *hemisphaerica* has a combination of features that are characteristic of *Appendisphaera* (thin and densely distributed processes) and *Mengeosphaera* (biform processes with a prominent basal expansion). For this reason, this species was tentatively placed in the genus *Appendisphaera* (Liu et al., 2014a). *Appendisphaera*? *hemisphaerica* is similar to several *Mengeosphaera* species in biform processes with a relatively long apical spine, such as *M. gracilis* Liu et al., 2014, *M. latibasis* Liu et al., 2014, and *M. uniformis* Liu et al., 2014. The main differentiator is the size and shape of the basal expansion. For reference, the basal expansion is 7–8 µm, 10–15 µm, and ~5 µm wide, respectively, for the holotypes of the three *Mengeosphaera* species listed above. Both *M. latibasis* and *M. uniformis* have an obtusely domical basal expansion, whereas *M. gracilis* has a conical basal expansion. However, specimens illustrated as *Mengeosphaera gracilis* in Liu and Moczydłowska (2019) have measurements of process size, shape, and density overlapping those of the holotype of *A.*? *hemisphaerica*. It is possible that *A.*? *hemisphaerica* and *Mengeosphaera gracilis* are synonymous, in which case the former species would take priority. At present, we follow Liu et al. (2014a) and treat *A.*? *hemisphaerica* and *Mengeosphaera gracilis* as two distinct species, with the processes of the latter species bearing a relatively larger basal expansion and a relatively shorter apical spine.

A specimen illustrated as *Appendisphaera*? *hemisphaerica* in Ouyang et al. (2015) was subsequently identified by Ouyang et al. (2021) as *Appendisphaera heliaca* (Liu and Moczydłowska, 2019) Ouyang et al., 2021, because the basal expansions of the processes in this specimen are thought to be a taphonomic artifact related to degradation. As discussed under *Appendisphaera grandis*, the specimen illustrated as *A.*? *hemisphaerica* in Hawkins et al. (2017) has basally separate biform processes with a clearly defined basal expansion. Thus, this specimen belongs to *A.*? *hemisphaerica* rather than *A. grandis*.

Appendisphaera longispina Liu et al., 2014
Figures 13, 14

2014a *Appendisphaera longispina* Liu et al., p. 21, figs. 17, 18, and synonyms therein.
2014a *Appendisphaera crebra* (Zang in Zang and Walter, 1992); Liu et al., p. 17, figs. 10, 11.
2019 *Appendisphaera longispina*; Liu and Moczydłowska, p. 54, fig. 25.
2019 *Appendisphaera longispina*; Shang et al., p. 8, fig. 4C, D.
2021 *Appendisphaera longispina*; Ouyang et al., fig. 11G, H.

Holotype.—IGCAGS–NPIII–141, reposited at Institute of Geology, Chinese Academy of Geological Sciences, from the upper member III of the Ediacaran Doushantuo Formation at Niuping section in the Yangtze Gorges area, Hubei Province, South China (Liu et al., 2014a, fig. 18.3, 18.4).

Occurrence.—Ediacaran of South China and northern India. South China: member II of the Doushantuo Formation at Jiuqunao and Xiaofenghe sections (Liu and Moczydłowska, 2019) and at Wuzhishan section (Ouyang et al., 2021), Yangtze Gorges area, Hubei Province; member III of the Doushantuo Formation at Niuping section in the Yangtze Gorges area, Hubei Province (described as *A. crebra* and *A. longispina* in Liu et al., 2014a); Doushantuo Formation at Liujing section in Guizhou Province (Shang et al., 2019). Northern India: Krol A Formation in the Solan area (this paper).

Description and measurements.—Large spherical vesicles with long, homomorphic, and evenly spaced processes that have a conical basal expansion gradually transitioning into a thin apical spine. Processes open to vesicle interior. Vesicle diameter ~250–300 µm, as estimated from two specimens (Fig. 13.1, 13.4). Processes 21–32 µm in length (~10% of vesicle diameter), densely distributed, ~16–24 processes per 100 µm of vesicle periphery, mostly in contact at base, but can be spaced at 1–2 µm. Basal expansion conical or slightly deflated (Fig. 13.2),

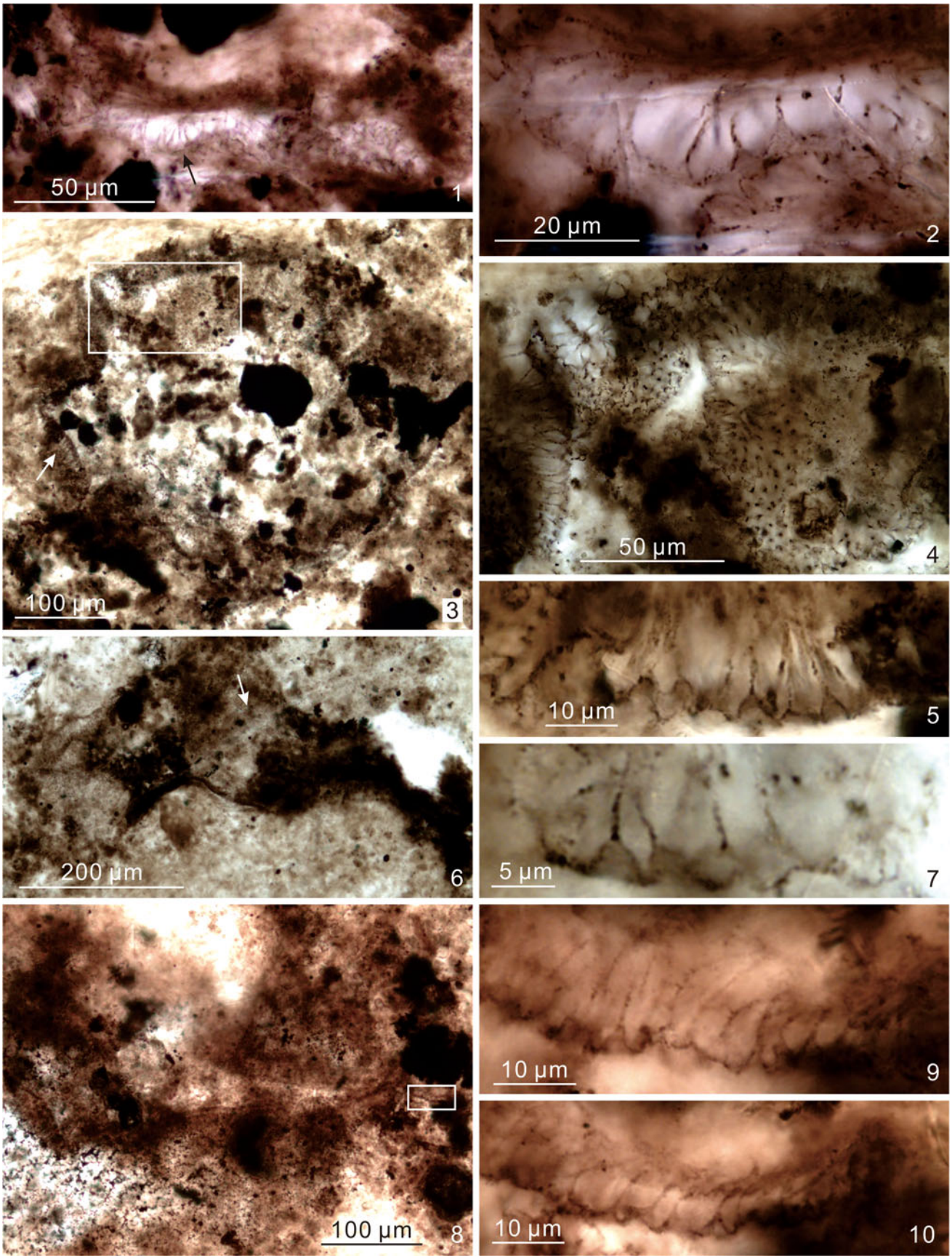

Figure 9. *Appendisphaera*? *hemisphaerica*. (**1, 2**) DH-14-67.0-A-2, 24.0 × 117.8, EF-D17-2, VPIGM-4844, arrow in (**1**) marks area shown in (**2**) at a different focal level; (**3–5**) S4-4-F2-5-2, 2.2 × 130.5, EF-AA31-1, VPIGM-4883, rectangle and arrow in (**3**) mark areas shown in (**4, 5**), respectively, at different focal levels; (**6, 7**) S4-4-F2-5-2, 5.6×129.0, EF-W29-4, VPIGM-4884, arrow in (**6**) marks area shown in (**7**) at a different focal level; (**8–10**) S4-4-F1-3, 16.3 × 125.9, EF-M26-1, VPIGM-4870, rectangle in (**8**) marks area shown in (**9, 10**) at different focal levels.

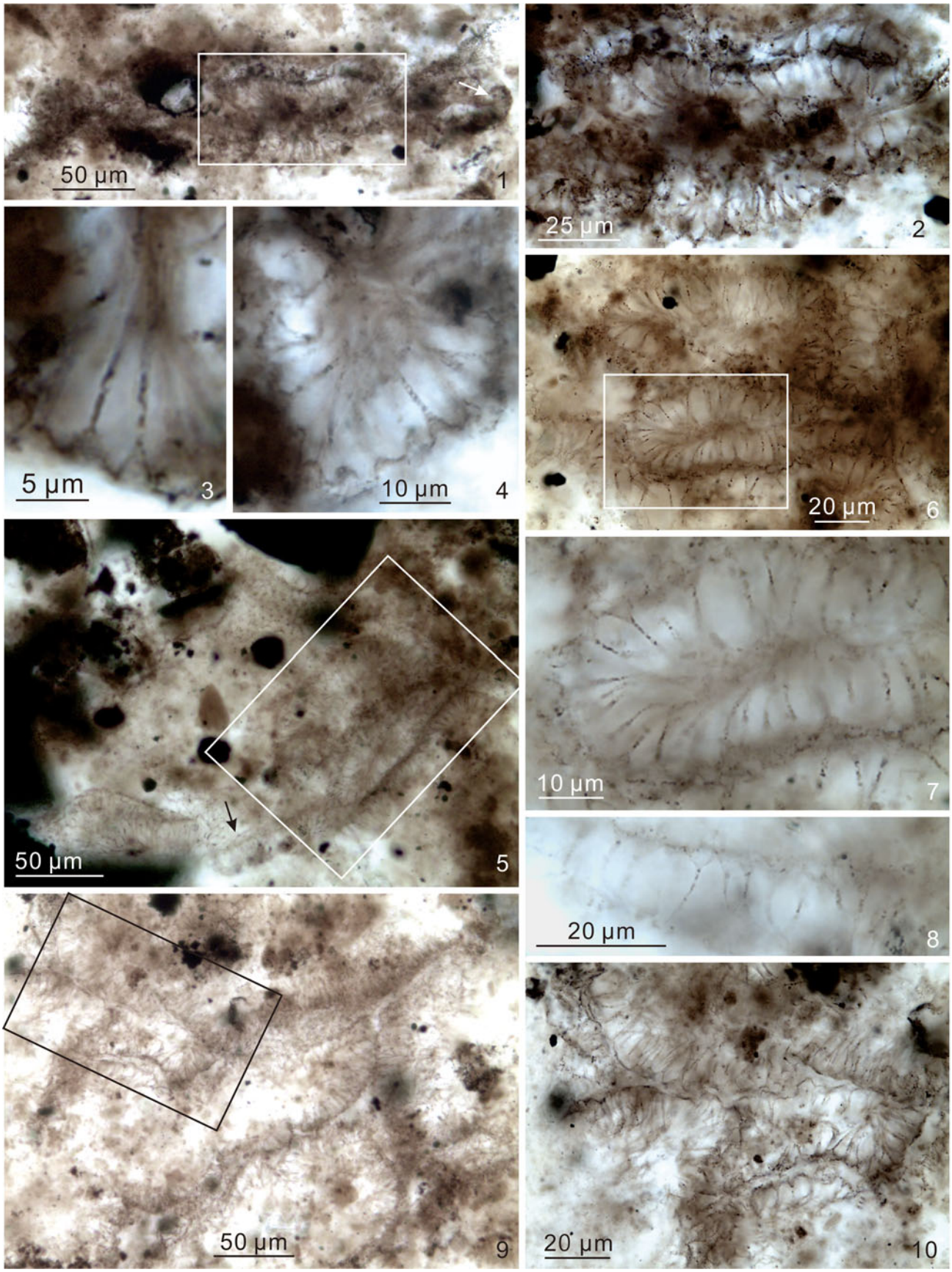

Figure 10. *Appendisphaera*? *hemisphaerica*. (**1–4**) S4-4-F2-15, 13.0 × 139.0, EF-P39-1, VPIGM-4899, rectangle in (**1**) marks area shown in (**2**), arrow in (**1**) marks area shown in (**3, 4**) at different focal levels and with slight rotations; (**5–8**) S4-4-F2-7, 10.3 × 129.3, EF-S29, VPIGM-4885, rectangles in (**5, 6**) mark areas shown in (**6, 7**), respectively, and arrow in (**5**) marks area shown in (**8**) at a different focal level and with a slight rotation; (**9, 10**) S4-4-F2-15, 21.9 × 138.0, EF-F38-3, VPIGM-4901, rectangle in (**9**) marks area shown in (**10**).

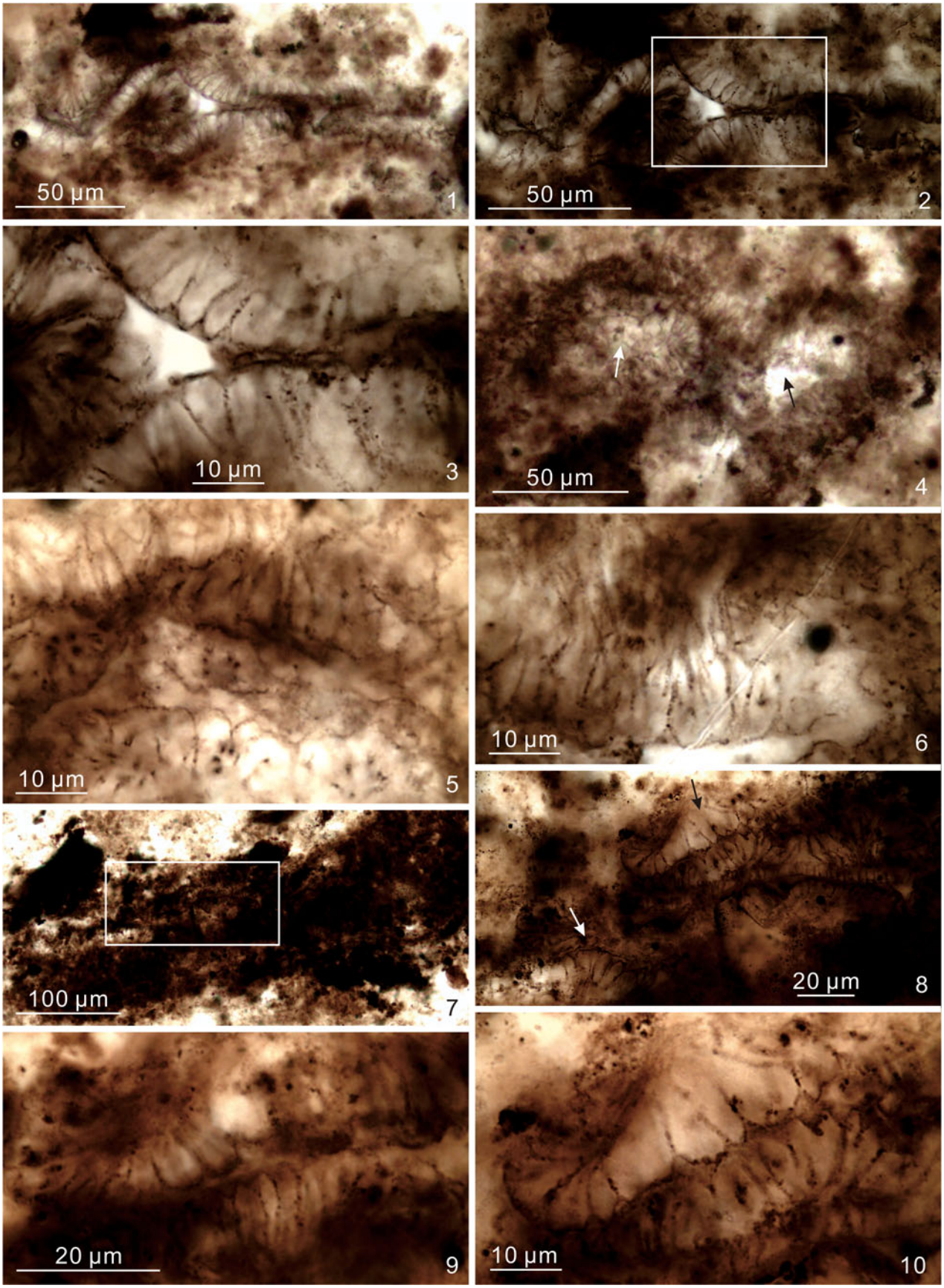

Figure 11. *Appendisphaera*? *hemisphaerica*. (**1–3**) DH-14-67.0-C-2, 11.1 × 140.8, EF-Q41-3, VPIGM-4851, (**1**) and (**2**) show roughly the same area at different focal levels, rectangle in (**2**) marks area shown in (**3**); (**4–6**) S4-4-F2-5-2, 18.5 × 140.5, EF-K40-2, VPIGM-4882, white and black arrows in (**4**) mark areas shown in (**5, 6**), respectively, at different focal levels; (**7–10**) DH-14-67.0-C-2, 15.8 × 141.4, EF-M41-3/4, VPIGM-4856, rectangle in (**7**) marks area shown in (**8**), white and black arrows in (**8**) mark areas shown in (**9**) (at a different focal level) and (**10**), respectively.

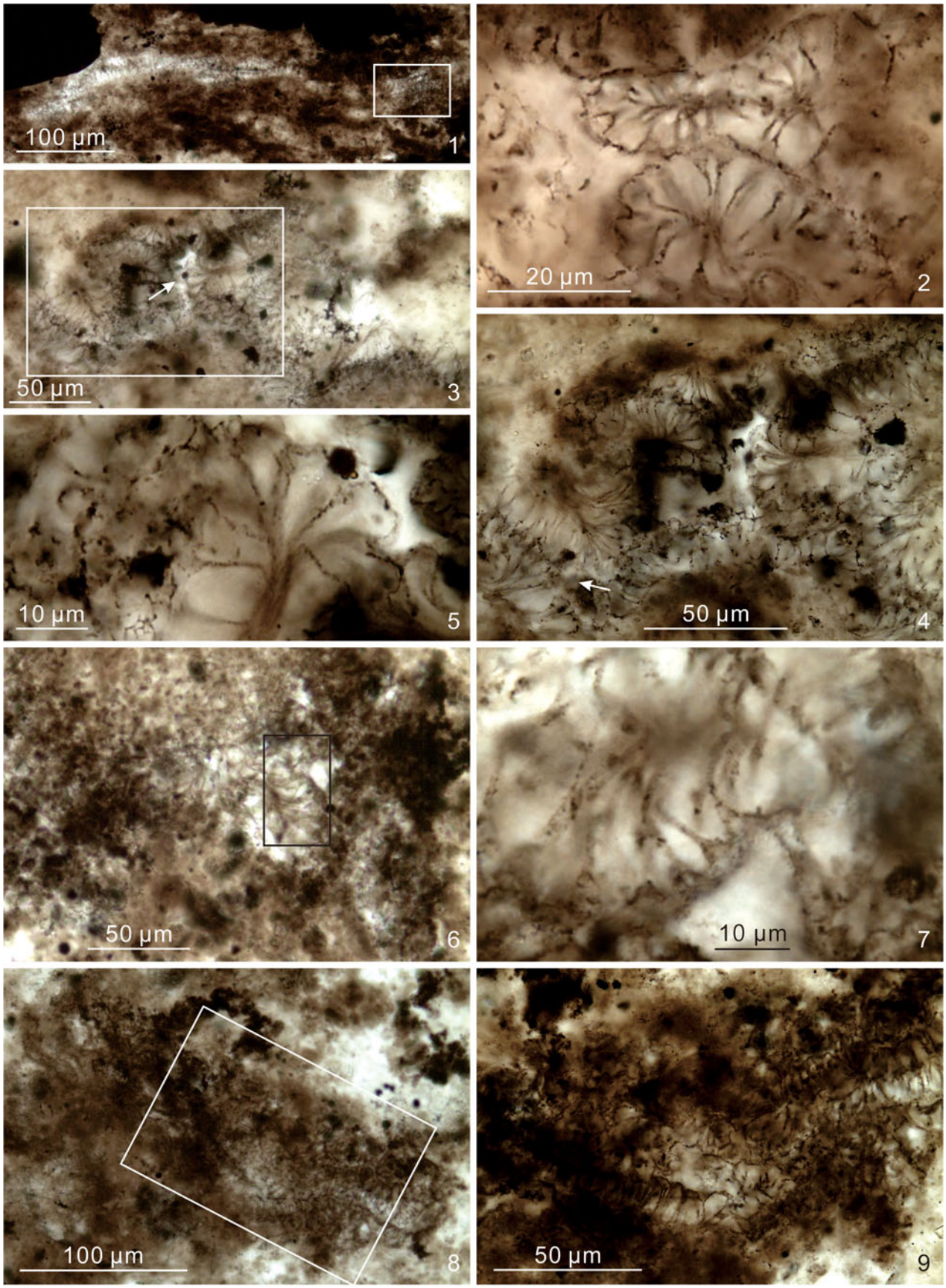

Figure 12. *Appendisphaera*? *hemisphaerica*. (**1, 2**) DH-14-67.0-A-2, 24.3 × 112.3, EF-D12, VPIGM-4845, rectangle in (**1**) marks area shown in (**2**) at a different focal level; (**3–5**) DH-14-68.0-B-2, 10.0 × 106.3, EF-T7-1, VPIGM-4865, rectangle and arrow in (**3**) mark areas shown in (**4**) and (**5**) (at a different focal level), respectively; (**6, 7**) S4-4-F2-5, 11.8 × 114.3, EF-Q14-4, VPIGM-4874, rectangle in (**6**) marks area shown in (**7**) at a different focal level; (**8, 9**) S4-4-F2-7, 13.2 × 108.5, EF-P8, VPIGM-4886, rectangle in (**8**) marks area shown in (**9**).

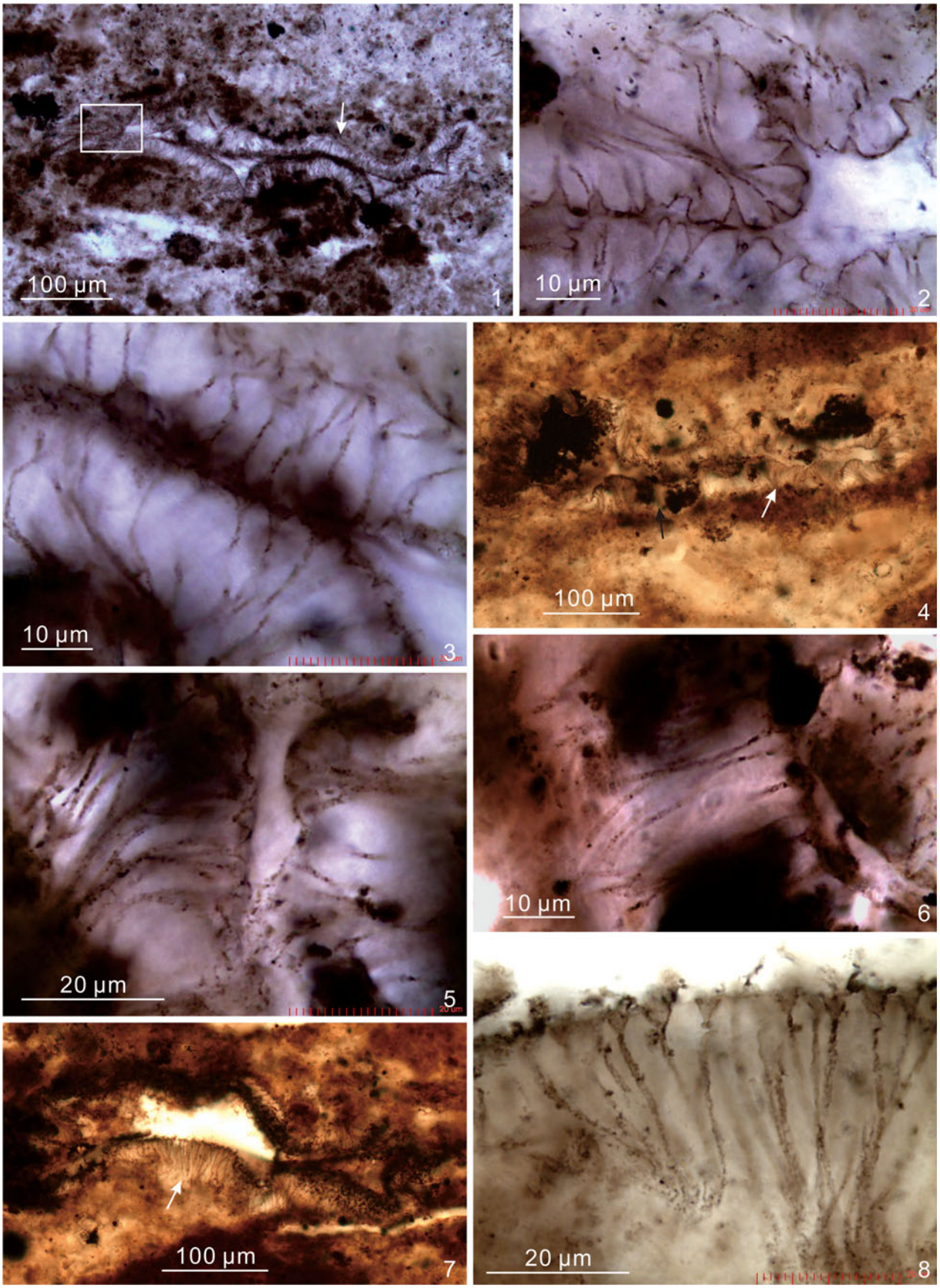

Figure 13. *Appendisphaera longispina*. (**1–3**) DH-14-67.0-C, 8.7 × 127.2, EF-T27, VPIGM-4850, rectangle and arrow in (**1**) mark areas shown in (**2, 3**), respectively, at different focal levels; (**4–6**) DH-14-67.0-C, 14.0 × 133.3, EF-N33-4, VPIGM-4849, white and black arrows in (**4**) mark areas shown in (**5, 6**), respectively, at different focal levels; (**7, 8**) DH-14-67.0-C-2, 18.7 × 133.2, EF-K33-1, VPIGM-4857, arrow in (**7**) marks area shown in (**8**).

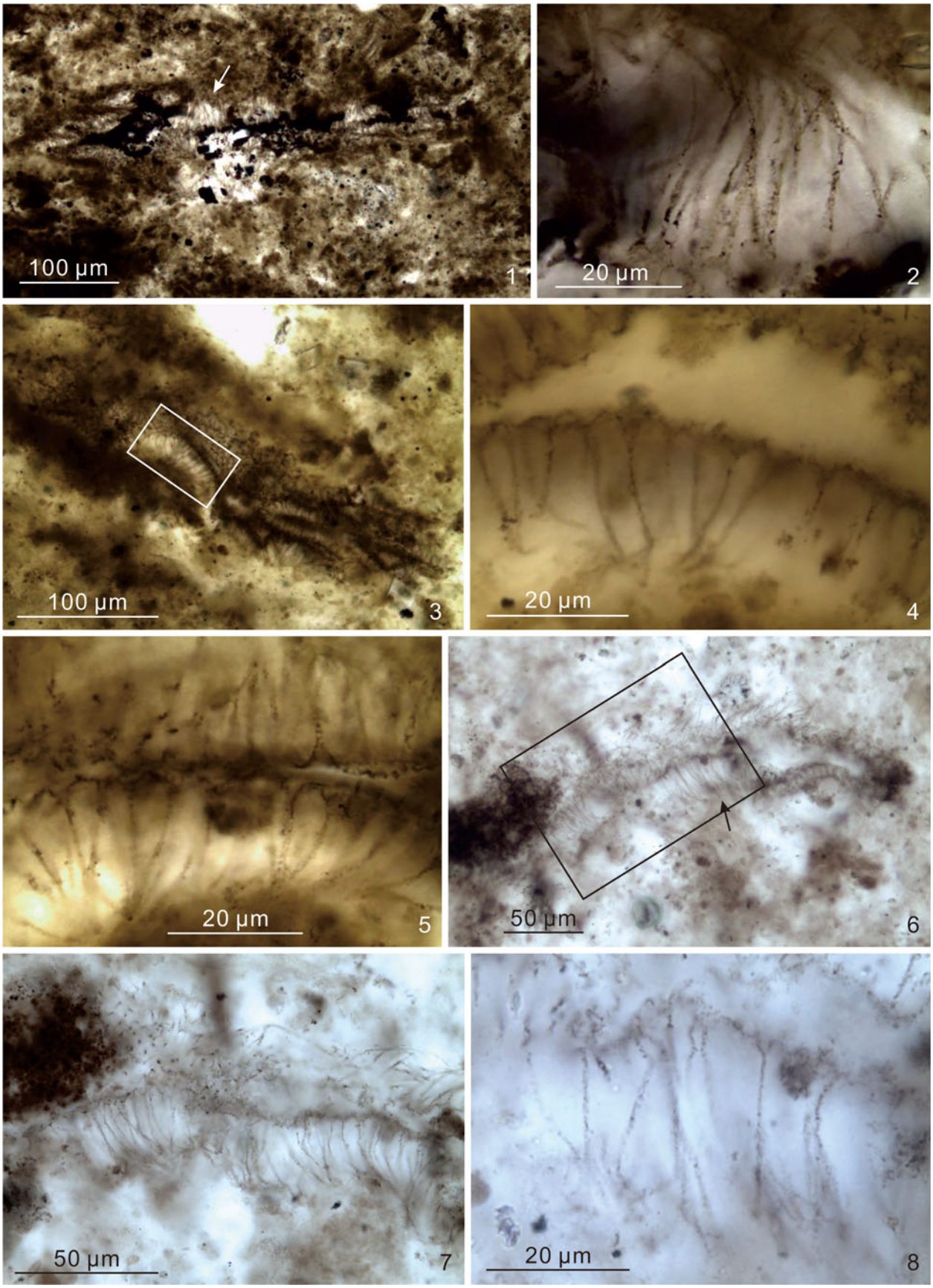

Figure 14. *Appendisphaera longispina*. (**1, 2**) DH-14-68.0-B, 11.5 × 140.1, EF-Q40-1, VPIGM-4864, arrow in (**1**) marks area shown in (**2**); (**3–5**) S4-4-F2-8-A, 17.3 × 109.6, EF-K9-4, VPIGM-4906, rectangle in (**3**) marks area shown in (**4, 5**) at two different focal levels; (**6–8**) S4-4-F2-15, 14.2 × 140.4, EF-O40, VPIGM-4900, rectangle and arrow in (**6**) mark areas shown in (**7, 8**), respectively, at different focal levels.

3–5 µm in width, and 2–5 µm in height. Apical spine thin and cylindrical, ~1 µm in width, and 19–30 µm in length.

Materials.—Six illustrated specimens (Figs. 13, 14) and 11 additional specimens.

Remarks.—*Appendisphaera longispina* is somewhat similar to *A. grandis* and *A.*? *hemisphaerica*. However, the basal expansion in *A. longispina* is more prominent than in *A. grandis*. Relative to *A.*? *hemisphaerica*, *A. longispina* has longer processes, a taller or longer basal expansion, and a more gradual transition from the basal expansion to the apical spine. The current specimens better fit the diagnosis of *A. longispina* than *A.*? *hemisphaerica*.

Following Liu and Moczydłowska (2019), specimens illustrated by Liu et al. (2014a) as *Appendisphaera crebra* (Zang in Zang and Walter, 1992) Liu et al., 2014 are transferred to *Appendisphaera longispina*.

Appendisphaera setosa Liu et al., 2014
Figures 15, 16

2014a *Appendisphaera setosa* Liu et al., p.31, figs. 21, 22, and synonyms therein.
2019 *Appendisphaera setosa*; Liu and Moczydłowska, p. 56, fig. 27.
2019 *Appendisphaera setosa*; Shang et al., p. 10, fig. 4E–J.
?2020 *Appendisphaera setosa*; Grazhdankin et al., fig. 3A.
2021 *Appendisphaera setosa*; Ouyang et al., fig. 11K, O.

Holotype.—IGCAGS–NPIII–592, reposited at Institute of Geology, Chinese Academy of Geological Sciences, from the upper member III of the Ediacaran Doushantuo Formation at Niuping section in the Yangtze Gorges area, Hubei Province, South China (Liu et al., 2014a, fig. 22.8, 22.9).

Occurrence.—Ediacaran of South China and northern India, and possibly early Cambrian of northern Siberia. South China: member II of the Doushantuo Formation at Jinguadun and Wuzhishan sections, Yangtze Gorges area, Hubei Province (Ouyang et al., 2021); member III of the Doushantuo Formation at Niuping and Wangfenggang sections (Liu et al., 2014a) as well as Baiguoyuan, Dishuiyan, and Chenjiayuanzi sections (Liu and Moczydłowska, 2019), Yangtze Gorges area, Hubei Province; Doushantuo Formation at Liujing section in Guizhou Province (Shang et al., 2019). Northern India: Ediacaran Krol A Formation in the Solan area (this paper). Possible occurrence in Siberia: upper Ediacaran or lower Cambrian Oppokun Formation, Khastakhskaya borehole, Lena-Anabar Basin, north-central Siberia (Grazhdankin et al., 2020).

Description and measurements.—Specimens assigned to this species are characterized by large vesicles and thin, cylindrical, hollow, homomorphic, evenly distributed, basally separate, and relatively straight processes that lack a basal expansion. Processes open to vesicle interior (Fig. 15.4), but the communication between hollow process and vesicle interior is often obscured by the accumulation of organic matter within the extremely thin processes. Vesicle diameter ~250 µm, as estimated from one completely preserved specimen (Fig. 15.1). Processes 19–29 µm in length (~11% of vesicle diameter, estimated from specimen in Fig. 15.1) and ~1.5 µm in diameter, ~9–12 processes per 100 µm of vesicle periphery, and process spacing 7–18 µm.

Materials.—Four illustrated specimens (Figs. 15, 16).

Remarks.—*Appendisphaera setosa* is somewhat similar to *A. tenuis* and *A. fragilis*. However, *A. tenuis* has relatively shorter and slightly conical processes. The holotype of *A. fragilis* is poorly preserved, with a small number of cylindrical processes covering a small area of the vesicle (Moczydłowska et al., 1993, text-fig. 6A, B). Although its process length (11–20 µm; Moczydłowska et al., 1993) is comparable to that of the holotype of *A. setosa* (16 µm; Liu et al., 2014a), the proportional process length is much greater in *A. fragilis* (16–19% of vesicle diameter; Moczydłowska, 2005) than in *A. setosa* (estimated ~10% of vesicle diameter; Liu et al., 2014a). On the other hand, specimens illustrated as *A. fragilis* in Shang et al. (2019) have much smaller proportional process length (e.g., 7–11% of vesicle diameter) relative to the holotype. Considering their relatively large vesicles and relatively straight processes, which are characteristic of *A. setosa*, the Krol A specimens are better placed in *A. setosa* than in *A. fragilis*.

A specimen illustrated as *Appendisphaera setosa* (Grazhdankin et al., 2020, fig. 3A) is similar to the holotype in vesicle size, process width, and absolute and proportional process length. However, some of its processes have a slightly expanded base. Thus, we regard its identification as *A. setosa* provisional. A possible alternative would be *A. tenuis*.

Appendisphaera tenuis Moczydłowska, Vidal, and Rudavskaya, 1993, emend. Moczydłowska, 2005
Figure 17

1993 *Appendisphaera tenuis* Moczydłowska et al., p. 506, text-fig. 7.
2005 *Appendisphaera tenuis*; emend. Moczydłowska, p. 296, fig. 5.
2014 *Appendisphaera grandis*; Shukla and Tiwari, p. 215, fig. 4D, E.
2016 *Appendisphaera grandis*; Sharma et al., fig. 4B.
2016 *Appendisphaera tenuis*; Prasad and Asher, p. 44, pl. 3, figs. 3–6.
2019 *Appendisphaera tenuis*; Liu and Moczydłowska, p. 61, figs. 29, 30, and synonyms therein.
2019 *Appendisphaera tenuis*; Anderson et al., p. 509, fig. 6H, I.
2019 *Appendisphaera tenuis*; Shang et al., p. 10, fig. 5.
2020 *Appendisphaera tenuis*; Shang and Liu, p. 157, fig. 5A, B.
2020 *Appendisphaera tenuis*; Vorob'Eva and Petrov, p. 370, pl. I, figs. 3, 4.
2021 *Appendisphaera tenuis*; Ouyang et al., fig. 11Q, R.

Holotype.—PMU-Sib.1-M/33, reposited at Uppsala University, from the Ediacaran Khamaka Formation, Zapad 742 borehole at

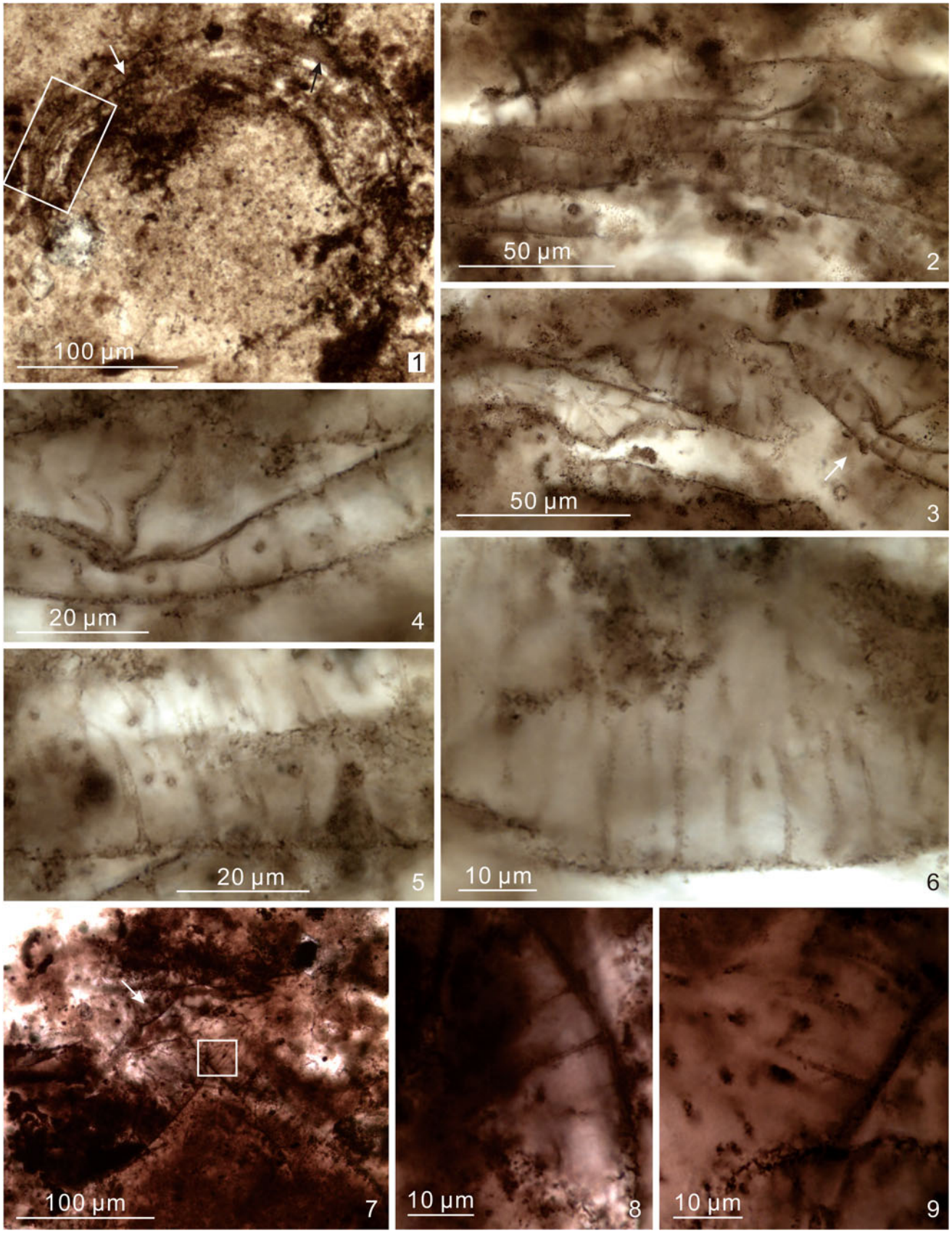

Figure 15. *Appendisphaera setosa*. (**1–6**) S4-4-F2-5, 19.4 × 131.9, EF-J32-1, VPIGM-4875, rectangle in (**1**) marks area shown in (**2, 3**) at different focal levels, white arrow in (**3**) marks area shown in (**4**), and white and black arrows in (**1**) mark areas shown in (**5, 6**), respectively; (**7–9**) DH-14-66.0-C-2, 11.9 × 117.3, EF-Q17-2, VPIGM-4841, arrow and rectangle in (**7**) mark areas shown in (**8, 9**), respectively, at a different focal level.

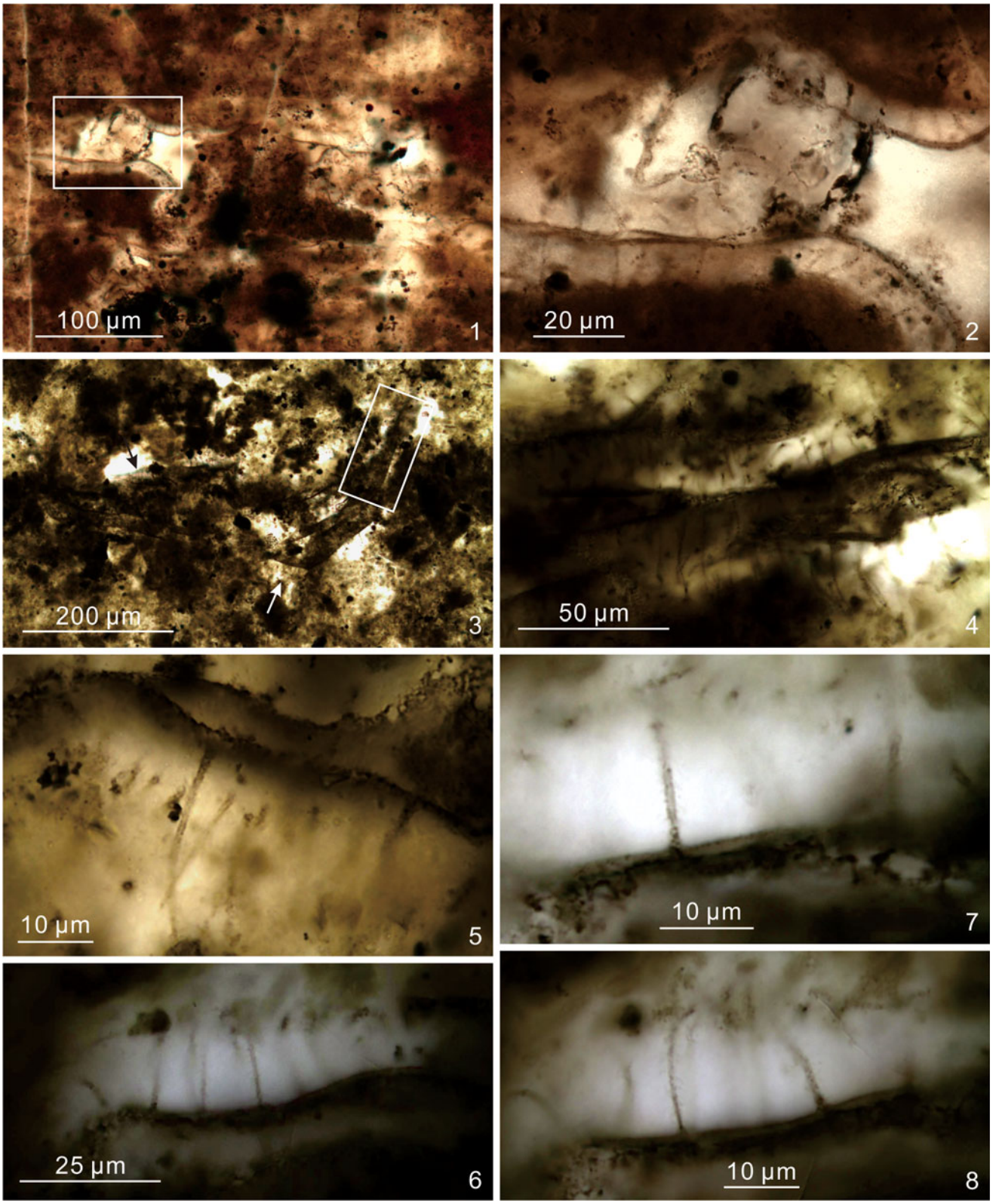

Figure 16. *Appendisphaera setosa*. (**1, 2**) DH-14-65.0-D, 11.6 × 140.6, EF-Q40-2, VPIGM-4837, rectangle in (**1**) marks area shown in (**2**); (**3–8**) S4-4-F2-18A, 21.5 × 133.2, EF-E33-3, VPIGM-4910, rectangle and white arrow in (**3**) mark areas shown in (**4, 5**), respectively; (**6–8**) show the same area indicated by the black arrow in (**3**) at different focal levels.

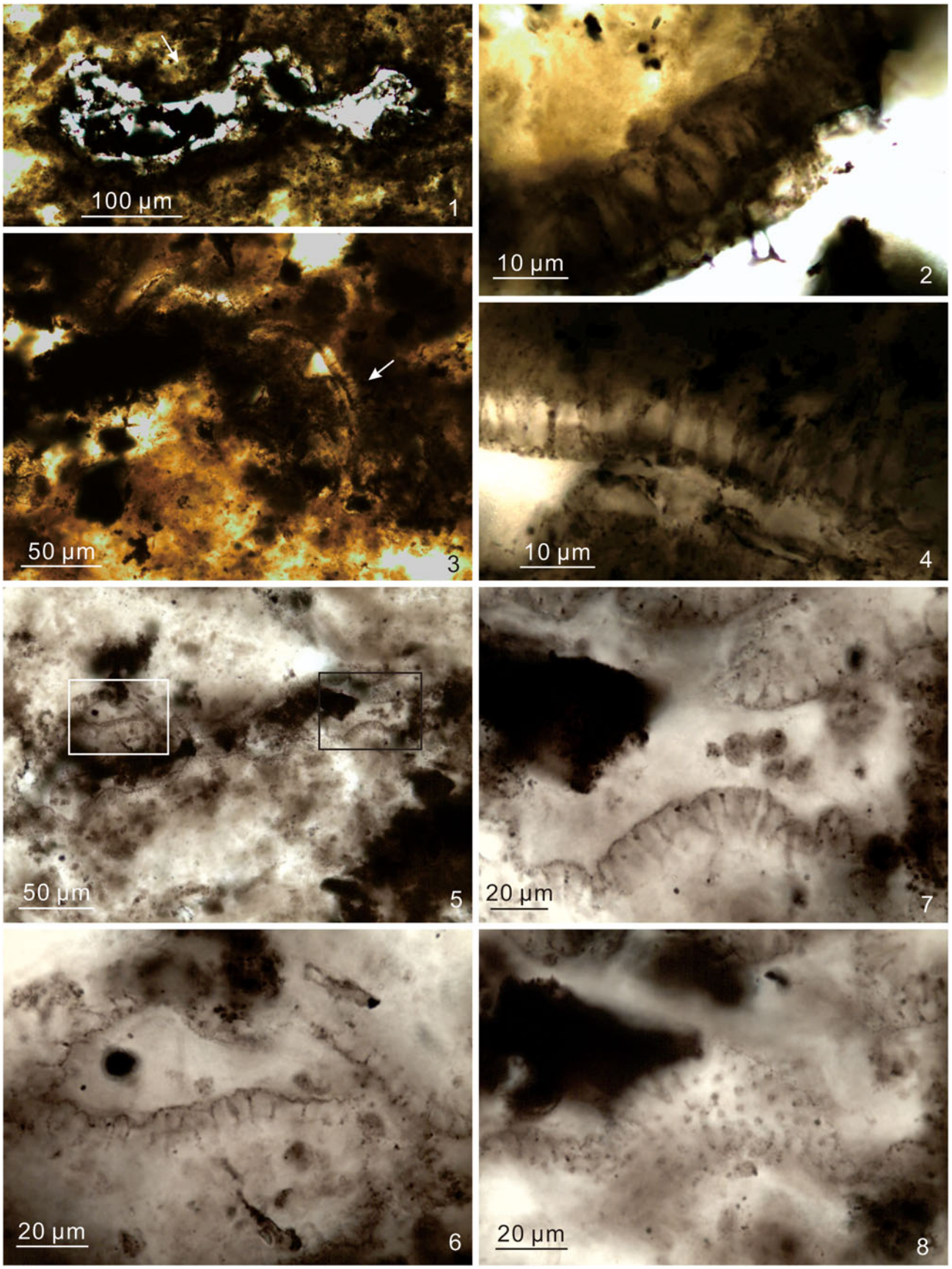

Figure 17. *Appendisphaera tenuis*. (**1, 2**) S4-4-F2-6-A, 9.3 × 110.7, EF-T10-2, VPIGM-4904, arrow in **1** marks area shown in (**2**); (**3, 4**) S4-4-F2-12-A, 12.0 × 142.8, EF-Q42-2, VPIGM-4907, arrow in (**3**) marks area shown in (**4**); (**5–8**) DH-14-67.0-C-2, 11.1 × 139.3, EF-Q39-4, VPIGM-4858, white and black rectangles in (**5**) mark areas magnified in (**6, 7**), respectively, and (**8**) illustrates the same area as (**7**) at a different focal level, showing the hollow nature of processes, as seen in transverse cross section.

a depth of 1887.0–1894.0 m, Nepa-Botuoba region, Yakutia, Siberian (Moczydłowska et al., 1993, p. 506, text-fig. 7).

Occurrence.—Ediacaran of South China, Siberia, Australia, and India (see Liu and Moczydłowska, 2019; Shang et al., 2019, for detailed occurrence information). *Appendisphaera tenuis* has been reported from the upper Khesen Formation at Urandush Uul in northern Mongolia (Anderson et al., 2017, 2019), which is regarded as terminal Ediacaran, although the uppermost Khesen Formation contains Cambrian-age detrital zircons (Anttila and Macdonald, 2020). It has also been reported from the Semri Group of the Lower Vindhyan Supergroup in the Chambal Valley of eastern Rajasthan of central-western India (Prasad and Asher, 2016). As discussed under *Appendisphaera grandis*, the Semri Group in central India is widely regarded as Paleo-/Mesoproterozoic in age (Rasmussen et al., 2002; Ray et al., 2002), and it is important to verify the occurrence of *Appendisphaera grandis* and *A. tenuis* in this unit.

Description and measurements.—Large vesicles with short, thin, hollow, slightly conical, evenly spaced, and basally separate processes. Vesicle ~265–364 µm in diameter (Fig. 17.1, 17.5; the specimen illustrated in Fig. 17.3 is poorly preserved, but has a medium-sized vesicle). Approximately 22–33 processes per 100 µm of vesicle periphery, process length 7–12 µm (or 2–3% of vesicle diameter), process spacing 2–4 µm at base, and process width 0.7–0.9 µm. Some processes in the specimen illustrated in Fig. 17.5–17.8 appear to have an expanded base (~2 µm wide and ~1.3 µm high), but this is an inconsistent feature (e.g., Fig. 17.6, 17.7) and seems an artifact resulting from degradation of the vesicle wall. Thus, we choose to place this specimen in *Appendisphaera tenuis* rather than *A. clava*.

Materials.—Three illustrated specimens (Fig. 17) and 33 additional specimens.

Remarks.—The Krol A specimens are identified as *Appendisphaera tenuis* based on their short, thin, hollow, and slightly conical processes, although they are larger in vesicle size than the holotype. *Appendisphaera tenuis* is similar to *A. clava* and *Cymatiosphaeroides forabilatus* in having relatively short processes. However, the processes of *A. clava* are more densely arranged and have a well-defined, albeit small basal expansion, and *C. forabilatus* has presumably solid processes that penetrate an outer membrane. Admittedly, when poorly preserved, these features can be difficult to discern. For example, strong degradation and displacement of organic matter by mineral recrystallization at the junction between cell wall and basal processes may give a false impression of a basal expansion, and hollow processes may appear solid due to accumulation of organic matter within the processes. In such cases, we depend on consistent process morphology and coherent preservation of organic walls to make a taxonomic decision, but even so, there are specimens that cannot be confidently assigned to one versus another species.

As discussed under *Appendisphaera grandis*, the two specimens illustrated as *A. grandis* in Shukla and Tiwari (2014) and in Sharma et al. (2016) have been re-assigned to *A. tenuis* because of their short processes (Liu and Moczydłowska, 2019). Also, as discussed under *Appendisphaera setosa*, a Cambrian acanthomorph identified as *A. setosa* (Grazhdankin et al., 2020, fig. 3A) may belong to *A. tenuis*, although a closer examination is needed to confirm or reject this suspicion.

Finally, specimens identified as *A. tenuis* from the Semri Group of the Lower Vindhyan Supergroup in the Chambal Valley of eastern Rajasthan of India (Prasad and Asher, 2016) have important biostratigraphic implications if the hosting rocks turn out to be Mesoproterozoic (Hughes, 2017). The Semri specimens have relatively smaller vesicles (50–80 µm in diameter) than the holotype of *A. tenuis* (115–148 µm in diameter; Moczydłowska et al., 1993), and as such, their relative process length (as a percentage of vesicle diameter) is greater, but they are otherwise similar to the holotype in process density and absolute process length. Perhaps both *A. grandis* and *A. tenuis* have extremely long stratigraphic ranges, from the Paleo–Mesoproterozoic (Prasad and Asher, 2016) to the terminal Ediacaran–Cambrian (Anderson et al., 2019; Grazhdankin et al., 2020).

Genus *Asterocapsoides* Yin and Li, 1978, emend. Xiao et al., 2014

Type species.—*Asterocapsoides sinensis* Yin and Li, 1978, emend. Xiao et al., 2014.

Other species.—*Asterocapsoides fluctuensis* Liu and Moczydłowska, 2019; *A. robustus* Xiao et al., 2014; *A. wenganensis* (Chen and Liu, 1986) Xiao et al., 2014.

Remarks.—In addition to the named species, several unnamed specimens of *Asterocapsoides* have been reported from Ediacaran deposits, including (1) *Asterocapsoides* sp. from the Infra-Krol Formation in the Solan area of the Lesser Himalaya, northern India (Tiwari and Knoll, 1994; Tiwari and Pant, 2004), which may be *A. wenganensis*; (2) *Asterocapsoides* sp. A and sp. B from the Krol A Formation in the Khanog and Rajgarh synclines of the Lesser Himalaya, northern India (Shukla and Tiwari, 2014), which have acutely conical processes (<10 µm in length) that are much shorter than those of existing species of *Asterocapsoides*; (3) *Asterocapsoides* sp. from the Doushantuo Formation at Baizhu of Hubei Province, South China (Yang et al., 2020), which resembles *A. wenganensis*, but has occasionally branching processes; (4) two specimens of *Asterocapsoides* sp. from the Doushantuo Formation at Chaoyang of Jiangxi Province, South China (Zhou et al., 2002), one of which has been assigned to *A. sinensis* by Xiao et al. (2014); and (5) two specimens of *Asterocapsoides* sp. from the Vychegda Formation at Keltma, Timan Ridge, East European Platform, Russia (Vorob'Eva et al., 2009), one of which may be *A. sinensis* (see Remarks under *A. sinensis*).

Asterocapsoides sinensis Yin and Li, 1978, emend. Xiao et al., 2014

Figure 18

1978 *Asterocapsoides sinensis* Yin and Li, p. 87, pl. 9, fig. 7.
?1992 *Asterocapsoides sinensis*; Knoll, p. 762, pl. 6, figs. 5, 6.
1998 *Asterocapsoides sinensis*; Zhang et al., p. 24, fig. 5.10 (neotype).
2002 *Asterocapsoides sinensis*; Yuan et al., p. 70, fig. 87.
2002 *Asterocapsoides* sp.; Zhou et al., pl. 2, fig. 6 (part).
?2004 *Asterocapsoides sinensis*; Tiwari and Pant, p. 10, fig. 5C–F.
2007 *Asterocapsoides sinensis*; Yin et al., pl. 13, fig. 1.
2009 *Asterocapsoides sinensis*; Liu et al., fig. 2g.
2009 *Asterocapsoides* sp.; Vorob'Eva et al., p. 175, fig. 7.10 (part).
?2012 *Asterocapsoides sinensis*; Sharma et al., fig. 4k, l.
2014 *Asterocapsoides sinensis*; Xiao et al., p. 11, fig. 5.1–5.3, and synonyms therein.
2014a *Asterocapsoides sinensis*; Liu et al., p. 31, fig. 24.1, 24.2.
2017 *Asterocapsoides sinensis*; Hawkins et al., fig. 8F.
?2021 *Asterocapsoides sinensis*; Sharma et al., fig. 9B, C.

Neotype.—The holotype designated by Yin and Li (1978) was damaged and a neotype was subsequently designated by Zhang et al. (1998). The neotype is reposited in the Nanjing Institute of Geology and Palaeontology (thin section R-19-3; Zhang et al., 1998, fig. 5.10).

Occurrence.—Ediacaran of South China, northern India, and Russia. South China: Doushantuo Formation at Tianzhushan, Changyang, Hubei Province (Yin and Li, 1978; Zhang et al., 1998); upper Doushantuo Formation at Chaoyang, Shangrao, Jiangxi Province (Zhou et al., 2002); Doushantuo Formation at Wangfenggang, Yangtze Gorges area, Hubei Province (Yin et al., 2007); member III of Doushantuo Formation at Wangfenggang and Niuping, Yangtze Gorges area, Hubei Province (Liu et al., 2014a); member II of Doushantuo Formation at Siduping, Hunan Province (Hawkins et al., 2017); lower Doushantuo Formation (equivalent to unit 4 at Weng'an or upper member II in the Yangtze Gorges area) at Wanjiagou section, Zhangcunping, Hubei Province (Liu et al., 2009); Doushantuo Formation at Weng'an, Guizhou Province (Yuan et al., 2002; Xiao et al., 2014). Northern India: Krol A Formation, Solan area (this paper).

Veis et al. (2006) and Vorob'Eva et al. (2006) mentioned the occurrence of *Asterocapsoides sinensis* in the Ediacaran Vychegda Formation in the Timan Ridge, East European Platform, Russia, but did not provide illustrations. Subsequently, Vorob'Eva et al. (2009) illustrated two specimens as *Asterocapsoides* sp., one of which, in our opinion, can be assigned to *A. sinensis* (see Remarks below). However, *A. sinensis* specimens from the Scotia Group of Svalbard (Knoll, 1992) and the Infra-Krol and Krol A formations in northern India (Tiwari and Pant, 2004; Sharma et al., 2012, 2021, fig. 9B) have acutely conical processes and their identification as *A. sinensis* remains uncertain (see Remarks below).

Description and measurements.—Large spheroidal vesicles with sparsely distributed processes open to vesicle interior. Processes conical, often obtuse, and basally separate from each other. An inner wall is present within the vesicle, and remnants of an outer membrane also may be present. Vesicle diameter 300–400 µm, only a few (<10) processes per circumferential view, process spacing 12 µm or more at base, process width ~30 µm at base, process length 20–40 µm (5–14% of vesicle diameter).

Materials.—Two poorly preserved specimens illustrated in Figure 18.

Remarks.—One could conceivably argue that the sparse processes in the specimens illustrated in Figure 18 may be deformation artifacts. Indeed, both specimens in our collection are deformed, particularly the inner wall. However, the processes on the vesicle wall do not coincide spatially with the deformation in the inner wall, leading us to favor the interpretation that the processes are biological structures rather than deformational folds of the vesicle wall. If our interpretation is correct, then the Krol A specimens best fit *Asterocapsoides sinensis* on the basis of their large vesicle size, the presence of an inner wall, as well as sparse, widely separate, and mostly obtusely conical processes.

Two specimens of *Asterocapsoides* sp. (Zhou et al., 2002, pl. 2, fig. 6; Vorob'Eva et al., 2009, fig. 7.10) from the Doushantuo Formation in South China and the Vychegda Formation in Russia also display these features, and thus can be regarded as *A. sinensis*. On the other hand, specimens of *A. sinensis* from the Infra-Krol Formation (Tiwari and Pant, 2004; Sharma et al., 2012) and Krol A Formation in northern India (Sharma et al., 2021, fig. 9B) have basally separate and acutely conical processes, as do specimens of *Asterocapsoides* sp. from the same formation (Tiwari and Knoll, 1994; Tiwari and Pant, 2004); these may be either *A. robustus* or *A. wenganensis*. One of the Krol A specimens illustrated as *A. sinensis* in Sharma et al. (2021, fig. 9C) is poorly preserved and does not exhibit diagnostic features of this species. Finally, the specimen illustrated as *A. sinensis* from the Scotia Group of Svalbard (Knoll, 1992) has sparsely distributed, basally separate, and acutely conical processes that seem to be divided internally by transverse septa; this specimen is akin to *A. wenganensis* or *Weissiella grandistella* Vorob'Eva et al., 2009, depending on future verification of the presence of transverse septa within processes.

Genus *Cavaspina* Moczydłowska, Vidal, and Rudavskaya, 1993

Type species.—*Cavaspina acuminata* (Kolosova, 1991) Moczydłowska, Vidal, and Rudavskaya, 1993.

Other species.—*Cavaspina basiconica* Moczydłowska, Vidal, and Rudavskaya, 1993; *C. conica* Liu and Moczydłowska, 2019; *C. uria* (Nagovitsin and Faizullin in Nagovitsin et al., 2004) Nagovitsin and Moczydłowska in Moczydłowska and Nagovitsin, 2012.

Remarks.—Liu and Moczydłowska (2019) regarded *Cavaspina amplitudinis* Willman in Willman and Moczydłowska, 2011, as a junior synonym of *Appendisphaera tenuis* Moczydłowska, Vidal, and Rudavskaya, 1993.

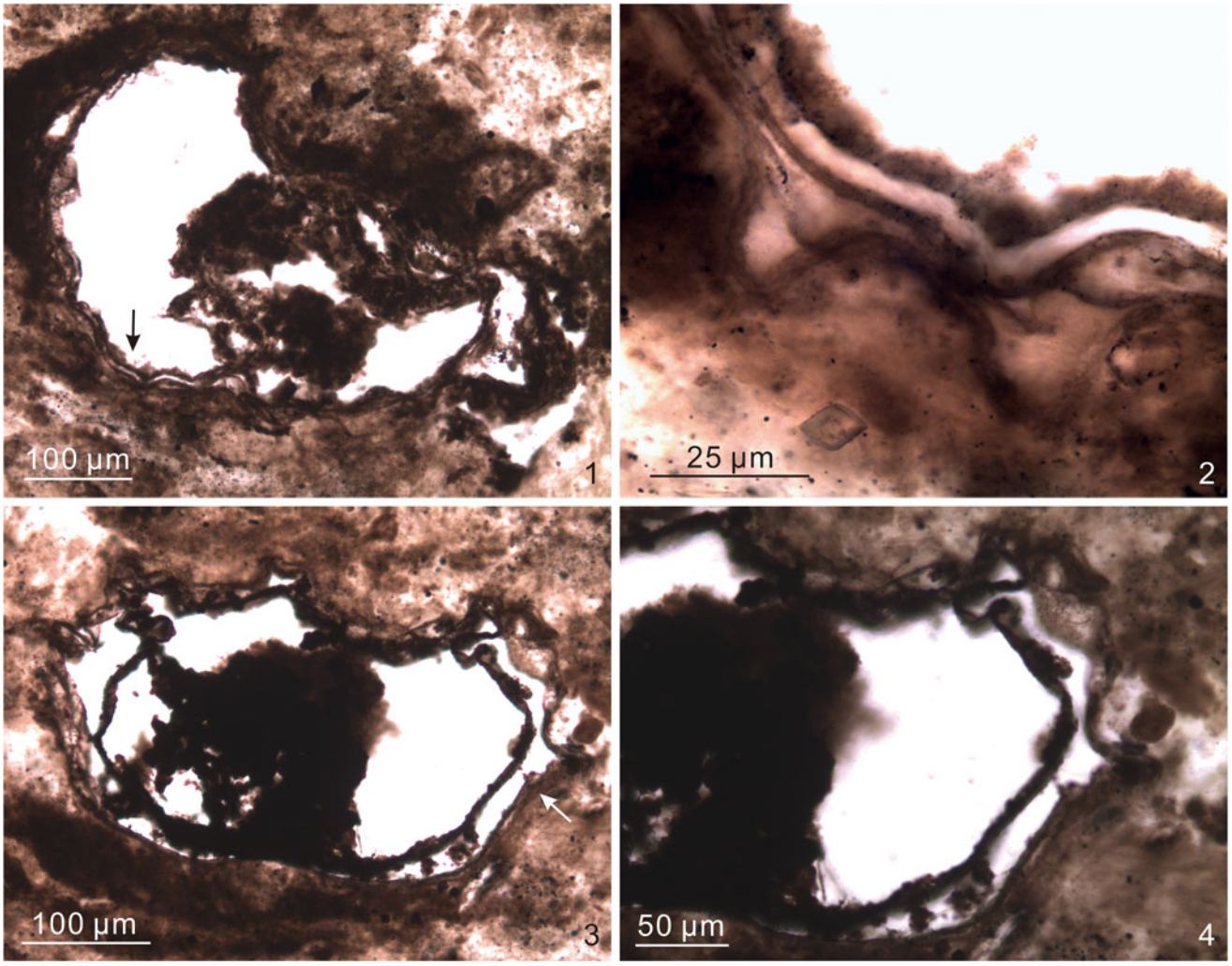

Figure 18. *Asterocapsoides sinensis*. (**1, 2**) DH-14-65.0-B, 14.3 × 134.6, EF-N34-4, VPIGM-4833, arrow in (**1**) marks area shown in (**2**) at a different focal level; (**3, 4**) DH-14-65.0-B, 15.8 × 132.0, EF-M31-2, VPIGM-4834, arrow in (**3**) marks area shown in (**4**).

Cavaspina tiwariae Xiao new species
Figure 19

2014 Unnamed Form A, Shukla and Tiwari, p. 219, fig. 6C, D.

Holotype.—VPIGM-4830, thin section DH-14-65.0-A, Olympus BX-51 coordinates 14.5 × 130.0, England Finder coordinates N30-1, illustrated in Figure 19, reposited in Museum of Geosciences at Virginia Tech, from Krol A Formation in Solan area, Lesser Himalaya, northern India.

Diagnosis.—A species of *Cavaspina* with a medium-sized vesicle bearing sparse, deflated, and obtusely conical processes.

Occurrence.—Thus far only known from the Ediacaran Krol A Formation in the Solan area, Lesser Himalaya, northern India (Shukla and Tiwari, 2014; this paper).

Description and measurements.—Medium-sized spherical vesicles with sparsely distributed and widely separate processes that are short, deflated, obtusely conical, and open to vesicle interior. The transition from processes to vesicle wall is gradual. Vesicle diameter ~150 µm, fewer than 20 processes per circumferential view, process spacing 19–28 µm at apex (spacing at base is difficult to measure because the transition from processes to vesicle wall is gradual), process width up to 8 µm at base, process length up to 5 µm (~3% of vesicle diameter).

Etymology.—In honor of Dr. Meera Tiwari, who pioneered the study of microfossils from the Infra-Krol and Krol A formations in the Lesser Himalaya and published a specimen that is here regarded as conspecific to this new species (Shukla and Tiwari, 2014, fig. 6C, D).

Material.—One illustrated specimen, the holotype (Fig. 19) and a previously published specimen from the Krol A Formation in the Solan area (Shukla and Tiwari, 2014, fig. 6C, D).

Remarks.—The specimen illustrated here is somewhat similar to *Asterocapsoides sinensis* (Fig. 18) in its sparsely distributed, relatively short, and obtusely conical processes. However, it

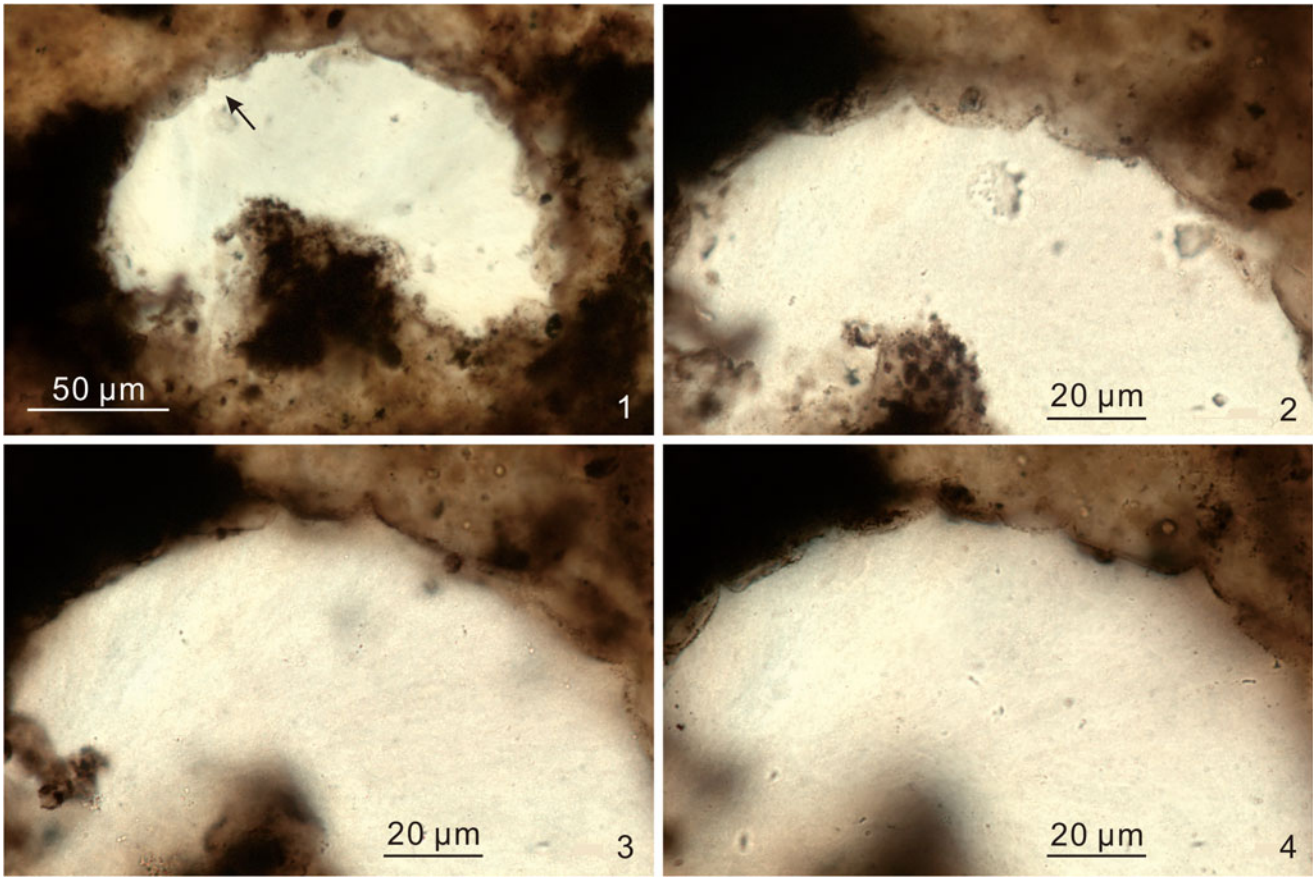

Figure 19. *Cavaspina tiwariae* Xiao new species. (**1–4**) Holotype, DH-14-65.0-A, 14.5 × 130.0, EF-N30-1, VPIGM-4830, (**2–4**) show the same area indicated by the arrow in (**1**) at different focal levels.

can be distinguished by its deflated processes, much smaller vesicle size, and the lack of an inner wall and an outer wall, which are thought to be diagnostic of *A. sinensis* (Liu and Moczydłowska, 2019), although Xiao et al. (2014) pointed out that these additional walls (particularly the inner wall) could be lost during diagenesis. This specimen is also similar to *Polygonium* sp. of Liu et al. (2014a) in its sparsely distributed processes that gradually transition at base to vesicle wall, but its processes are much smaller than those of the latter species. It better fits the genus *Cavaspina*, which is characterized by relatively short and sparsely distributed processes that are generally conical in shape (Moczydłowska et al., 1993). In particular, it is similar to the type species of *Cavaspina*, *C. acuminata*, in its sparsely distributed, relatively short, and conical processes. However, the Krol A specimen can be differentiated by its larger vesicle as well as its deflated and obtusely conical processes, which are distinct from the acutely conical processes (1 μm wide and 3–5 μm long) of *C. acuminata*. The Krol A specimen is also somewhat similar to *Cavaspina uria* in process size, but the latter species has a smaller vesicle size (80–130 μm), acutely conical processes (5–11 μm long and 4–12 μm wide at base), and more closely spaced processes (>15 processes in circumferential view; estimated from Moczydłowska and Nagovitsin, 2012, fig. 4G, I). More importantly, the processes of *C. uria* are not deflated. Thus, a new species is erected here on the basis the specimen illustrated in Figure 19 and a morphologically similar specimen previously published from the same stratigraphic unit in the same area (Shukla and Tiwari, 2014).

Genus *Cymatiosphaeroides* Knoll, 1984, emend. Shang et al., 2019

Type species.—*Cymatiosphaeroides kullingii* Knoll, 1984, emend. Shang et al., 2019

Other species.—*Cymatiosphaeroides forabilatus* Liu and Moczydłowska, 2019; *C. yinii* Yuan and Hofmann, 1998.

Remarks.—*Cymatiosphaeroides dilutopilum* Zang in Zang and Walter (1992) and *C. pilatopilum* Zang in Zang and Walter (1992) were synonymized and transferred to *Appendisphaera dilutopila* (Zang in Zang and Walter, 1992) Grey, 2005, although some non-holotype specimens illustrated in Zang and Walter (1992) as *C. dilutopilum* and *C. pilatopilum* have been reassigned by Grey (2005) to *Appendisphaera barbata* and *Knollisphaeridium triangulum* (Zang in Zang and Walter, 1992) Willman and Moczydłowska, 2008, respectively. More recently, Liu and Moczydłowska (2019, p. 61) considered *Appendisphaera dilutopila* as a synonym of *Appendisphaera tabifica*.

The genus *Cymatiosphaeroides* was originally diagnosed as a double-walled acanthomorph with thin and solid processes

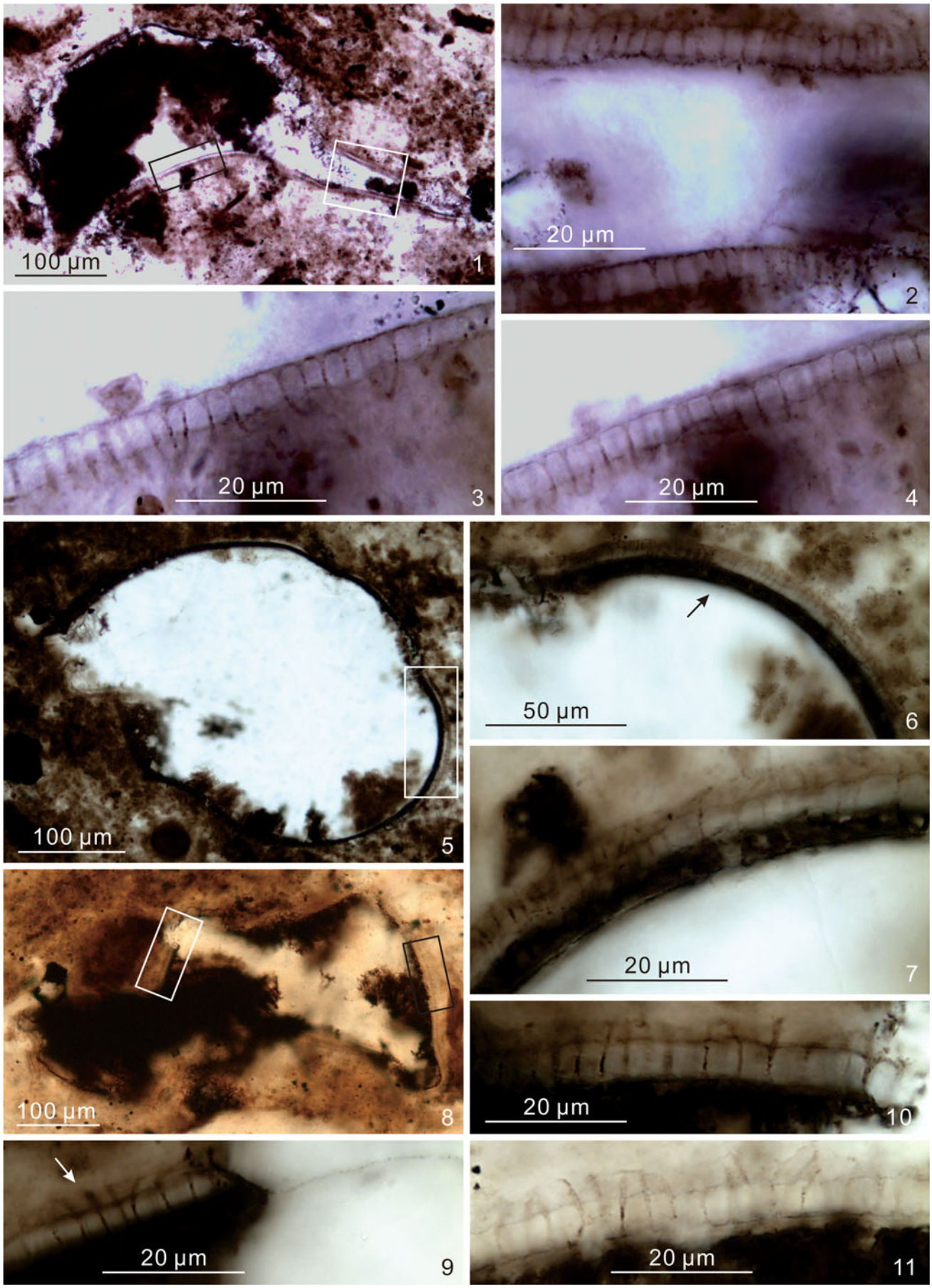

Figure 20. *Cymatiosphaeroides forabilatus*. (**1–4**) DH-14-67.0-C, 11.8 × 139.0, EF-Q39-1, VPIGM-4848, white rectangle in (**1**) marks area shown in (**2**) at a different focal level, and black rectangle in (**1**) marks area shown in (**3, 4**) at two different focal levels; (**5–7**) DH-14-67.0-C-2, 12.0 × 135.9, EF-Q36-3, VPIGM-4852, rectangle in (**5**) marks area shown in (**6**) at a different focal level, and arrow in (**6**) marks area shown in (**7**) at a different focal level and with a rotation; (**8–11**) DH-14-67.0-C-2, 15.2 × 137.3, EF-N37, VPIGM-4854, white and black rectangles in (**8**) mark areas shown in (**9**) and (**11**), respectively, and arrow in (**9**) marks area magnified in (**10**).

arising from the inner wall and supporting the outer wall (Knoll, 1984). It was later emended to emphasize that the outer wall can be a single-layered or multilamellate structure (Knoll et al., 1991). The diagnosis was recently emended again by Shang et al. (2019), who diagnosed the genus *Cymatiosphaeroides* as a double-walled acanthomorph with thin, hollow, and cylindrical processes. It remains to be verified whether the holotype of the type species, *C. kullingii*, has hollow processes; this feature cannot be determined with confidence from the published illustrations (Knoll, 1984, fig. 9A, B) because the processes are extremely thin (~1 μm in width). Nonetheless, we follow the emendation of Shang et al. (2019) so that *C. forabilatus*, which has hollow processes (see below), can be included in the genus *Cymatiosphaeroides*.

The genus *Cymatiosphaeroides* and its type species, *C. kullingii*, have extremely long stratigraphic distributions. The oldest known occurrences of *C. kullingii* are from the ~1.6 Ga Chitrakoot Formation in the Vindhyan Basin, central India (Anbarasu, 2001; Singh and Sharma, 2014). Specimens identified as *Shuiyousphaeridium echinulatum* Yin and Gao, 1999, from the Chitrakoot Formation (Singh and Sharma, 2014) have been reassigned to *C. kullingii* by Liu and Moczydłowska (2019). Examples of Tonian *C. kullingii* are from the Svanbergfjellet and Draken formations of the Akademikerbreen Group in northeastern Svalbard (Knoll et al., 1991; Butterfield et al., 1994), the Fifteenmile Group in Northwest Canada (Allison and Awramik, 1989), and the Chuar Group in the Grand Canyon of the western U.S. (Vidal and Ford, 1985). Examples of Ediacaran *Cymatiosphaeroides* include *C. kullingii* from the Doushantuo Formation in South China (see Liu and Moczydłowska, 2019, for details).

Cymatiosphaeroides forabilatus Liu and Moczydłowska, 2019, emend. Shang et al., 2019
Figures 20–22

1992 Form B, Tiwari and Azmi, p. 390, pl. 1, fig. 15.
1994 *Ericiasphaera spjeldnaesii* Vidal, 1990; Tiwari and Knoll, p. 198, pl. 1, fig. 1 (part).
1994 Unclassified acanthomorphic acritarch; Tiwari and Knoll, p. 198, pl. 1, fig. 6.
2014 Unnamed Form E; Shukla and Tiwari, p. 222, fig. 7E–G.
2019 *Cymatiosphaeroides forabilatus* Liu and Moczydłowska, p. 81, fig. 41.
2019 *Cymatiosphaeroides forabilatus*; emend. Shang et al., p. 22, figs. 9, 10A–C.

Holotype.—IGCAGS–D2XFH212, thin section XFH0946-1-10, reposited at the Institute of Geology, Chinese Academy of Geological Sciences, from member II of the Ediacaran Doushantuo Formation at Xiaofenghe section in the Yangtze Gorges area, Hubei Province, South China (Liu and Moczydłowska, 2019, fig. 41A, B).

Occurrence.—Ediacaran of South China and northern India. South China: member II of Doushantuo Formation at northern and southern Xiaofenghe sections, Yangtze Gorges area, Hubei Province (Liu and Moczydłowska, 2019); Doushantuo Formation at Liujing section in Guizhou Province (Shang et al., 2019). Northern India: Krol A Formation, Solan area (this paper).

Description and measurements.—Large double-walled spheroidal vesicles with densely and evenly distributed processes. Processes arise from the inner wall and penetrate the outer wall. They are thin, short, uniform in length, and basally separate. Processes are apparently solid at the distal end, but many of them are hollow at least at the base, with a small basal expansion tapering distally toward a thin filament (e.g., Fig. 20.2–20.4). Vesicle diameter ~315–430 μm (estimated from Fig. 20.1, 20.5, 20.8), 28–41 processes per 100 μm of vesicle periphery, process length 6–10 μm (~1.5–2.4% of vesicle diameter), process spacing 1–3 μm at base, basal expansion (when discernable) 1–2 μm wide at base and 1–2 μm in height, apical spine ~0.5–0.9 μm wide and 5–7 μm long. Inner and outer walls ~5 μm apart.

Materials.—Ten illustrated specimens (Figs. 20–22) and 21 additional specimens.

Remarks.—The Krol A specimens are identified as *Cymatiosphaeroides forabilatus* based on their double-walled vesicles that bear processes arising from the inner wall and penetrating the outer wall. Processes are extremely thin and it is difficult to determine whether they are solid or hollow. However, in several better-preserved specimens, it can be seen that the processes have a small basal expansion and is hollow at least at the basal part (e.g., Fig. 20.2–20.4). Shang et al. (2019) also noted that the processes of *C. forabilatus* are "slightly widened at the bases" in some specimens and that they are hollow in nature.

The specimen illustrated in Figure 22.8–22.10 is strongly degraded and obscured by the accumulation of organic matter. Nonetheless, remnants of processes extruding beyond the outer wall can be seen in the upper left of Figure 22.10. Thus, we regard this specimen as a poorly preserved example of *C. forabilatus*.

In sharp contrast to *Cymatiosphaeroides kullingii*, which has an extremely long stratigraphic range, *C. forabilatus* is restricted to the Ediacaran based on biostratigraphic data available thus far. Indeed, this is one of the common species in the Ediacaran Doushantuo Formation in South China and Infra-Krol–Krol A formations in northern India. Several previously published specimens from the Infra-Krol–Krol A formations are characterized by large double-walled vesicles with thin processes arising from the inner wall and penetrating the outer wall. These specimens are similar to the specimens described here in

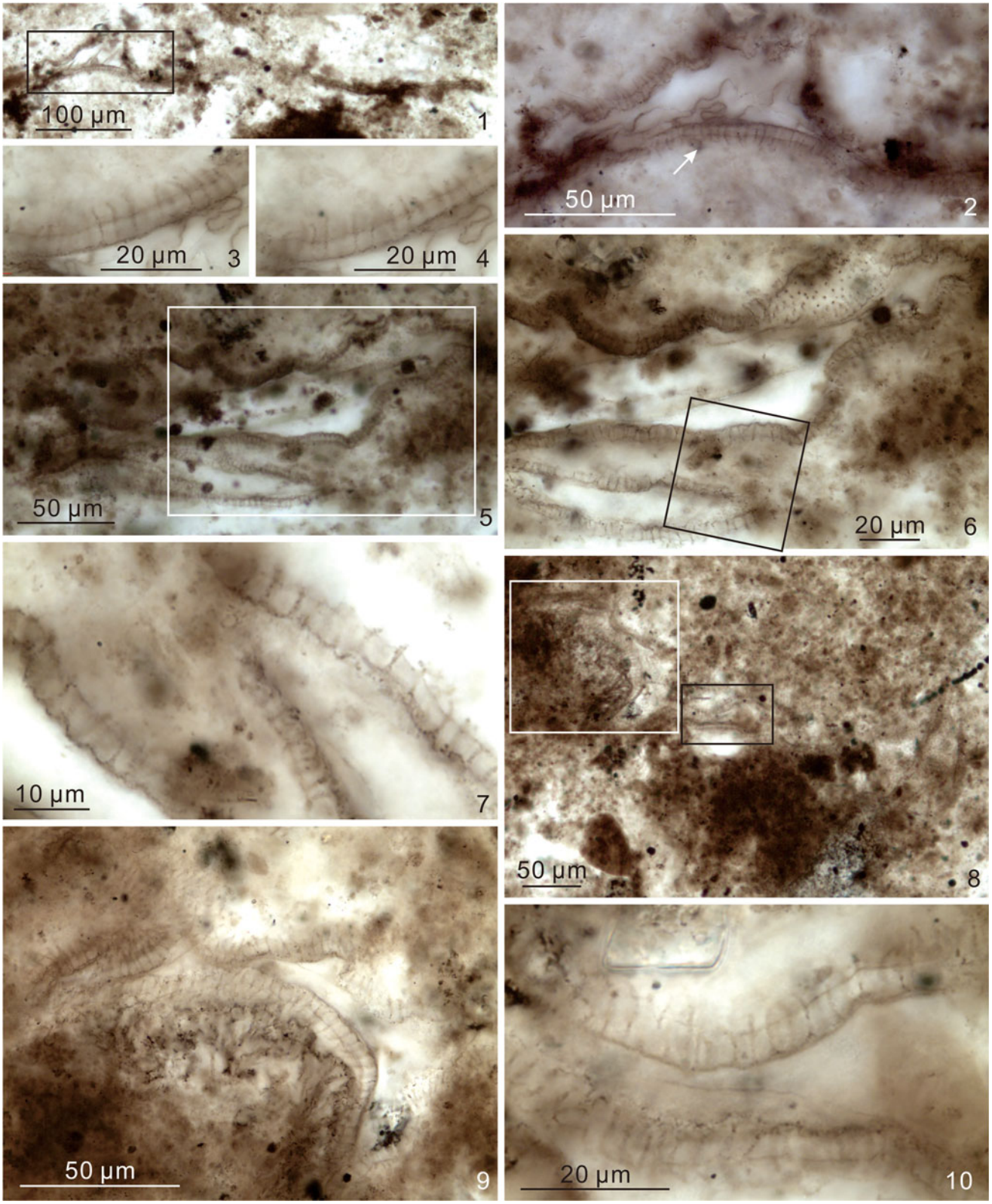

Figure 21. *Cymatiosphaeroides forabilatus*. (**1–4**) DH-14-67.0-B-2, 12.5 × 136.7, EF-P37-3, VPIGM-4846, rectangle in (**1**) marks area shown in (**2**), and arrow in (**2**) marks area shown in (**3, 4**) at different focal levels; (**5–7**) DH-14-67.0-C-2, 15.3 × 137.7, EF-M37-3, VPIGM-4855, rectangles in (**5, 6**) mark areas shown in (**6, 7**), respectively; (**8–10**) S4-4-F2-5, 8.4 × 128.8, EF-U29-1, VPIGM-4876, white and black rectangles in (**8**) mark areas shown in (**9, 10**), respectively, at a different focal levels.

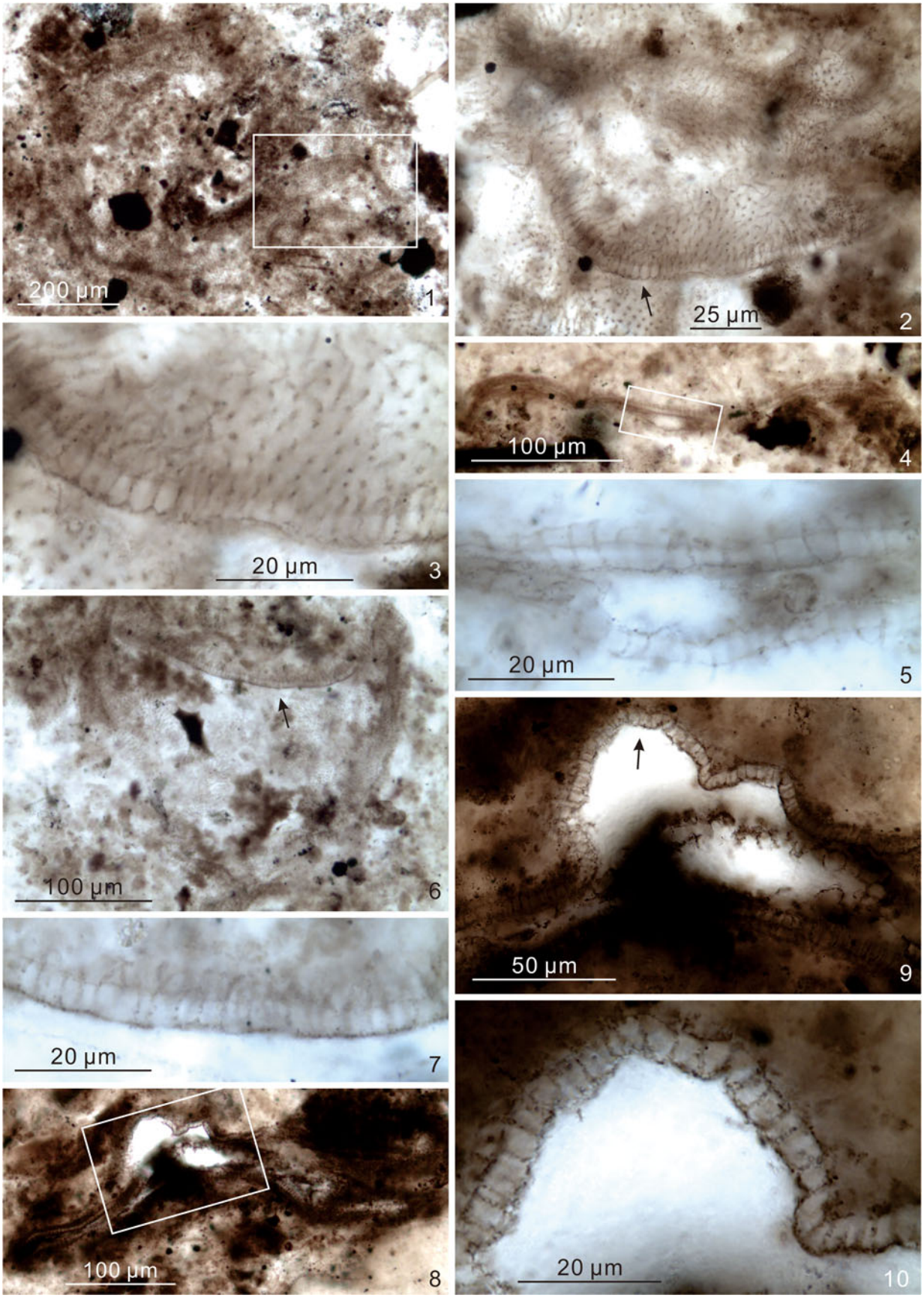

Figure 22. *Cymatiosphaeroides forabilatus*. (**1–3**) S4-4-F2-15, 10.3 × 129.7, EF-S30-1, VPIGM-4898, rectangle in (**1**) marks area shown in (**2**) with 180° rotation, and arrow in (**2**) marks area shown in (**3**); (**4, 5**) S4-4-F2-15, 22.3 × 106.4, EF-F6, VPIGM-4902, rectangle in (**4**) marks area shown in (**5**); (**6, 7**) S4-4-F2-14, 22.8 × 134.7, EF-E34-4, VPIGM-4897, arrow in (**6**) marks area shown in (**7**); (**8–10**) S4-4-F2-9, 16.4 × 135.5, EF-M35, VPIGM-4895, rectangle in (**8**) marks area shown in (**9**), and arrow in (**9**) marks area shown in (**10**).

vesicle size, process length and width, and spacing between double walls, and some of them have a small expansion at the base of the processes (e.g., Shukla and Tiwari, 2014). These specimens include (1) Form B in Tiwari and Azmi (1992), which was subsequently described as *Ericiasphaera spjeldnaesii* in Tiwari and Knoll (1994); (2) Unclassified acanthomorphic acritarch in Tiwari and Knoll (1994), which was later assigned to *Tianzhushania spinosa* (Zhang et al., 1998); and (3) Unnamed Form E of Shukla and Tiwari (2014). These specimens are here considered to be *Cymatiosphaeroides forabilatus*. Additionally, specimens illustrated as *Tianzhushania spinosa* (Shukla et al., 2008, pl. 3, figs. 1, 2) and *Echinosphaeridium maximum* (Shukla et al., 2008, pl. 2, figs. 13, 14) appear to have double-walled vesicles bearing processes that arise on the inner wall and penetrate the outer wall; these may also be *C. forabilatus*, but further examination is needed to verify this suspicion because the specimens are poorly preserved.

Genus *Dictyotidium* Eisenack, 1955, emend. Staplin, 1961

Type species.—*Dictyotidium dictyotum* Eisenack, 1955

Other species.—Two additional species have been reported from the Precambrian: *Dictyotidium fullerene* Butterfield in Butterfield et al. (1994) from the Tonian Algal Dolomite Member of the Svanbergfjellet Formation at Geerabukta of Spitsbergen, and *Dictyotidium ambonum* Zang in Zang and Walter (1992) from the Ediacaran Pertatataka Formation at Rodinga 4 drill core in Amadeus Basin, central Australia. Other species are listed in Eisenack et al. (1979) and Fensome et al. (1990).

Dictyotidium grazhdankinii Xiao new species
Figure 23

Holotype.—VPIGM-4832, thin section DH-14-65.0-A-2, Olympus BX-51 coordinates 10.6 × 108.8, England Finder coordinates R9-3, illustrated in Figure 23.1–23.5, reposited in Museum of Geosciences at Virginia Tech, from Krol A Formation in Solan area, Lesser Himalaya, northern India.

Diagnosis.—A species of *Dictyotidium* with a delicate network consisting of polygonal reticular fields that are 1–5 μm in dimension and defined by thin ridges 0.2–1.0 μm in thickness. No processes are present.

Occurrence.—Ediacaran Krol A Formation in the Solan area, Lesser Himalaya, northern India (this paper).

Description and measurements.—Medium-sized to large vesicles consisting of a reticulate framework with apparent absence of a continuous vesicle wall. Vesicle diameter 100–400 μm (holotype 120 μm, Fig. 23.1). Polygonal fields 1–5 μm in size (2–4 μm in holotype, Fig. 23.2–23.5). Ridges 0.2–1.0 μm in thickness (0.2–0.4 μm in holotype, Fig. 23.5).

Etymology.—In recognition of Dr. Dmitriy Grazhdankin's contributions to Ediacaran paleontology and his service to the Ediacaran Subcommission.

Materials.—Two illustrated specimens (Fig. 23). Additionally, there are as many as 30 poorly preserved specimens that may be this species, although some of them may simply be degraded sphaeromorphs.

Remarks.—One may argue that the reticulate pattern of the Krol A specimens is a result of degradation or taphonomic alteration of the vesicle wall. For example, recrystallization of quartz crystals may displace and concentrate organic residues along crystal interfaces to form polygonal crystal rings (Brasier et al., 2006). There is no doubt that Krol A fossils have been subjected to taphonomic processes, including alteration related to crystal growth. This can be seen in numerous cases of discontinuous carbonaceous particles that outline microfossil structures (e.g., processes of *Appendisphaera*? *hemisphaerica*, Fig. 8.10). However, close examination of the best-preserved specimens, here identified as *Dictyotidium grazhdankinii* Xiao n. sp., led us to believe that their reticulate pattern is not a taphonomic artifact. First, observation under cross-polarized light microscopy shows that the fossils are replicated by microcrystalline silica and the reticulate pattern does not match any crystal extinction pattern when observed under crossed nicols. Second, microscopic observation by adjusting the focal level confirms that the organic ridges are one-dimensional thread-like structures that are relatively continuous, uniform in thickness, and weaved into a reticulate sheet (Fig. 23.2–23.4). Importantly, when the fossil is deformed, the reticulate sheet is also folded accordingly, without any disruption of the reticulate pattern (Fig. 23.2–23.4). These observations are in sharp contrast to polygonal crystal rings (Brasier et al., 2006) that form three-dimensional spongy networks consisting of discontinuous carbonaceous particles distributed along crystal interfaces and often are concentrated at multi-crystal junctions (where incongruent crystal morphologies result in open space where organic matter accumulates). Thus, for the best-preserved specimens (e.g., Fig. 23.1–23.5), the regular reticulate morphology is unlikely a taphonomic artifact. In some specimens, parts of the vesicle show a regular reticulate sheet, whereas the other parts have more degraded patterns (e.g., Fig. 23.6, 23.7); these are interpreted as *Dictyotidium grazhdankinii* Xiao n. sp. specimens that have been unevenly altered by taphonomic processes.

Herkomorphs are acritarchs with their vesicle walls divided into polygonal fields. Examples include *Cymatiosphaera* Wetzel, 1933; *Dictyosphaera* Xing and Liu, 1973; *Dictyosphaeridium* Wetzel, 1952; and *Dictyotidium* Eisenack, 1955. In *Cymatiosphaera*, the polygonal fields are defined by fence-like structures perpendicular to the vesicle wall, thus distinct from the reticulate ridges in the Krol A specimens. In the other three genera, the polygonal fields are defined by ridges on the vesicle wall (typically manifested as polygonal platelets in *Dictyosphaera*; Agić et al., 2015). However, *Dictyosphaeridium* bears processes, and *Dictyosphaera* may represent a different ontogenetic stage of the acanthomorphic herkomorph *Shuiyousphaeridium* Yan in Yan and Zhu, 1992 (Xiao et al., 1997; Agić et al., 2015). Thus, given its lack of processes, the Krol A specimens are best referred to the genus *Dictyotidium*.

Dictyotidium grazhdankinii Xiao n. sp. can be distinguished from the other Ediacaran species of *Dictyotidium*

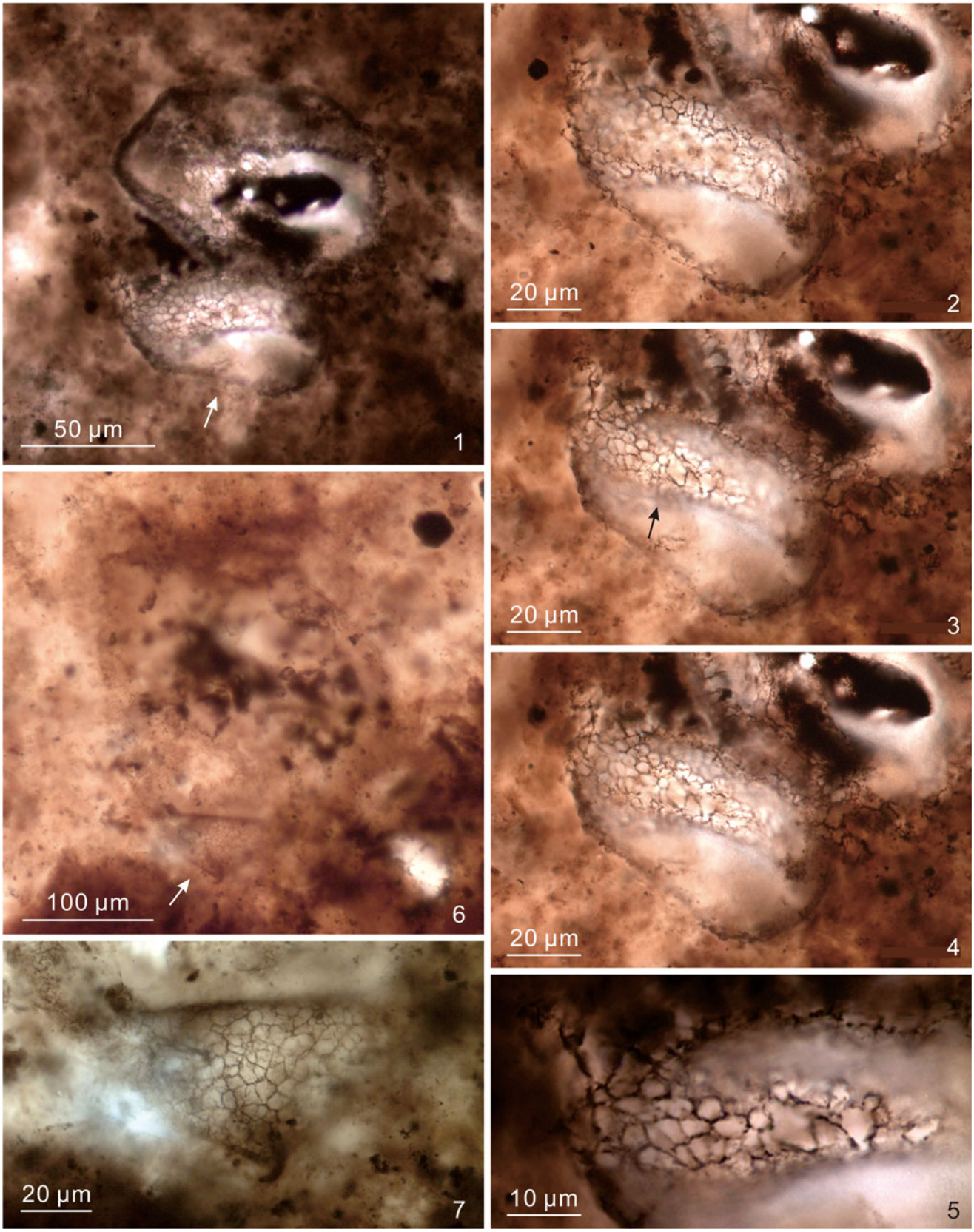

Figure 23. *Dictyotidium grazhdankinii* Xiao new species. (**1–5**) Holotype, DH-14-65.0-A-2, 10.6 × 108.8, EF-R9-3, VPIGM-4832, arrow in (**1**) marks area shown in (**2–4**) at different focal levels, and arrow in (**3**) marks area magnified in (**5**); (**6, 7**) S4-4-F2-5-2, 11.9 × 128.5, EF-Q28-4, VPIGM-4881, arrow in (**6**) marks area magnified in (**7**).

(*D. ambonum* Zang *in* Zang and Walter, 1992) by its larger overall size but smaller reticulum size, as well as its apparent lack of a continuous vesicle wall. It is similar to the Tonian species *D. fullerene* Butterfield in Butterfield et al. (1994) in that both taxa apparently lack a continuous vesicle wall. However, *D. fullerene* has short processes at the corners of polygonal fields and has thicker and more robust ridges. The apparent lack of a continuous vesicle wall is probably a taphonomic artifact; perhaps the vesicle wall was thin and had been preferentially degraded.

A specimen illustrated as "reticulate acanthomorphic acritarch" from the upper Ediacaran or Cambrian Oppokun Formation in north-central Siberia (Grazhdankin et al., 2020) also has a vesicle consisting of a reticulate network, and is similar to *Dictyotidium grazhdankinii* Xiao n. sp. in vesicle size, reticulum size, and ridge thickness. However, the Oppokun specimen seems to have minute and faintly preserved processes.

Genus *Mengeosphaera* Xiao et al., 2014

Type species.—*Mengeosphaera chadianensis* (Chen and Liu, 1986) Xiao et al., 2014.

Other species.—*Mengeosphaera angusta* Liu et al., 2014; *M. bellula* Liu et al., 2014; *M. constricta* Liu et al., 2014; *M. eccentrica* Xiao et al., 2014; *M. flammelata* Liu and Moczydłowska, 2019; *M. gracilis* Liu et al., 2014; *M. grandispina* Liu et al., 2014; *M. latibasis* Liu et al., 2014; *M. lunula* Liu and Moczydłowska, 2019; *M. matryoshkaformis* Ouyang et al., 2021; *M. membranifera* Shang et al., 2019; *M. minima* Liu et al., 2014; *M. reticulata* (Xiao and Knoll, 1999) Xiao et al., 2014; *M. spinula* Liu et al., 2014; *M. stegosauriformis* Liu et al., 2014; *M. uniformis* Liu et al., 2014.

Remarks.—The genus *Mengeosphaera* is characterized by closely and evenly arranged biform processes (Xiao et al., 2014). However, the definition of biform processes varies. According to Grey (2005, p. 175), a biform process has "a conical base and tapering or ciliate distal portion." Following this definition, a gradually tapering process (e.g., in *Tanarium conoideum* Kolosova, 1991; see simplified diagrams in Fig. 24.2–24.4) would be regarded as biform. Subsequently, a biform process was defined as a process with "a basal expansion and an apical spine or lateral spine, often separated by an inflection point" (Xiao et al., 2014, p. 4), emphasizing the distinct and recognizable boundary between the basal and apical parts of the process (Fig. 24.5–24.10). An inflection point can represent a gradual transition from an inflated basal expansion to a distally tapering or cylindrical apical spine (e.g., Fig. 24.5). This is analogous to the mathematical inflection point where a convex curve changes to a concave curve and where the second derivative of the curve is zero (or where the distally decreasing slope of the inflated basal expansion transitions to the distally increasing slope of the deflated apical spine). From a practical point of view, an inflection point of a biform process also can represent an abrupt change in slope between the basal expansion and apical spine, regardless of whether the basal expansion is inflated (Fig. 24.6–24.10). In contrast, a process with a concave (or deflated) basal expansion continuing into an apical spine without an inflection point in between is not regarded as a biform process (Fig. 24.2–24.4), even if it would fit the definition of Grey (2005).

The genus *Mengeosphaera* was diagnosed by its biform processes with a conical or domical, often inflated, basal expansion that tapers rapidly and supports an apical spine that is acutely conical, often very thin, and tapers gradually (Xiao et al., 2014). An inflection point separates the basal expansion and apical spine. This feature is best seen in the holotype of the type species, *Mengeosphaera chadianensis* (Chen and Liu, 1986). Xiao et al. (2014) described two additional species of *Mengeosphaera*, *M. reticulata* and *M. eccentrica*, both of which are characterized by biform processes.

Liu and Moczydłowska (2019) commented that the inflated basal expansion of *Mengeosphaera* processes could be a taphonomic artifact unique to silica or phosphate mineralization, but not in shale preservation. We understand that an originally inflated basal expansion could become deflated due to degradation, contraction, and compression, regardless of preservation mode of mineralization and carbonaceous compression. However, it is difficult to understand how an originally deflated or otherwise non-inflated basal expansion would become consistently inflated during fossil mineralization, particularly when the basal expansion is preserved with structural integrity and show no evidence of organic displacement due to mineral recrystallization. Silicification or phosphatization is fundamentally a process of microcrystal precipitation on organic substrates, resulting in a mold and/or cast of the organic structure (Oehler and Schopf, 1971; Xiao and Tang, 2022). Organic structures such as basal expansions can be preserved with structural integrity when they are coated with or embedded in phosphate and silica. If they are disintegrated or destroyed by mineral recrystallization, organic walls or membranes would be disrupted to form irregular structures. It is unlikely for a deflated basal expansion to become consistently inflated during mineralization/recrystallization and to still maintain its structural integrity.

Liu and Moczydłowska (2019) further stated that neither *M. reticulata* nor *M. eccentrica* have biform processes. They did not define what they meant by biform processes. Following either of the definitions of Grey (2005) or Xiao et al. (2014), as clarified above and schematically illustrated in Figure 24, it is indisputable that all three species of *Mengeosphaera* described in Xiao et al. (2014) have biform processes with clear inflection points. This key feature is clearly present in the holotypes of *M. chadianensis*, *M. reticulata*, and *M. eccentrica*, illustrated in Chen and Liu (1986, pl. 2, figs. 2, 4), Xiao and Knoll (1999, fig. 11H), and Xiao et al. (2014, fig. 26.1), respectively. It should be pointed out that these holotypes are all three-dimensionally phosphatized and acid-extracted specimens that were imaged using scanning electron microscopy so that the biform nature of the processes is best seen in lateral views, but not discernable in apical views. Additionally, the fragile apical spines may be abraded during taphonomic reworking or acid extraction, and they may not be retained at all if the specimens are preserved as internal molds (Xiao and Knoll, 1999). Despite these complications, the processes in the holotypes of the above-

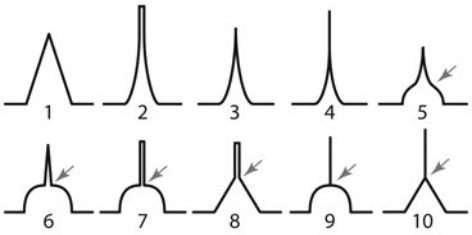

Figure 24. Schematic illustration of non-biform (**1–4**) and biform processes (**5–10**). Arrows point to inflection points in biform processes.

mentioned species were clearly illustrated, with an inflection point separating an inflated basal expansion and an apical spine, although the distal part of the apical spine is often not intact.

Liu et al. (2014a) established 13 new species of *Mengeosphaera*, four of which are discussed here because of their uncertain placement in this genus. *Mengeosphaera*? *cuspidata* has conical or even deflated basal expansions and, as a result, was published as an open nomenclature to acknowledge its uncertain placement in *Mengeosphaera*. This species was subsequently transferred to the genus *Tanarium* Kolosova, 1991, becoming *T. cuspidatum* (Liu et al., 2014) Liu and Moczydłowska, 2019. Similarly, Liu et al. (2014a) noted that the basal expansion of *M. triangularis* was not clearly inflated and this species was tentatively placed in the genus *Mengeosphaera*. This species also was transferred to the genus *Tanarium* and became *T. triangulare* (Liu et al., 2014) Liu and Moczydłowska, 2019, an orthographic correction of *T. triangularis* as spelled in Liu and Moczydłowska (2019, p. 143, 151). In the same paper, however, Liu and Moczydłowska (2019, p. 129) listed *M. triangularis* as an accepted species of *Mengeosphaera*, likely as an unintended error. Liu and Moczydłowska (2019) mentioned in passing that *M. spicata* Liu et al., 2014, is a junior synonym of *M. constricta*, but provided no explanation or justification. Although the holotypes of these two species are notably different in vesicle size, process density, process spacing, and the presence of a constriction at process base (compare fig. 56.1, 56.2 and fig. 64.1, 64.2 of Liu et al., 2014a), we do acknowledge that there are specimens (e.g., Liu et al., 2014a, fig. 58) that are morphologically transitional between the two holotypes. Thus, we tentatively follow the synonymization of these two species proposed by Liu and Moczydłowska (2019). Finally, the species *M.*? *gracilis* was placed in open nomenclature because, relative to other *Mengeosphaera* species, it has somewhat densely arranged processes with somewhat long and thin apical spines, which are features typically associated with species of *Appendisphaera* (Liu et al., 2014a). Liu and Moczydłowska (2019), however, removed the ambiguity in genus placement (although it was still listed as *M.*? *gracilis* in Liu and Moczydłowska, 2019, p. 129), a proposition followed by subsequent authors (e.g., Shang et al., 2019) and in this paper.

Mengeosphaera gracilis Liu et al., 2014
Figure 25

2014a *Mengeosphaera*? *gracilis* Liu et al., p. 96, fig. 60.
2019 *Mengeosphaera gracilis*; Liu and Moczydłowska, p. 132, fig. 71.
2019 *Mengeosphaera gracilis*; Shang et al., p. 25, fig. 14F, G.
2020 *Mengeosphaera gracilis*; Shang and Liu, p. 158, fig. 6F–L.
2021 *Mengeosphaera gracilis*; Ouyang et al., fig. 16K–M.

Holotype.—IGCAGS–WFG–727, reposited at Institute of Geology, Chinese Academy of Geological Sciences, from the lower member III of the Ediacaran Doushantuo Formation at Wangfenggang section in the Yangtze Gorges area, Hubei Province, South China (Liu et al., 2014a, fig. 60.1, 60.2).

Occurrence.—Ediacaran of South China and northern India. South China: member II of Doushantuo Formation at Wuzhishan (Ouyang et al., 2021), Jiuqunao, Nantuocun, Niuping, Wangfenggang, and northern and southern Xiaofenghe sections (Liu and Moczydłowska, 2019), as well as member III of Doushantuo Formation at Wangfenggang, Niuping, Xiaofenghe, Baiguoyuan, Chenjiayuanzi, Dishuiyan, and Liuhuiwan sections, Yangtze Gorges area, Hubei Province (Liu et al., 2014a); lower Doushantuo Formation (probably equivalent to member II) at Tianping section, Hunan Province (Shang and Liu, 2020); Doushantuo Formation at Liujing section in Guizhou Province (Shang et al., 2019). Northern India: Krol A Formation, Solan area (this paper).

Description and measurements.—Large spheroidal vesicles with densely and evenly distributed processes open to vesicle interior. Processes biform, with a conical to slightly inflated basal expansion supporting a thin and distally tapering apical spine. Vesicle diameter ~280 µm (Fig. 25.8), 13–18 processes per 100 µm of vesicle periphery, process length 6–14 µm (~5% of vesicle diameter, as estimated from specimen illustrated in Fig. 25.8), process spacing 1–3 µm at base, basal expansion 4–6 µm wide at base, and 3–4 µm in height, apical spine ~1 µm wide and 4–10 µm long.

Materials.—Four illustrated specimens (Fig. 25) and three additional specimens.

Remarks.—Liu et al. (2014a) commented on the similarities and differences among *M. gracilis*, *Cavaspina basiconica*, and *Appendisphaera*? *hemisphaerica*, all of which are characterized by processes with a basal expansion supporting a thin apical spine. The processes of *C. basiconica* do not have an inflated basal expansion and typically are shorter than the two other species. Relative to *M. gracilis*, *A.*? *hemisphaerica* was said to have narrower and more-inflated basal expansion, as well as proportionally longer and more densely arranged processes. As discussed under *A.*? *hemisphaerica*, however, these two species may be synonymous. The specimen of *M. gracilis* illustrated in Shang and Liu (2020) is poorly preserved, with its biform processes barely visible; therefore its taxonomic identification is tentative.

Genus *Tanarium* Kolosova, 1991, emend. Moczydłowska, Vidal, and Rudavskaya, 1993

Type species.—*Tanarium conoideum* Kolosova, 1991, emend. Moczydłowska, Vidal, and Rudavskaya, 1993.

Other species.—*Tanarium acus* Liu et al., 2014; *T. araithekum* Grey, 2005; *T. capitatum* Liu and Moczydłowska, 2019; *T. cuspidatum* (Liu et al., 2014) Liu and Moczydłowska, 2019; *T. digitiforme* (Nagovitsin and Faizullin in Nagovitsin et al., 2004) Sergeev et al., 2011; *T. elegans* Liu et al., 2014; *T. gracilentum* (Yin in Yin and Liu, 1988) Ouyang et al., 2021; *T. irregulare* Moczydłowska, Vidal, and Rudavskaya, 1993; *T. mattoides* Grey, 2005; *T. megaconicum* Grey, 2005; *T.*? *minimum* Liu et al., 2014; *T.*? *muntense* Grey, 2005; *Tanarium obesum* Liu et al., 2014; *T. paucispinosum* Grey, 2005; *T. pilosiusculum* Vorob'Eva, Sergeev, and Knoll, 2009; *T. pluriprotensum* Grey, 2005; *T. pycnacanthum* Grey, 2005; *T. triangulare* (Liu et al., 2014) Liu and Moczydłowska, 2019, an orthographic correction of *T. triangularis* as published in Liu and Moczydłowska (2019); *T. tuberosum* Moczydłowska, Vidal, and Rudavskaya, 1993; *T. uniformum* Liu and Moczydłowska, 2019; *T. varium* Liu et al., 2014; *T. victor* Xiao et al., 2014.

Remarks.—Together with *Appendisphaera* and *Mengeosphaera*, *Tanarium* is one of the richly speciose genera of Ediacaran acanthomorphs. This is due to the very broad definition of this genus. For example, according to Moczydłowska et al.'s (1993) emendation, *Tanarium* is an acanthomorph with hollow processes that are conical or cylindrical, tapering or rounded distally, simple or branching. A number of acanthomorphs—including *Papillomembrana* Spjeldnaes, 1963, and *Xenosphaera* Yin, 1987 (see Liu et al., 2014a)—would fit in this definition, in which case *Tanarium* would be rendered a junior synonym. Grey's (2005) emendation restricts *Tanarium* to acanthomorphs with heteromorphic processes longer than 20% of vesicle diameter. This restriction would exclude a few species, including *T.*? *minimum* and *T. pilosiusculum* Vorob'Eva et al., 2009, from the genus of *Tanarium*. But even this restriction would still include *Xenosphaera* and its type species, *X. liantuoensis* Yin, 1987, rendering *Tanarium* a junior synonym. It is probably time to split the genus *Tanarium* as currently recognized into several genera on the basis of, for example, process length and morphologies.

Moczydłowska and Nagovitsin (2012) listed *Tanarium stellatum* Nagovitsin and Faizullin in Nagovitsin et al., 2004, as a junior synonym of *T. tuberosum*, and Liu and Moczydłowska (2019) listed *Tanarium obesum* Liu et al., 2014, as a junior synonym of *T. tuberosum*, but no explanation was provided to justify these synonymization proposals. Liu et al. (2014a, p. 113) diagnosed *T. obesum* as a species of *Tanarium* "with a small to medium-sized vesicle covered with a moderate number of relatively large, acutely conical, and heteromorphic processes that occasionally bifurcate." Additionally, *T. obesum* has more numerous, more closely arranged, and more acutely conical processes than does *T. tuberosum*. In this paper, we follow Liu et al. (2014a) and treat *T. obesum* as a distinct species (see also Ouyang et al., 2021).

Tanarium cf. *T. conoideum* Kolosova, 1991, emend. Moczydłowska, Vidal, and Rudavskaya, 1993
Figure 26

cf. 1991 *Tanarium conoideum* Kolosova, p. 57, fig. 5.1–15.3.
cf. 1993 *Tanarium conoideum*; emend. Moczydłowska et al., p. 514, text-fig. 10C, D.

Occurrence.—Ediacaran Krol A Formation, Solan area, Lesser Himalaya, northern India (this paper).

Description and measurements.—A poorly preserved specimen with numerous long and conical processes. Estimated maximum vesicle diameter 247 µm (Fig. 26.1), process length up to 60 µm (~24% of vesicle diameter), and process basal width up to 7 µm. Some processes appear to be biform (Fig. 26.4, 26.5), with a basal expansion 14 µm wide and 8 µm high, supporting an apical spine 4 µm in basal width and 45 µm in length.

Materials.—One specimen illustrated in Figure 26.

Remarks.—The specimen is similar to the holotype of *Tanarium conoideum* in morphology and proportional length of processes (cf., Kolosova, 1991, fig. 5.1, 5.2). It is about twice as large in vesicle diameter and its process density is greater than the holotype (although Kolosova, 1991, illustrated another specimen of *T. conoideum* with a greater density of processes than in the holotype). Some processes in the current specimen appear to be biform in shape, a feature that is not present in the holotype. Alternatively, these apparently biform processes may be a taphonomic artifact; a torn and dislodged process with its base attached to a small piece of the vesicle wall may appear to be biform. On the other hand, Grey (2005) emended the diagnosis of the genus *Tanarium* to emphasize its heteromorphic (morphologically variable) processes that are longer than 20% of vesicle diameter. She also commented that the processes of the Australian specimens of *T. conoideum* have a conspicuously widened base (e.g., Grey, 2005, fig. 212D), although she did not specifically describe their processes as biform. Considering the uncertainty about the biform nature of the processes in the only available specimen from the Krol A Formation, we tentatively place this specimen in an open nomenclature. An alternative taxonomic home for this specimen would be the genus *Mengeosphaera*, if its biform processes can be confirmed with better-preserved specimens that show the intact transition from process base to vesicle wall.

Tanarium digitiforme (Nagovitsin and Faizullin in Nagovitsin et al., 2004) Sergeev et al., 2011
Figure 27

2004 *Goniosphaeridium digitiforme* Nagovitsin and Faizullin in Nagovitsin et al., p. 13, pl. 2, figs. 4, 5.
2008 Unnamed form with processes; Vorob'Eva et al., fig. 2h.
2010 "*Goniosphaeridium*" *digitiforme*; Golubkova et al., pl. 4, fig. 3.

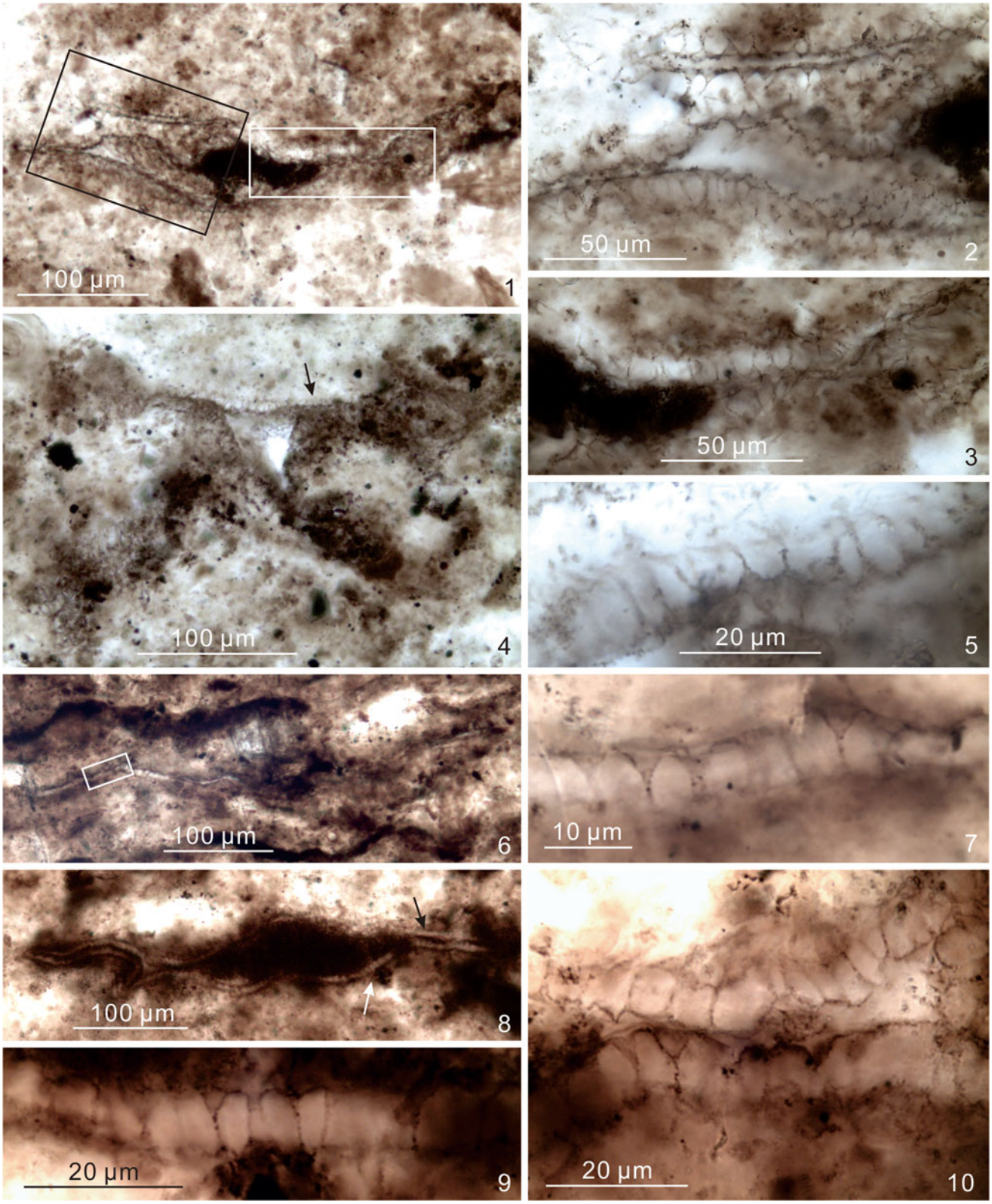

Figure 25. *Mengeosphaera gracilis*. (**1–3**) S4-4-F2-8-2, 12.2 × 108.2, EF-Q8-3, VPIGM-4894, black and white rectangles in (**1**) mark areas shown in (**2, 3**), respectively; (**4, 5**) S4-4-F2-14, 10.9 × 104.4, EF-S4-2, VPIGM-4896, arrow in (**4**) marks area shown in (**5**) at a different focal level; (**6, 7**) S4-4-F1-2, 18.3 × 102.8, EF-K3-3, VPIGM-4869, rectangle in (**6**) marks area shown in (**7**) at a different focal level; (**8–10**) S4-4-F1-4, 9.2 × 129.0, EF-T29-3, VPIGM-4872, white and black arrows in (**8**) mark areas shown in (**9, 10**), respectively, at different focal levels.

2011 *Tanarium digitiformum* (Nagovitsin and Faizullin in Nagovitsin et al., 2004) Sergeev et al., p. 1006, fig. 7.6.
2012 *Tanarium digitiformum*; Moczydłowska and Nagovitsin, p. 19, fig. 8D–8F.
2014 *Tanarium digitiforme*; Xiao et al., p. 53, Fig. 34.1–34.3.
2020 *Tanarium digitiforme*; Yang et al., p. 7, fig. 2L–M.

Holotype and paratype.—Holotype (specimen N2, preparation PN8/17-2, number 673; illustrated in Nagovitsin et al., 2004, pl. 2, fig. 4) and paratype (PN8/4-17/7-3; illustrated in Moczydłowska and Nagovitsin, 2012, fig. 8E) are reposited in the Central Siberian Geological Museum of the United Institute of Geology, Geophysics, and Mineralogy, Siberian Branch of the Russian Academy of Sciences, Novosibirsk, Russia.

Occurrence.—Ediacaran of East Siberia, South China, and northern India. East Siberia: Ura Formation of the Zhuya-Lena area (Nagovitsin et al., 2004; Vorob'Eva et al., 2008; Golubkova et al., 2010; Sergeev et al., 2011; Moczydłowska and Nagovitsin, 2012). South China: Doushantuo Formation at Weng'an, Guizhou Province (Xiao et al., 2014) and Baizhu, Hubei Province (Yang et al., 2020). Northern India: Krol A Formation, Solan area (this paper).

Description and measurements.—Medium-sized spheroidal vesicles with a moderate number of basally separate, digitate, hollow, and cylindrical to clavate processes that open to vesicle interior. Vesicle diameter up to 144 µm (Fig. 27.3), ~5 processes per 100 µm of vesicle periphery, process length at least 19–22 µm (~19% of vesicle diameter), process width 13–17 µm, and process spacing ~9 µm at base.

Materials.—Two specimens illustrated in Figure 27.

Remarks.—The specimens available are poorly preserved. In particular, the full length of the processes is not captured in thin sections. Most processes are captured in transverse or oblique sections (Fig. 27.2, 27.6, 27.8), making them appear to be circular, elliptical, or conical (Fig. 27.1, 27.2, lower center of Fig. 27.3), but the axially cut processes are cylindrical (Fig. 27.5) or clavate (Fig. 27.7). Overall, the process size, morphology, and density, as well as the vesicle size, of the Krol A specimens match the diagnosis of *Tanarium digitiforme*. Alternatively, these specimens could be assigned to *Papillomembrana boletiformis* Xiao et al., 2014, a taxon characterized by cylindrical processes with a bulbous or clavate termination. As noted above, *Papillomembrana* and the broadly defined *Tanarium* may be synonymous, and Xiao et al. (2014) commented that some Doushantuo specimens of *Papillomembrana compta* Spjeldnaes, 1963, are better assigned to *T. digitiforme*. Indeed, *P. compta* has been recorded previously from the Infra-Krol Formation in the Nainital area of the Lesser Himalaya (Table 1). The Krol A specimens illustrated here, however, have relatively longer processes (~19% of vesicle diameter) than *P. compta* (6–8% of vesicle diameter) and *P. boletiformis* (~5% of vesicle diameter). In light of Grey's (2005) attempt to differentiate *Tanarium* from other acanthomorphs on the basis of process length, we choose to place the Krol A specimens under *T. digitiforme*.

Genus *Weissiella* Vorob'Eva, Sergeev, and Knoll, 2009

Type species.—*Weissiella grandistella* Vorob'Eva, Sergeev, and Knoll, 2009.

Other species.—*Weissiella brevis* Xiao et al., 2014, emend. Ouyang et al., 2021.

Weissiella brevis Xiao et al., 2014, emend. Ouyang et al., 2021
Figure 28

2014 *Weissiella brevis* Xiao et al., p. 61, fig. 38.
2014 *Weissiella* cf. *grandistella*; Shukla and Tiwari, p. 219, fig. 8A–E.
2015 *Weissiella* cf. *brevis*; Ouyang et al., p. 221, pl. III, figs. 7–13.
2015 *Weissiella* sp.; Ouyang et al., p. 221, pl. IV, figs. 8–13.
2015 *Weissiella* sp.; Ye et al., p. 50, pl. I, figs. 15–19.
2016 *Weissiella* cf. *grandistella*; Sharma et al., fig. 4K (same as Shukla and Tiwari, 2014, fig. 8A).
2019 *Weissiella* sp.; Ouyang et al., fig. 10E–H.
2019 *Weissiella grandistella*; emend. Liu and Moczydłowska, p. 163, fig. 91A–E (part).
2019 *Weissiella grandistella*; Shang et al., p. 28, fig. 19A, B.
2020 *Weissiella* sp.; Tian et al., fig. 9K, L.
2021 *Weissiella grandistella*; Liu et al., fig. 5.3, 5.5.
2021 *Weissiella brevis*; emend. Ouyang et al., p. 40, figs. 6C, D, 23A–N.

Holotype.—VPIGM-4641 (WPB-3-4-4, 16.53132.6), reposited in the Museum of Geosciences at Virginia Polytechnic Institute, from unit 4A (probably equivalent to member II) of the Doushantuo Formation at Weng'an, Guizhou Province, South China (Xiao et al., 2014, fig. 38.1).

Occurrence.—Ediacaran of South China and northern India. South China: unit 4A (probably equivalent to member II) of Doushantuo Formation, Weng'an, Guizhou Province (Xiao et al., 2014); member II and equivalent strata of Doushantuo Formation at Zhangcunping (Ye et al., 2015; Ouyang et al., 2019; Tian et al., 2020), Jiulongwan (Ouyang et al., 2021), Jinguadun (Ouyang et al., 2015, 2021), Wuzhishan (Ouyang et al., 2021), Xiaofenghe (Liu and Moczydłowska, 2019), and Changyang (Liu et al., 2021), Hubei Province; Doushantuo Formation at Liujing, Guizhou Province (Shang et al., 2019). Northern India: Krol A Formation, Solan area (Shukla and Tiwari, 2014; Sharma et al., 2016; this paper).

Description and measurements.—Medium-sized spheroidal vesicle with numerous evenly distributed processes that open to vesicle interior. Processes are relatively short, slightly taper toward an often-truncated distal end. Process interior is subdivided by transverse cross-walls. Vesicle diameter ~160 µm (Fig. 28.1), ~6–7 processes per 100 µm of vesicle periphery, process length ~15 µm (~10% of vesicle diameter), process width ~15 µm at base, and process spacing ~3 µm at

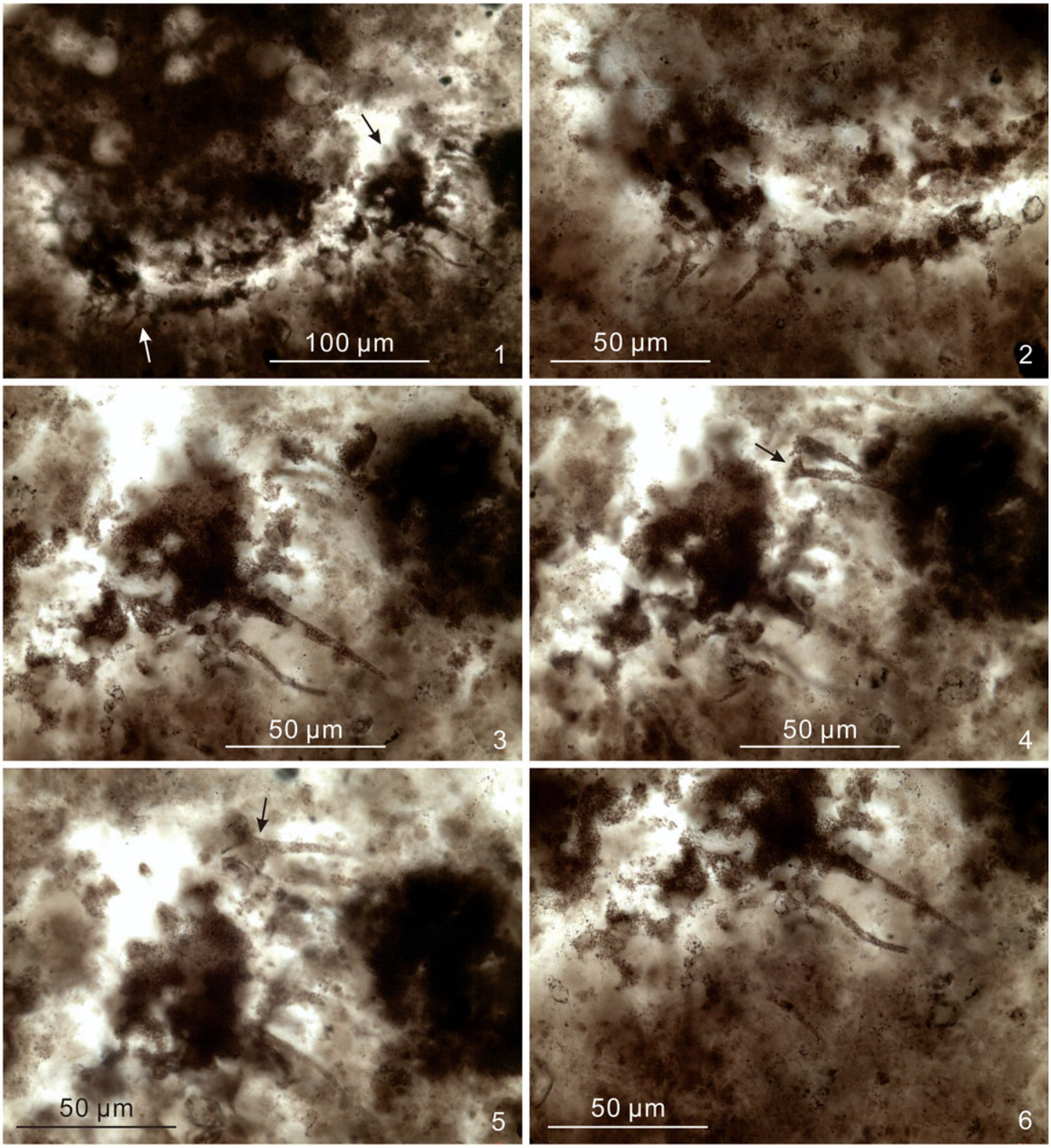

Figure 26. *Tanarium* cf. *T. conoideum*. S4-4-F2-7, 17.1 × 120.0, EF-L20-3, VPIGM-4888. (**1**) Specimen overview; (**2–6**) close-up views showing details of processes. White and black arrows in (**1**) mark areas magnified in (**2**) and (**3–6**) (same area at different focal levels), respectively. Arrows in (**4, 5**) mark possible biform processes with a basal expansion.

base. One or more cross-walls present in each process, with a spacing of ~6 µm between cross-walls.

Materials.—One specimen illustrated in Figure 28.

Remarks.—Liu and Moczydłowska (2019) proposed that *Weissiella brevis* be synonymized with *W. grandistella*. However, *W. brevis* has distinctly smaller vesicles and more numerous processes than *W. grandistella*. Importantly, *W. brevis* has proportionally smaller and shorter processes relative to its vesicle size. With more materials available, the distinction between these two species has become clearer, and we follow Ouyang et al. (2021) in regarding these two species as separate taxa. The distinction is

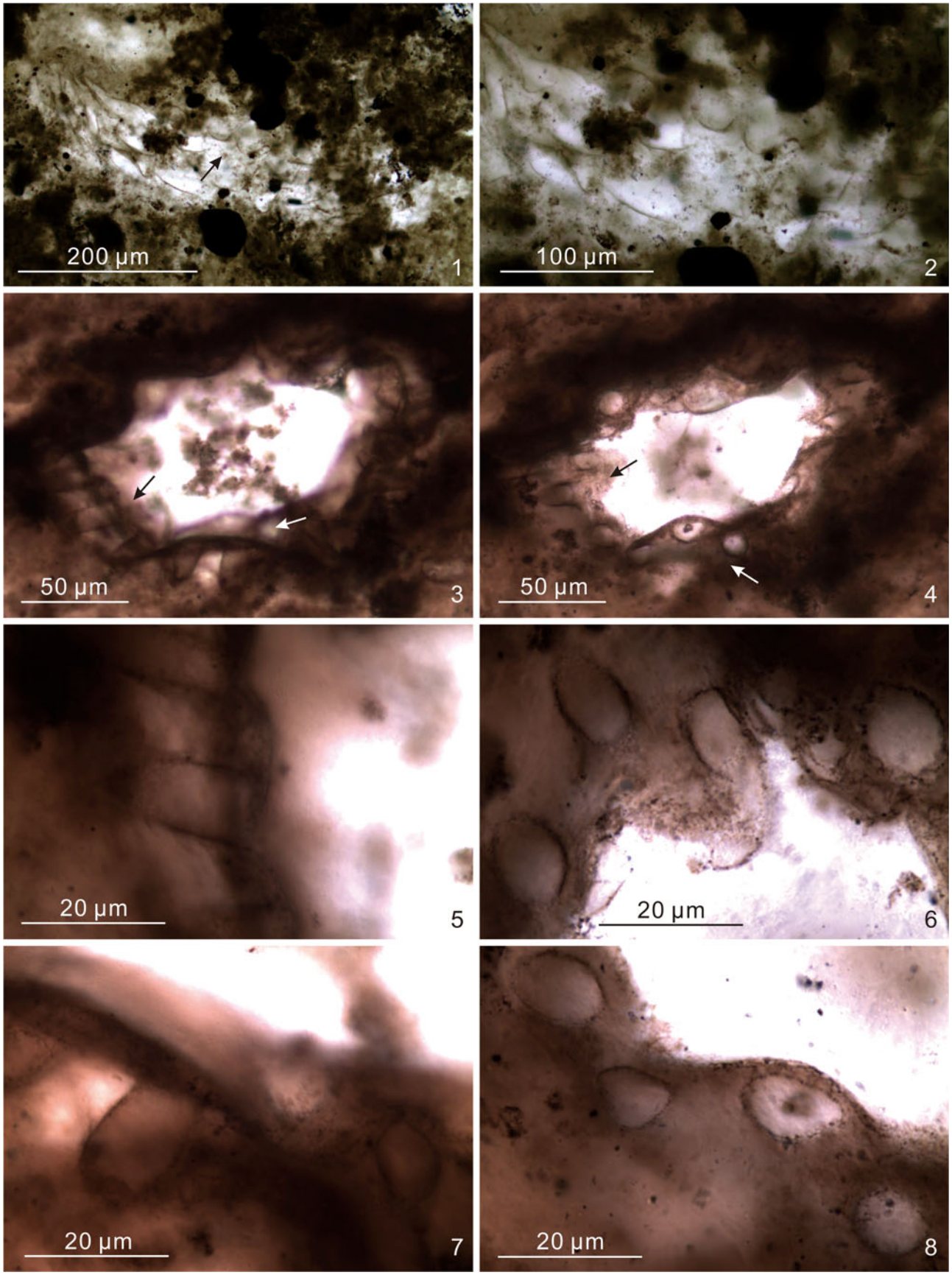

Figure 27. *Tanarium digitiforme* (Nagovitsin and Faizullin in Nagovitsin et al., 2004) Sergeev et al., 2011. (**1, 2**) DH-14-68.0-A, 21.3 × 130.3, EF-G30-1, VPIGM-4859, arrow in (**1**) marks area shown in (**2**), showing obliquely cut processes; (**3–8**) DH-14-65.0-A, 16.7 × 109.9, EF-L10-3, VPIGM-4831, (**3, 4**) the same area at two different focal levels, black and white arrows in (**3**) mark areas shown in (**5**) and (**7**), respectively, and black and white arrows in (**4**) mark areas shown in (**6**) and (**8**), respectively.

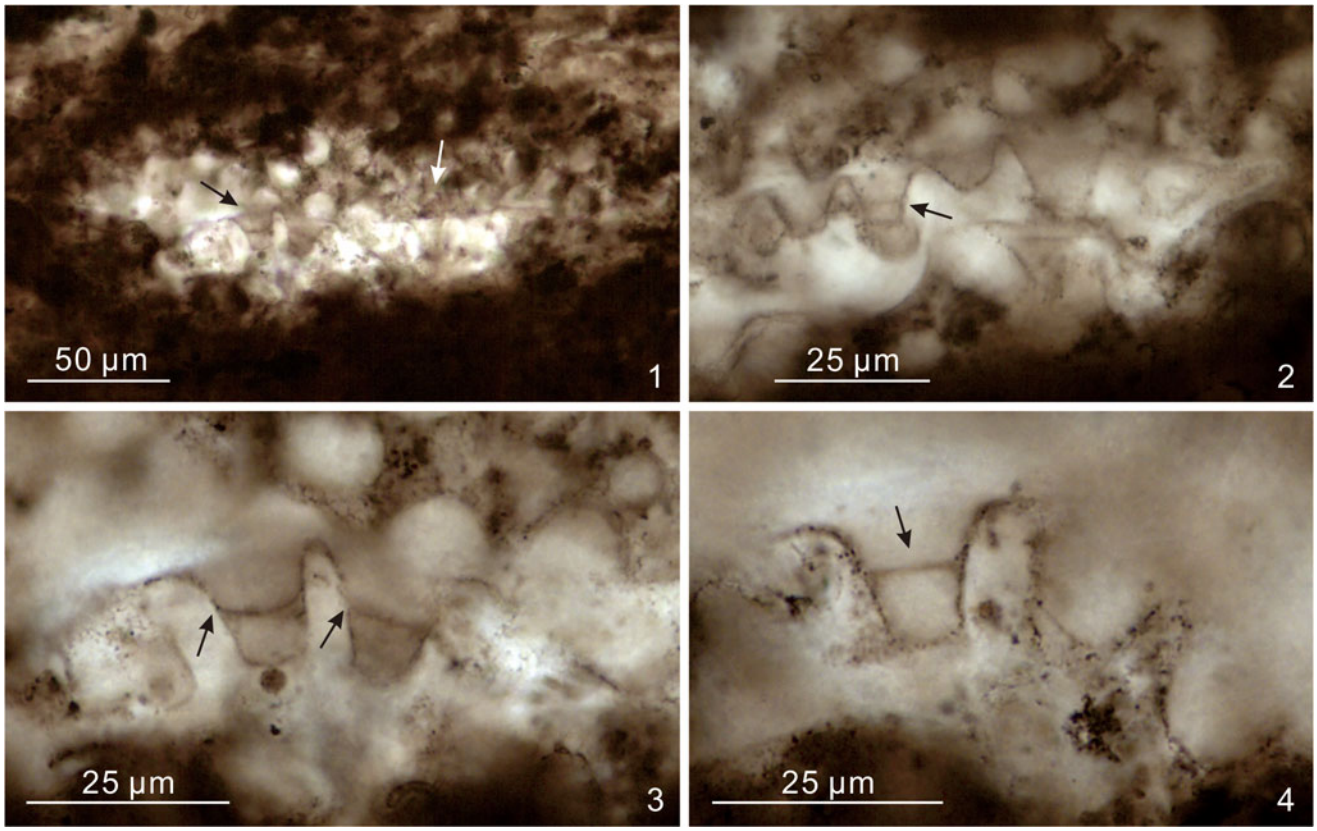

Figure 28. *Weissiella brevis*. (**1–4**) DH-14-68.0-C-2, 23.8 × 112.6, EF-D12-4, VPIGM-4868, white and black arrows in (**1**) mark areas shown in (**2**) and (**3, 4**) (at two different focal levels). Black arrows in (**2–4**) mark cross-walls within processes. Note that arrows in (**2, 3**) are placed outside processes, and arrow in (**4**) is inside the process.

even more apparent if the truncated distal end of *W. brevis* processes is a result of taphonomic breakage, because more completely preserved processes of *W. brevis* are expanded both basally and terminally (Ouyang et al., 2021), which is substantively different from the conical and distally tapering processes of *W. grandistella*. Based on the distinction between *W. brevis* and *W. grandistella*, as outlined in Ouyang et al. (2021), several specimens previously illustrated as *W. grandistella* (Liu and Moczydłowska, 2019; Shang et al., 2019; Liu et al., 2021), *W.* cf. *W. grandistella* (Shukla and Tiwari, 2014; Sharma et al., 2016), and *Weissiella* sp. (Ye et al., 2015; Ouyang et al., 2019; Tian et al., 2020) are here considered as *W. brevis*.

Results

Summary of $\delta^{13}C$ and $\delta^{18}O$ data.—$\delta^{13}C$ values of −8‰ to −15‰ occur in the first 30 m of the Krol A silty dolostones directly overlying the Krol Sandstone (Fig. 3.2; Table 2). The $\delta^{13}C$ values shift to positive at the uppermost part of Krol A, with highest values up to +5.5‰. Most of the $\delta^{13}C$ values of Krol B are in the range of +3.3‰ to +4.2‰, with a few down to +0.3‰ and −1.6‰. The $\delta^{13}C$ values of Krol C are mostly around +3.0‰, with a few lower values below +2.0‰ and the highest values up to +4.1‰ (Fig. 3.2). The $\delta^{18}O$ values of Krol A are very stable, with an average around −4‰ (Fig. 3.2, 3.3). In contrast, $\delta^{18}O$ values of Krol B and Krol C are variable between −6‰ and −11‰ and they do not show a co-variation with $\delta^{13}C$ values (Fig. 3.2, 3.3).

Summary of Krol A microfossils: taxonomic treatment and stratigraphic distribution.—We recovered 274 specimens of ornamented acritarchs, including 241 acanthomorph specimens belonging to 13 species and numerous specimens of the herkomorph species *Dictyotidium grazhdankinii* Xiao n. sp. (Table 3). The acanthomorphs can be divided into four groups based on their ornamentation, particularly size and shape of processes (Fig. 29; Table 4). The first and most common group of taxa—including *Appendisphaera clava*, *A. tenuis*, *Cymatiosphaeroides forabilatus*, and *Mengeosphaera gracilis*—is characterized by thin (<5 µm wide) and short processes (<15 µm and typically <10 µm long, or <5% of vesicle diameter), and accounts for 49% of ornamented acritarch specimens. The second group—including *Appendisphaera grandis*, *A.*? *hemisphaerica*, *A. longispina*, and *A. setosa*—accounts for 24% in abundance and is characterized by thin (<5 µm wide) and long processes (>10 µm and typically 15–30 µm long, or 5–10% of vesicle diameter). The third group, accounting for <2% in abundance, includes *Tanarium digitiforme*, *T.* cf. *T. conoideum*, and *Weissiella brevis*, which have thick processes (typically 10–15 µm wide) with variable lengths (typically 15–60 µm long, or 10–20% of vesicle diameter). The fourth group, representing 1% of the abundance, includes *Asterocapsoides sinensis* and *Cavaspina tiwariae* Xiao n. sp.,

Table 2. Sample number, stratigraphic height, lithology, and $\delta^{13}C$ and $\delta^{13}O$ data from the Krol A to Krol C formation at sections DH-14 and DH2-14. $\delta^{13}C$ and $\delta^{13}O$ data are plotted in Figure 3.

Sample	unit	height (m)	lithology	$\delta^{13}C$ (‰)	$\delta^{13}O$ (‰)
DH-14-40.4	Krol A	40.4	Shaly dolostone	−11.4	−5.1
DH-14-40.6	Krol A	40.6	Shaly dolostone	−12.3	−4.3
DH-14-42	Krol A	42.0	Shaly dolostone	−9.1	−0.7
DH-14-43	Krol A	43.0	Shaly dolostone	−12.4	−3.7
DH-14-43.6	Krol A	43.6	Shaly dolostone	−10.9	−4.0
DH-14-46.5	Krol A	46.5	Shaly dolostone	−10.5	−4.1
DH-14-48.5	Krol A	48.5	Shaly dolostone	−9.3	−3.6
DH-14-50.3	Krol A	50.3	Shaly dolostone	−8.5	−4.2
DH-14-51	Krol A	51.0	Shaly dolostone	−8.9	−3.9
DH-14-52	Krol A	52.0	Shaly dolostone	−11.9	−4.5
DH-14-52.5	Krol A	52.5	Shaly dolostone	−10.5	−3.6
DH-14-53	Krol A	53.0	Shaly dolostone	−11.4	−4.2
DH-14-54.3	Krol A	54.3	Shaly dolostone	−8.6	−4.4
DH-14-56.4	Krol A	56.4	Shaly dolostone	−11.3	−3.6
DH-14-57	Krol A	57.0	Shaly dolostone	−9.7	−4.1
DH-14-57.5	Krol A	57.5	Shaly dolostone	−10.2	−4.1
DH-14-57.8	Krol A	57.8	Shaly dolostone	−9.6	−4.7
DH-14-58.2	Krol A	58.2	Shaly dolostone	−7.5	−4.0
DH-14-58.3	Krol A	58.3	Shaly dolostone	−10.5	−4.5
DH-14-58.6	Krol A	58.6	Shaly dolostone	−11.2	−4.1
DH-14-59.9	Krol A	59.9	Shaly dolostone	−10.4	−4.3
DH-14-60	Krol A	60.0	Shaly dolostone	−13.7	−3.8
DH-14-60.3	Krol A	60.3	Shaly dolostone	−10.9	−3.4
DH-14-60.5	Krol A	60.5	Shaly dolostone	−10.7	−3.7
DH-14-61	Krol A	61.0	Shaly dolostone	−13.2	−4.6
DH-14-61.2	Krol A	61.2	Shaly dolostone	−12.3	−3.5
DH-14-62.2	Krol A	62.2	Shaly dolostone	−14.3	−4.1
DH-14-62.5	Krol A	62.5	Shaly dolostone	−12.8	−4.5
DH-14-62.8	Krol A	62.8	Shaly dolostone	−15.0	−3.7
DH-14-63.3	Krol A	63.3	Shaly dolostone	−12.5	−4.1
DH-14-63.5	Krol A	63.5	Shaly dolostone	−13.3	−3.3
DH-14-64.2	Krol A	64.2	Shaly dolostone	−12.9	−4.3
DH-14-65.1	Krol A	65.1	Shaly dolostone	−13.2	−4.1
DH-14-65.2	Krol A	65.2	Shaly dolostone	−12.7	−3.9
DH-14-65.5	Krol A	65.5	Shaly dolostone	−11.5	−4.5
DH-14-66.7	Krol A	66.7	Shaly dolostone	−8.5	−3.8
DH-14-67.1	Krol A	67.1	Shaly dolostone	−7.6	−4.2
DH-14-68	Krol A	68.0	Shaly dolostone	−8.4	−3.4
DH-14-69	Krol A	69.0	Shaly dolostone	−5.3	−3.4
DH-14-69.2	Krol A	69.2	Shaly dolostone	−5.5	−4.3
DH-14-70	Krol A	70.0	Shaly dolostone	−2.8	−3.5
DH-14-71	Krol A	71.0	Shaly dolostone	−0.8	−3.6
DH-14-72	Krol A	72.0	Shaly dolostone	0.8	−2.3
DH-14-72.5	Krol A	72.5	Shaly dolostone	−0.4	−3.0
DH-14-73	Krol A	73.0	Shaly dolostone	2.0	−1.3
DH-14-73.5	Krol A	73.5	Shaly dolostone	0.8	−3.4
DH-14-74	Krol A	74.0	Shaly dolostone	0.0	−3.4
DH-14-74.5	Krol A	74.5	Intraclastic dolowackestone	0.9	−3.3
DH-14-75	Krol A	75.0	Shaly dolostone	1.4	−3.9
DH-14-75.5	Krol A	75.5	Intraclastic dolowackestone	2.4	−3.4
DH-14-76	Krol A	76.0	Shaly dolostone	2.2	−3.9
DH-14-76.5	Krol A	76.5	Shaly dolostone	2.1	−5.4
DH-14-77	Krol A	77.0	Shaly dolostone	3.6	−3.1
DH-14-77.5	Krol A	77.5	Shaly dolostone	3.4	−2.8
DH-14-78	Krol A	78.0	Shaly dolostone	2.7	−4.4
DH-14-78.5	Krol A	78.5	Shaly dolostone	3.6	−2.9
DH-14-79	Krol A	79.0	Shaly dolostone	3.7	−3.7
DH-14-79.5	Krol A	79.5	Dolomudstone	4.6	−3.7
DH-14-80	Krol A	80.0	Dolomudstone	4.7	−3.1
DH2-14-0.4	Krol A	74.4	Shaly dolostone	0.8	−3.2
DH2-14-1	Krol A	75.0	Shaly dolostone	1.7	−3.3
DH2-14-1.8	Krol A	75.8	Shaly dolostone	1.8	−3.5
DH2-14-2	Krol A	76.0	Shaly dolostone	2.1	−3.7
DH2-14-2.2	Krol A	76.2	Shaly dolostone	2.1	−3.4
DH2-14-2.4	Krol A	76.4	Shaly dolostone	1.5	−3.2
DH2-14-2.8	Krol A	76.8	Shaly dolostone	2.4	−3.0
DH2-14-3	Krol A	77.0	Shaly dolostone	1.7	−3.7
DH2-14-3.2	Krol A	77.2	Shaly dolostone	2.5	−3.1
DH2-14-3.5	Krol A	77.5	Shaly dolostone	2.2	−3.4
DH2-14-3.7	Krol A	77.7	Shaly dolostone	2.7	−3.1
DH2-14-4	Krol A	78.0	Shaly dolostone	2.3	−3.3
DH2-14-4.3	Krol A	78.3	Shaly dolostone	1.7	−5.6
DH2-14-4.5	Krol A	78.5	Shaly dolostone	3.1	−2.7

Table 2. Continued.

Sample	unit	height (m)	lithology	$\delta^{13}C$ (‰)	$\delta^{13}O$ (‰)
DH2-14-5	Krol A	79.0	Shaly dolostone	2.7	−3.4
DH2-14-5.5	Krol A	79.5	Intraclastic dolowackestone	2.9	−5.6
DH2-14-6	Krol A	80.0	Shaly dolostone	3.5	−3.3
DH2-14-6.5	Krol A	80.5	Dolowackestone	3.3	−2.9
DH2-14-7	Krol A	81.0	Dolomudstone	3.3	−2.7
DH2-14-7.2	Krol A	81.2	Dolomudstone	3.5	−2.4
DH2-14-7.5	Krol A	81.5	Dolomudstone	3.7	−2.6
DH2-14-8	Krol A	82.0	Dolomudstone	4.2	−3.7
DH2-14-8.5	Krol A	82.5	Dolomudstone	4.1	−3.6
DH2-14-9	Krol A	83.0	Dolomudstone	5.0	−3.3
DH2-14-9.5	Krol A	83.5	Dolomudstone	5.2	−3.2
DH2-14-10	Krol A	84.0	Dolomudstone	5.3	−3.3
DH2-14-10.5	Krol A	84.5	Microcrystalline dolostone	5.5	−3.3
DH2-14-11	Krol A	85.0	Microcrystalline dolostone	5.5	−3.3
DH2-14-11.5	Krol A	85.5	Microcrystalline dolostone	5.5	−3.8
DH2-14-12	Krol A	86.0	Microcrystalline dolostone	5.5	−4.8
DH2-14-12.5	Krol A	86.5	Microcrystalline dolostone	5.5	−5.3
DH2-14-13	Krol A	87.0	Microcrystalline dolostone	4.4	−5.4
DH2-14-13.3	Krol A	87.3	Microcrystalline dolostone	5.2	−6.3
DH2-14-14.5	Krol B	88.5	Silty dolostone	3.8	−5.6
DH2-14-14.8	Krol B	88.8	Silty dolostone	4.3	−6.8
DH2-14-15	Krol B	89.0	Silty dolostone	4.2	−7.0
DH2-14-15.3	Krol B	89.3	Silty dolostone	4.4	−7.5
DH2-14-15.6	Krol B	89.6	Silty dolostone	4.1	−7.1
DH2-14-16	Krol B	90.0	Silty dolostone	3.7	−6.4
DH2-14-16.3	Krol B	90.3	Silty dolostone	3.7	−7.3
DH2-14-16.6	Krol B	90.6	Silty dolostone	3.9	−6.6
DH2-14-17	Krol B	91.0	Silty dolostone	3.7	−6.0
DH2-14-17.7	Krol B	91.7	Silty limestone	0.4	−5.0
DH2-14-18	Krol B	92.0	Silty limestone	1.7	−7.9
DH2-14-18.3	Krol B	92.3	Silty limestone	4.1	−6.7
DH2-14-18.6	Krol B	92.6	Silty limestone	1.1	−8.7
DH2-14-18.8	Krol B	92.8	Silty limestone	−1.6	−8.4
DH2-14-19	Krol B	93.0	Silty limestone	3.4	−10.3
DH2-14-19.3	Krol B	93.3	Silty limestone	2.6	−10.5
DH2-14-19.5	Krol B	93.5	Silty limestone	3.2	−10.7
DH2-14-19.8	Krol B	93.8	Silty limestone	2.9	−10.2
DH2-14-20	Krol B	94.0	Silty limestone	3.9	−10.2
DH2-14-20.3	Krol B	94.3	Silty limestone	3.8	−10.4
DH2-14-20.6	Krol B	94.6	Silty limestone	3.7	−10.4
DH2-14-21	Krol B	95.0	Silty limestone	3.7	−10.9
DH2-14-21.3	Krol B	95.3	Silty limestone	3.5	−9.0
DH2-14-21.5	Krol B	95.5	Silty limestone	3.5	−9.7
DH2-14-21.8	Krol B	95.8	Silty limestone	3.3	−9.2
DH2-14-22.2	Krol B	96.2	Silty limestone	3.3	−8.0
DH2-14-22.5	Krol B	96.5	Silty limestone	3.3	−7.4
DH2-14-22.8	Krol B	96.8	Dolomudstone	3.6	−6.6
DH2-14-23	Krol B	97.0	Dolomudstone	3.3	−7.5
DH2-14-23.5	Krol C	97.5	Dolomudstone	2.7	−6.7
DH2-14-24	Krol C	98.0	Dolomudstone	3.2	−7.8
DH2-14-25	Krol C	99.0	Dolomudstone	3.2	−7.8
DH2-14-25.5	Krol C	99.5	Lime mudstone	3.0	−7.6
DH2-14-26	Krol C	100.0	Lime mudstone	2.9	−8.2
DH2-14-26.5	Krol C	100.5	Lime mudstone	3.2	−8.4
DH2-14-27	Krol C	101.0	Lime mudstone	3.0	−8.2
DH2-14-28.5	Krol C	102.5	Lime mudstone	3.0	−8.3
DH2-14-29	Krol C	103.0	Lime mudstone	2.7	−6.6
DH2-14-29.5	Krol C	103.5	Lime mudstone	1.8	−6.7
DH2-14-30	Krol C	104.0	Lime mudstone	−0.3	−7.4
DH2-14-30.5	Krol C	104.5	Lime mudstone	1.5	−8.7
DH2-14-31	Krol C	105.0	Lime mudstone	3.3	−9.8
DH2-14-31.5	Krol C	105.5	Lime mudstone	0.9	−8.7
DH2-14-32	Krol C	106.0	Lime mudstone	2.6	−8.7
DH2-14-32.5	Krol C	106.5	Lime mudstone	3.2	−10.3
DH2-14-33	Krol C	107.0	Lime mudstone	3.6	−10.3
DH2-14-33.5	Krol C	107.5	Lime mudstone	2.9	−11.8
DH2-14-34	Krol C	108.0	Lime mudstone	3.8	−9.8
DH2-14-34.5	Krol C	108.5	Lime mudstone	3.1	−10.5
DH2-14-35	Krol C	109.0	Lime mudstone	3.8	−10.5
DH2-14-35.5	Krol C	109.5	Lime mudstone	3.4	−9.5
DH2-14-36	Krol C	110.0	Lime mudstone	2.1	−8.2
DH2-14-36.5	Krol C	110.5	Lime mudstone	2.7	−9.4
DH2-14-37	Krol C	111.0	Lime mudstone	4.3	−11.1
DH2-14-37.5	Krol C	111.5	Lime mudstone	4.4	−11.0

Table 2. Continued.

Sample	unit	height (m)	lithology	$\delta^{13}C$ (‰)	$\delta^{13}O$ (‰)
DH2-14-38	Krol C	112.0	Lime mudstone	3.6	−10.0
DH2-14-38.5	Krol C	112.5	Lime mudstone	3.7	−10.4
DH2-14-39	Krol C	113.0	Lime mudstone	2.4	−9.1
DH2-14-39.5	Krol C	113.5	Lime mudstone	3.2	−10.2
DH2-14-40	Krol C	114.0	Lime mudstone	3.5	−10.9
DH2-14-41	Krol C	115.0	Lime mudstone	3.1	−10.4
DH2-14-42	Krol C	116.0	Dolomudstone	3.3	−7.9
DH2-14-43	Krol C	117.0	Bituminous limestone	2.5	−6.7
DH2-14-44	Krol C	118.0	Bituminous limestone	2.4	−8.3
DH2-14-45	Krol C	119.0	Bituminous limestone	2.8	−7.1
DH2-14-46	Krol C	120.0	Bituminous limestone	3.0	−8.0
DH2-14-47	Krol C	121.0	Dolomudstone	2.9	−7.2
DH2-14-48	Krol C	122.0	Bituminous limestone	2.8	−7.8
DH2-14-49	Krol C	123.0	Bituminous limestone	2.8	−10.1
DH2-14-50	Krol C	124.0	Bituminous limestone	3.4	−10.8
DH2-14-51	Krol C	125.0	Bituminous limestone	2.4	−9.3
DH2-14-52	Krol C	126.0	Bituminous limestone	3.3	−10.1
DH2-14-53	Krol C	127.0	Bituminous limestone	3.4	−9.9
DH2-14-54	Krol C	128.0	Bituminous limestone	3.6	−10.3
DH2-14-55	Krol C	129.0	Bituminous limestone	3.9	−10.9
DH2-14-56	Krol C	130.0	Bituminous limestone	3.9	−9.8
DH2-14-57	Krol C	131.0	Bituminous limestone	3.8	−11.0
DH2-14-58	Krol C	132.0	Bituminous limestone	3.6	−10.4
DH2-14-59	Krol C	133.0	Bituminous limestone	2.5	−8.3
DH2-14-60	Krol C	134.0	Bituminous limestone	2.3	−7.4
DH2-14-61	Krol C	135.0	Bituminous limestone	3.4	−7.6
DH2-14-62	Krol C	136.0	Bituminous limestone	3.3	−7.9
DH2-14-63.0	Krol C	137.0	Bituminous limestone	3.8	−10.3
DH2-14-63.5	Krol C	137.5	Bituminous limestone	2.6	−10.5
DH2-14-64	Krol C	138.0	Bituminous limestone	3.2	−9.4
DH2-14-65	Krol C	139.0	Bituminous limestone	2.7	−8.1
DH2-14-66	Krol C	140.0	Lime mudstone	2.8	−7.9
DH2-14-67	Krol C	141.0	Lime mudstone	3.8	−11.1
DH2-14-68	Krol C	142.0	Lime mudstone	−0.3	−10.5
DH2-14-69	Krol C	143.0	Dolomudstone	2.1	−8.1

which are characterized by obtusely conical processes. Herkomorphs are represented by one species, *Dictyotidium grazhdankinii* Xiao n. sp., whose abundance is likely overestimated because some heavily degraded leiospheres may be misidentified as this species.

Taxonomic identification among species in the first two groups of acanthomorphs can be challenging, particularly when specimens are poorly preserved. Among the four species that have thin and short processes, *Cymatiosphaeroides forabilatus* is differentiated from the other species by its outer membrane, *Mengeosphaera gracilis* by its proportionally larger basal expansion relative to the apical spine, *Appendisphaera clava* by its small basal expansion and relatively long apical spine, and *A. tenuis* by its minute basal expansion or lack thereof. However, organic degradation and crystal growth can produce artifacts that resemble a basal expansion, taphonomic accumulation of organic material at the tip of processes with a uniform length can mimic an outer membrane, or the diaphanous outer membrane may be lost during diagenesis. In these cases, taxonomic identification relies on the consistency of morphological features (e.g., whether an outer membrane is continuous around the vesicle, whether a basal expansion is consistently present in most processes, and whether processes consistently penetrate the outer membrane, as in *C. forabilatus*). Still, many specimens have to be classified as unidentifiable (Table 3, Fig. 29, and many more that were not counted because of their poor preservation).

Similarly, among the four acanthomorph species with thin and long processes, *Appendisphaera*? *hemisphaerica* is unique in having clearly biform processes, a feature that belies its placement in the genus *Appendisphaera* (Liu et al., 2014a). The processes in *A. grandis* and *A. longispina* can have a basal expansion, but an inflection point is not apparent, thus these are not technically considered biform (see Fig. 24). The processes in *A. setosa* are largely cylindrical, without a basal expansion. The taxonomic identification of the rest of Krol A acanthomorphs—including *Tanarium digitiforme*, *T.* cf. *T. conoideum*, *Weissiella brevis*, *Asterocapsoides sinensis*, and *Cavaspina tiwariae* Xiao—is relatively straightforward, and their diagnostic features are schematically illustrated in Figure 29.

In addition to ornamented acritarchs, there are a number of sphaeromorphs in the Krol samples (several examples are illustrated in Fig. 30). Of importance are *Osculosphaera arcelliformis* Liu et al., 2014 (Fig. 30.4) and *Schizofusa zangwenlongii* Grey, 2005 (Fig. 30.5, 30.6). The former has been known previously from the Tonian Svanbergfjellet Formation in Svalbard (Butterfield et al., 1994) and the upper Doushantuo Formation (member III) at Wangfenggang, Xiaofenghe, and Niuping sections in the Yangtze Gorge area (Liu et al., 2014a). The latter species is an eponymous species of the second acritarch biozone (i.e., the *Tanarium tuberosum-Schizofusa zangwenlongii* Assemblage Zone) in the lower Doushantuo Formation of the Yangtze Gorges area (Liu and Moczydłowska, 2019).

To highlight their biostratigraphic significance of Krol A acritarchs, the stratigraphic occurrence and abundance of selected taxa—including all acanthomorphs, the herkomorph species *Dictyotidium grazhdankinii* Xiao n. sp., and the

Table 3. Summary of occurrence and abundance data for acanthomorphs, herkomorphs, and selected sphaeromorphs from the Krol A Formation. Number of specimens from each fossiliferous horizon is reported, with empty cells representing absence. A* = acanthomorphs; H* = herkomorphs; S* = sphaeromorphs. The abundance of *Dictyotidium grazhdankinii* Xiao n. sp. is probably an overestimate because poorly preserved sphaeromorphs may be mistakenly identified as this species. The abundance of unidentifiable acanthomorphs is likely underestimated because poorly preserved specimens may not be counted or photographed.

Sample number	Estimated stratigraphic height (m)	*Appendisphaera clava* A*	*Appendisphaera grandis* A*	*Appendisphaera? hemisphaerica* A*	*Appendisphaera longispina* A*	*Appendisphaera setosa* A*	*Appendisphaera tenuis* A*	*Asteroceapsoides sinensis* A*	*Cavaspina tivariae* n. sp. A*	*Cymatiosphaeroides forabilatus* A*	*Dictyotidium grazhdankinii* n. sp. H*	*Mengeosphaera gracilis* A*	*Tanarium* cf. *T. conoideum* A*	*Tanarium digitiforme* A*	*Weissiella brevis* A*	*Schizofusa zangwenlongii* S*	Unidentifiable acanthomorphs A*	subtotal
DH-14-52.6	52.6																	
DH-14-58.3	58.3																	
DH-14-60.6	60.6																	
DH-14-63.2	63.2																	
DH-14-64.1	64.1																	
DH-14-65.0	65.0	6	2			1		2	1	1	1			1			4	19
DH-14-66.0	66.0	1	3	4	2	1	1				6							25
DH-14-67.0	67.0	8	2	6	9		7			5	5	3					3	41
DH-14-68.0	68.0	5	3	1	1		5			1	4			1	1	1	13	36
DH2-14-3.1	77.1																	
DH2-14-3.7	77.7																	
DH2-14-4.3	78.3																	
DH2-14-7.1	81.1																	
S4-4-F1	77.1	8	1	1			3					2					3	18
S4-4-F2	77.7	31	9	12	5	2	20			24	16	2	1				13	135
S4-4-F3	78.3																	
subtotal		59	20	24	17	4	36	2	1	31	32	7	1	2	1	1	36	274
Grand total																		

sphaeromorph species *Schizofusa zangwenlongii*—are presented in Table 3 and plotted in Figure 3 along with $\delta^{13}C$ and $\delta^{18}O$ data.

Like many other Ediacaran chert nodules, the Krol A samples contain abundant coccoidal and filamentous taxa that are traditionally regarded as cyanobacteria. Filamentous microfossils of the form genus *Siphonophycus* Schopf, 1968, are the most abundant fossils in the Krol A, many of which are preserved in rip-up fragments of microbial mats (Fig. 31.1–31.4). Another common form is *Salome hubeiensis* Zhang, 1986 (Fig. 31.5, 31.6), which was first reported from, and is widely present in, the Doushantuo Formation (e.g., Zhang et al., 1998; Xiao, 2004b). Other filamentous forms include *Botominella lineata* Reitlinger, 1959 (Fig. 32.1, 32.2), *Obruchevella* sp. (Fig. 32.3, 32.4), *Oscillatoriopsis breviconvexa* Schopf and Blacic, 1971 (Fig. 32.5–32.7), and *Polytrichoides lineatus* Hermann, 1974 (Fig. 32.8, 32.9). These filamentous forms are common, but they have very long stratigraphic ranges and thus have limited biostratigraphic significance.

Finally, confirming previous reports (e.g., Shukla et al., 2008), we have identified a number of multicellular algae from the Krol A chert nodules. Identification of three-dimensionally silicified multicellular algae in thin sections is a challenge (Zhang et al., 1998; Xiao et al., 2004). Nonetheless, several taxa are recognizable on the basis of their cell arrangement patterns. For example, closely arranged and nested cell packets are identified as *Sarcinophycus radiatus* Xiao and Knoll, 1999 (Fig. 33.1), spherical thalli with compact parenchymatous cells are regarded as *Wengania minuta* Xiao, 2004 (Fig. 33.2) and *W. exquisita* Zhang et al., 1998 (Fig. 33.5–33.6), and pseudoparenchymatous thalli consisting of linearly aligned cells but without a well-defined cortex-medulla differentiation are identified as *Thallophycoides phloeatus* Zhang and Yuan, 1992 (Fig. 33.3, 33.4). These taxa have been reported previously from the Doushantuo Formation in South China (Zhang, 1989; Zhang and Yuan, 1992; Zhang et al., 1998; Xiao, 2004b; Xiao et al., 2004; Liu et al., 2014a; Shang et al., 2019; Ouyang et al., 2021). It is worth mentioning that *W. exquisita* also has been reported from phosphorite of the Ediacaran Birmania Formation in Rajasthan of western India (Hughes et al., 2015), and multicellular algal fossils have been reported previously from the Infra-Krol Formation (Tiwari and Pant, 2004) and the approximately equivalent Chambaghat Formation in the western Krol Belt (Shukla et al., 2005a), as well as from the Krol C Formation in the Garhwal syncline of the Krol Belt (Singh and Rai, 2013). Currently available data seem to indicate that, although these multicellular algal taxa have important implications for the evolution of multicellularity, they have long stratigraphic ranges and thus are not useful in refining Ediacaran biostratigraphy.

Discussion

Chemostratigraphic correlation.—The overall $\delta^{13}C$ and $\delta^{18}O$ values of the Krol A–Krol C interval are within the range of isotope values of early–middle Ediacaran strata at other sections of the Krol Belt (Kaufman et al., 2006). However, the negative $\delta^{13}C$ excursion at the Krol B-C transition from other sections (Kaufman et al., 2006) is not well displayed in the

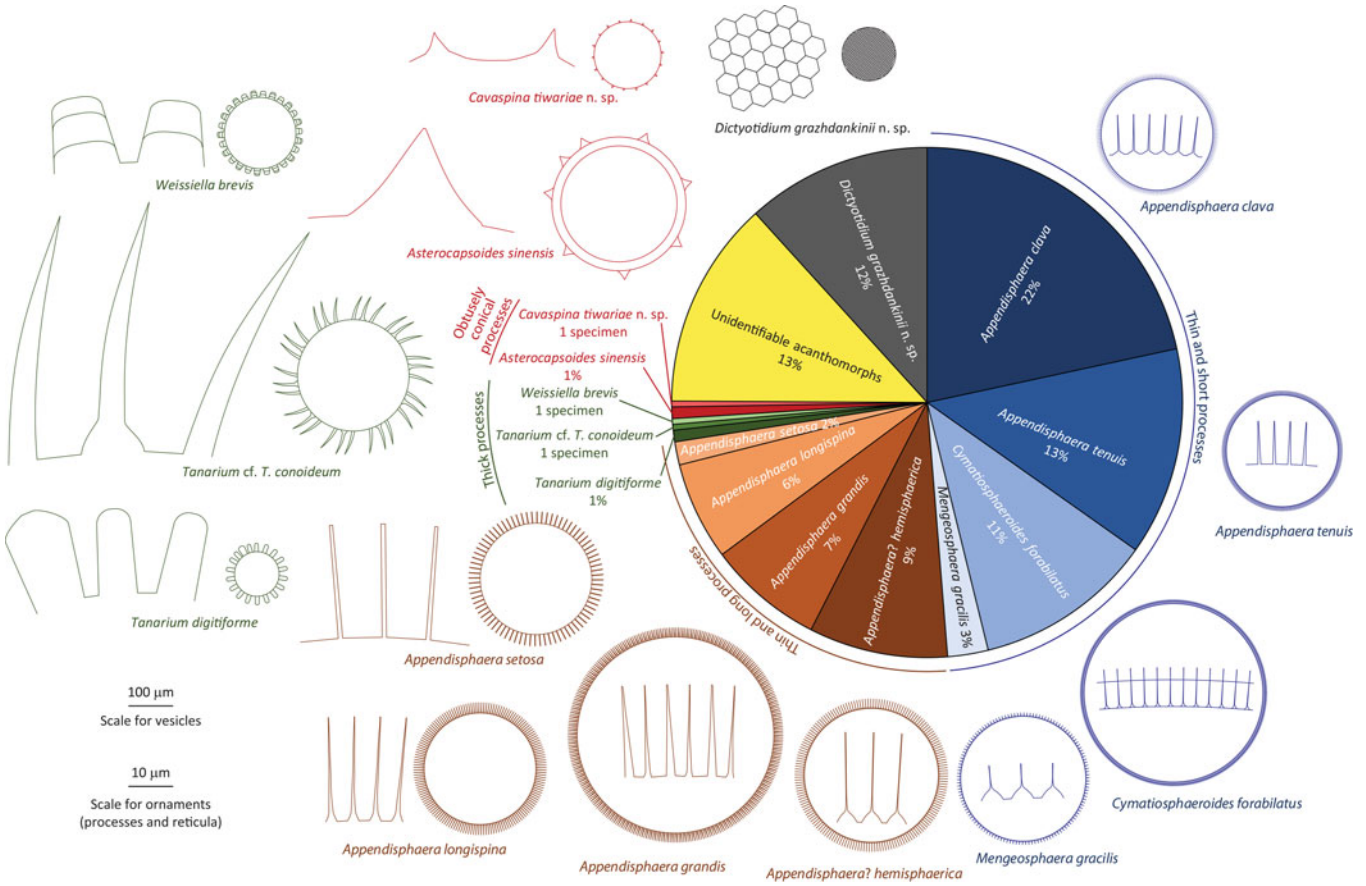

Figure 29. Pie diagram showing relative abundance of acanthomorphic and herkomorphic taxa from the Krol A Formation. The four acanthomorph groups, as discussed in the text, are color coded (blue, thin and short processes; brown, thin and long processes; green, large and thick processes; red, obtuse processes) to show that the assemblage is dominated by acanthomorphs with thin processes. Schematic diagrams denoting the vesicle size and ornament morphology are shown. Note that scales are different for vesicles and ornaments (processes in acanthomorphs and reticula in herkomorphs).

section analyzed in this study. The potential cause could be that the upper part of Krol B Formation is truncated in the current section, as evinced by the presence of a sandstone layer at the top of the Krol B Formation. The negative $\delta^{13}C$ excursion from the lower Krol A was not documented in previous studies due to the lack of exposure, although a few negative $\delta^{13}C$ values at the transition from Krol Sandstone to the Krol A Formation and its correlative interval were reported in Kaufman et al. (2006). Negative $\delta^{13}C$ values of the lower Krol A correspond with $\delta^{18}O$ values consistently around −4‰ (Fig. 3.3), implying either that the $\delta^{18}O$ values have not been significantly modified by diagenesis or that diagenesis may have uniformly reset the $\delta^{18}O$ values to −4‰. The latter is more likely, considering the more variable $\delta^{18}O$ values of Krol B and Krol C in the same section and the very low $\delta^{13}C$ values down to −15‰ in the lower Krol A. Therefore, even though we consider that the negative shift in $\delta^{13}C$ in the lower Krol A may represent a real chemostratigraphic excursion, the magnitude of this excursion may have been exaggerated by diagenetic alteration.

In combination with previously published isotope data from the Krol Belt (Kaufman et al., 2006; Etienne et al., 2011), we construct a composite $\delta^{13}C$ curve for the Ediacaran strata (Infra-Krol–Krol C) of the Krol Belt and propose a correlation with the $\delta^{13}C$ record of the Doushantuo and Dengying formations in the Yangtze Platform (Fig. 34). Accepting Kaufman et al.'s (2006) correlation of the negative $\delta^{13}C$ excursions at Krol B-C and upper Doushantuo Formation (EN3, which is widely regarded as equivalent to the Shuram negative $\delta^{13}C$ excursion, Jiang et al., 2007; McFadden et al., 2008), the negative $\delta^{13}C$ excursion in the lower Krol A is most parsimoniously correlated with the negative $\delta^{13}C$ excursion EN2 in the uppermost member II of the Doushantuo Formation in the Yangtze Gorges area in South China (Fig. 34). This chemostratigraphic correlation can illuminate and be further tested by biostratigraphic correlation.

Biostratigraphic correlation.—In this section, we consider possible biostratigraphic correlation between the Krol Group in the Lesser Himalaya and the Doushantuo Formation in the Yangtze Gorges area. Biostratigraphic investigations of the early–middle Doushantuo Formation in the Yangtze Gorges area in the past four decades (e.g., Yin and Li, 1978; Zhang et al., 1998; Zhou et al., 2007; McFadden et al., 2009; Yin et al., 2009; Xiao et al., 2012; Liu et al., 2013, 2014a, b; Liu and Moczydłowska, 2019; Ouyang et al., 2021) have established a foundation for acritarch-based biostratigraphy. Earlier studies of Doushantuo acritarchs led to the recognition of two biozones separated by the negative $\delta^{13}C$ excursion

Table 4. Summary of measurements of acanthomorphs, herkomorphs, and selected sphaeromorphs from the Krol A Formation.

					process morphologies														
group	species	vesicle diameter (μm)	outer membrane	inner membrane	density (#/100 μm unless otherwise indicated)	basal spacing (μm)	total length (μm)	length as % of vesicle diameter	biform	basal width (μm)	conical base height (μm)	apical spine max width (μm)	apical spine length (μm)	distal truncation	internal tabulae	cross-walls per process	Cross-wall spacing (μm)	reticulum diameter (μm)	ridge thickness (μm)
1	*Appendisphaera clava*	likely >200	N	N	19–34	1–3	4–10	<5% (?)	Y	2–3	1–2	0.5	2–10	N	N				
	Appendisphaera tenuis	265–364	N	N	22–33	2–4	7–12	2–3	N	0.7–0.9				N	N				
	Cymatiosphaeroides forabilatus	315–430	Y	N	28–41	0.6–2.8	6–10	1.5–2.4	some	0.3–2	1–2 (when discernable)	0.5–0.9	5–7	N	N				
	Mengeosphaera gracilis	280	N	N	13–18	1–3	6–14	5	Y	4–6	3–4	1	4–10	N	N				
2	*Appendisphaera grandis*	440	N	N	15–50	0–1.4	17–21	5% (?)	some	0.5 (cylindrical processes)	3–4 (when discernable)	0.5	12–17	N	N				
	Appendisphaera? *hemisphaerica*	~300	N	N	13–21	1–3	12–29	4–6	Y	3–6	2–4	1	7–25	N	N				
	Appendisphaera longispina	250–300	N	N	16–24	0–2	21–32	~10	Y	3–5	2–5	1	19–30	N	N				
	Appendisphaera setosa	~250	N	N	9–12	7–18	19–29	11	N	1.3–1.8				N	N				
3	*Tanarium* cf. *T. conoideum*	247	N	N			60	24	some	14	8	4	45	N	N				
	Tanarium digitiforme	up to 144	N	N	5	9	19–22	19	N	13–17				N	N				
	Weissiella brevis	160	N	N	6–7	3	15	10	N	15				Y	Y	1–2	6		
4	*Asterocapsoides sinensis*	300–400	N	Y	9 per circumference	12 or more	20–40	5–14	N	30				N	N				
	Cavaspina tiwariae n. sp.	156	N	N	<20 per circumference	19–28 (apical spacing)	5	3	N	8				N	N				
	Dictyotidium grazhdankinii n. sp.	100–400	N	N														1–5	0.2–1
	Schizofusa zangwenlongii	196																	

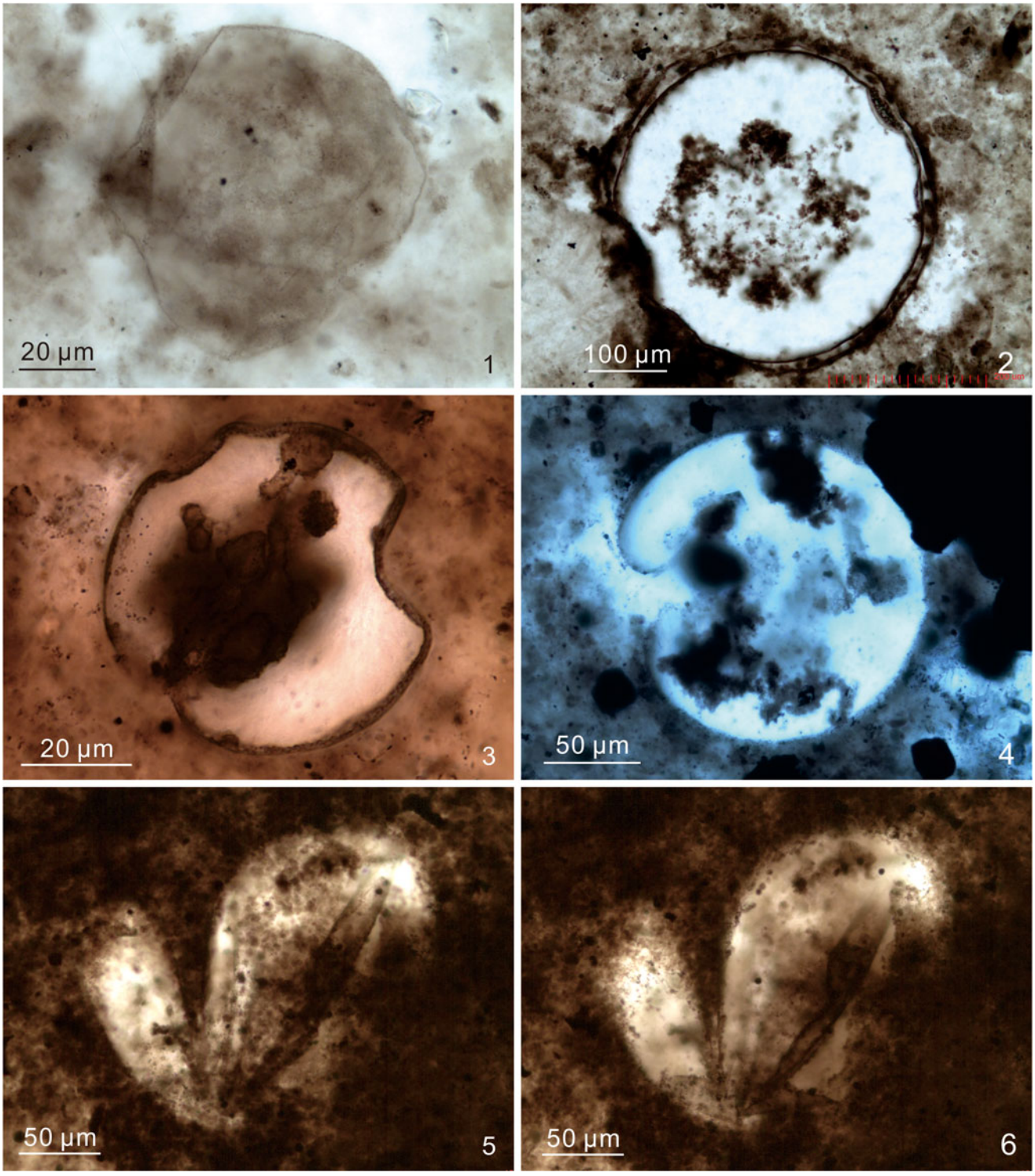

Figure 30. Representative sphaeromorphs. (**1**) *Leiosphaeridia tenuissima* Eisenack, 1958, S4-4-F2-7, 13.0 × 137.1, EF-P37-3, VPIGM-4892; (**2**) *Leiosphaeridia jacutica* (Timofeev, 1966) Mikhailova and Jankauskas in Jankauskas et al., 1989, S4-4-F2-7, 7.3 × 136.1, EF-V36-1, VPIGM-4893; (**3**) *Leiosphaeridia crassa* (Naumova, 1949) Jankauskas in Jankauskas et al., 1989, DH-14-65.0-D-2, 15.2 × 127.8, EF-N27-2, VPIGM-4838; (**4**) *Osculosphaera arcelliformis* Liu et al., 2014, DH-14-64.1-C, 13.5 × 137.2, EF-O37-1/3, VPIGM- 4829; (**5, 6**) *Schizofusa zangwenlongii* Grey, 2005, DH-14-68.0-A-2, 15.2 × 130.8, EF-N30-4, VPIGM-4861, same specimen at different focal levels, showing asymmetrical split and elongate folds.

EN2 (McFadden et al., 2008, 2009; Yin et al., 2009; Liu et al., 2014a; Xiao et al., 2014). These two biozones (the *Tianzhushania spinosa* biozone in member II and the *Tanarium conoideum-Hocosphaeridium scaberfacium-H. anozos* biozone in member III of the Doushantuo Formation) were vaguely understood as acme biozones characterized by the abundant occurrence of the eponymous species (Xiao et al., 2014). However, Liu et al. (2014a) indicated that the

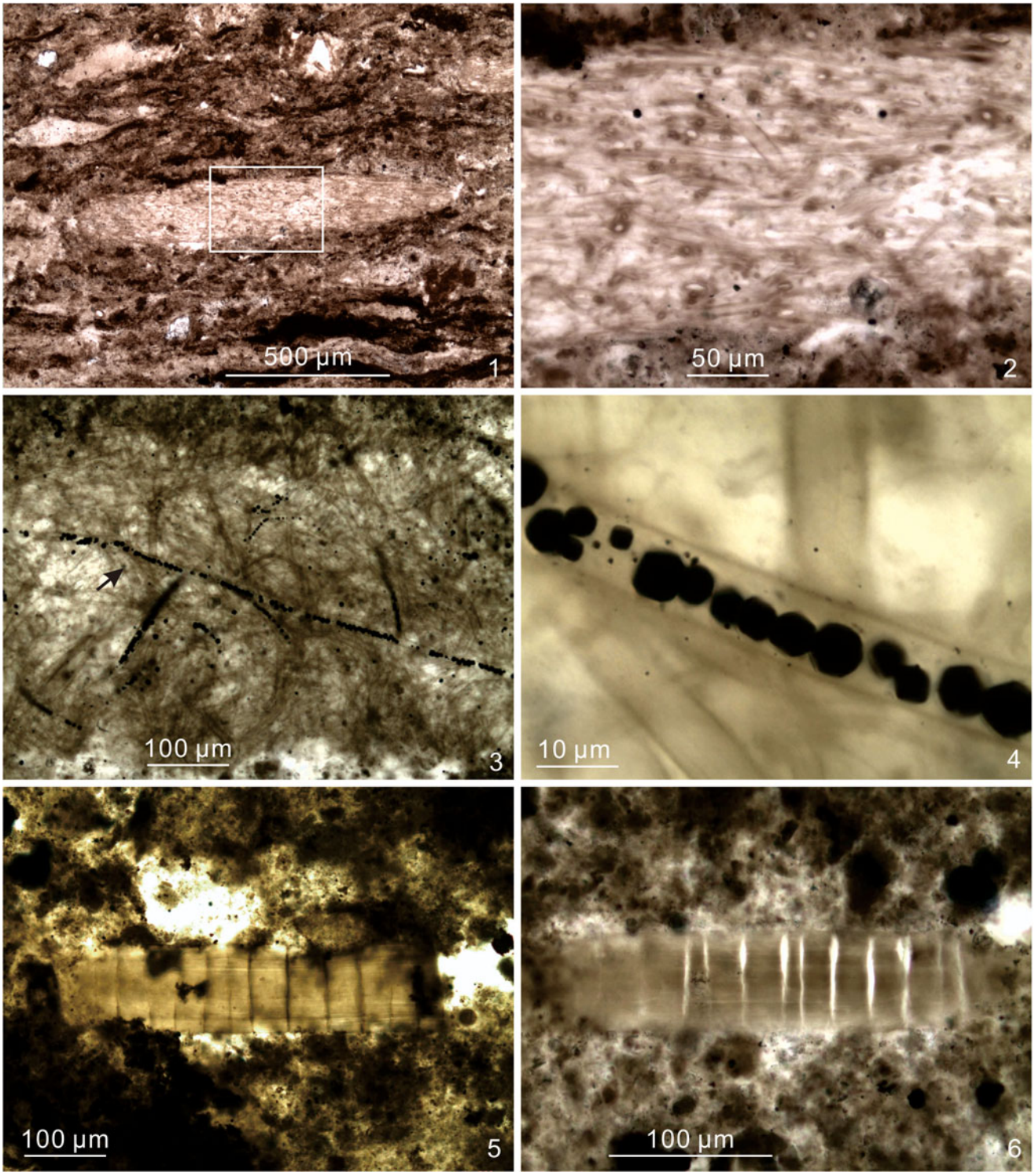

Figure 31. Filamentous microfossils. (**1, 2**) Fragments of microbial mat consisting of entangled sheaths of *Siphonophycus* spp., DH-14-65.0-B-2, 18.5 × 117.5, EF-J17, VPIGM-4836, rectangle in (**1**) marks area magnified in (**2**); (**3, 4**) fragment of microbial mat with *Siphonophycus* filaments, some of which are partially pyritized, S4-4-F2-5-A, 15.1 × 121.0, EF-N21-1, VPIGM-4903, arrow in (**3**) marks area magnified in (**4**); (**5, 6**) *Salome hubeiensis* Zhang, 1986; (**5**), S4-4-F2-7-A, 21.1 × 132.2, EF-F32-3, VPIGM-4905; (**6**), S4-4-F2-14-A, 9.6 × 129.9, EF-S30-1, VPIGM-4909.

lower boundaries of these two biozones could be defined by the first occurrence of *T. spinosa* in member II and *H. anozos* in member III, respectively. Subsequent investigation revealed that the four eponymous species have overlapping stratigraphic ranges; for example, *T. conoideum* and *H. anozos* are found co-occurring with *T. spinosa* in the Doushantuo Formation at Weng'an in South China (Xiao et al., 2014), and both *H. scaberfacium* Zang in Zang and Walter, 1992, and *H. anozos* (Willman in Willman and Moczydłowska, 2008) Xiao et al., 2014, extend down-section to member II of the Doushantuo

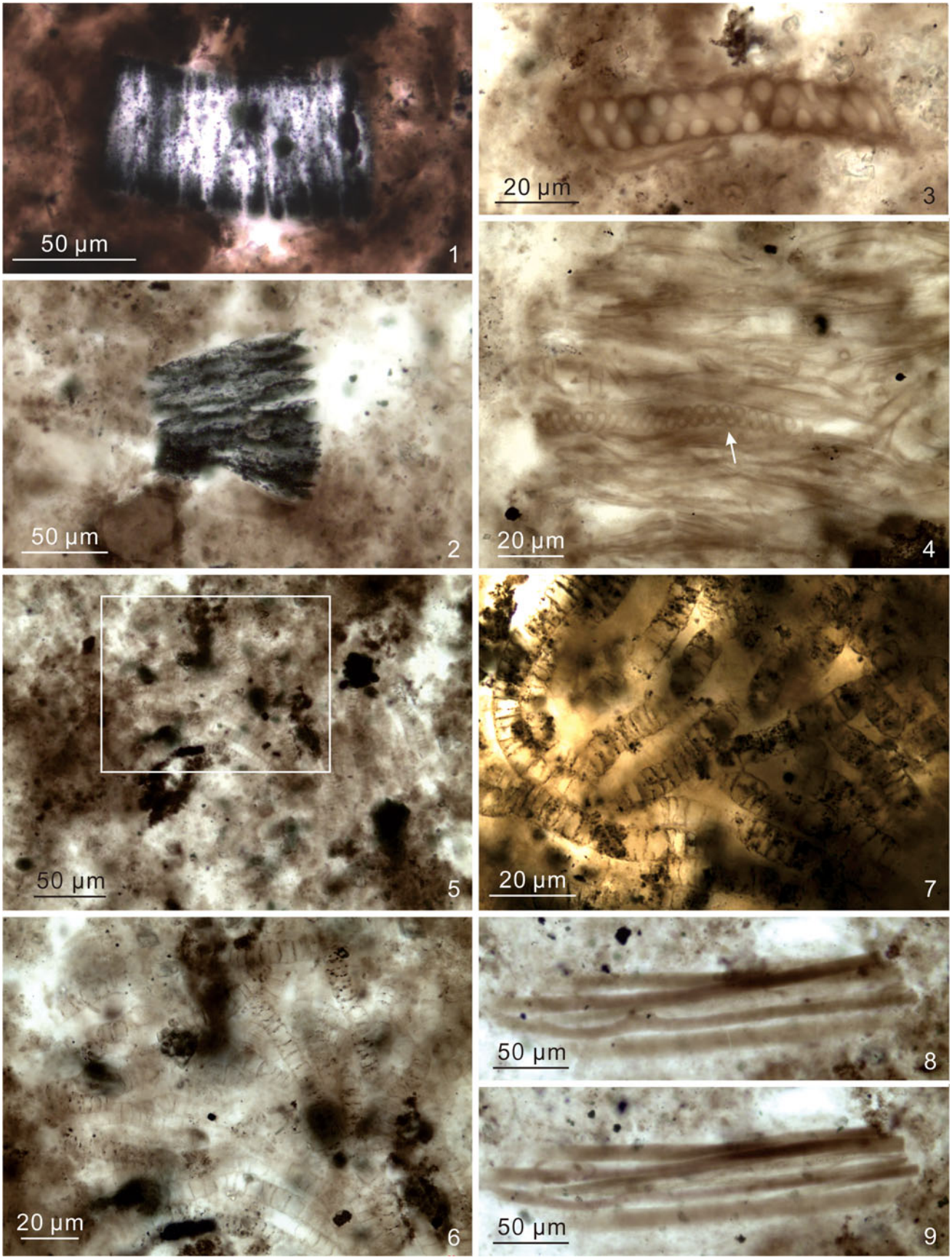

Figure 32. Filamentous microfossils. (**1, 2**) Carbonized filaments identified by Sharma et al. (2021) as *Botominella lineata* Reitlinger, 1959; (**1**), DH-14-65.0-B, 18.6 × 107.0, EF-J7-3, VPIGM-4835; (**2**), DH-14-68.0-A-2, 4.5 × 116.2, EF-Y16-1, VPIGM-4862; (**3**) *Obruchevella* sp., S4-4-F2-5, 12.5 × 109.5, EF-Q9-2, VPIGM-4877; (**4**) *Obruchevella* sp. (arrow) and *Siphonophycus* spp., DH-14-68.0-B-2, 14.5 × 118.5, EF-O18-2, VPIGM-4866; (**5–7**) *Oscillatoriopsis breviconvexa* Schopf and Blacic, 1971; (**5, 6**), S4-4-F2-7, 11.1 × 110.8, EF-R11-3, VPIGM-4891, rectangle in (**5**) marks area magnified in (**6**); (**7**), DH-14-68.0-A, 12.0 × 131.2, EF-Q31-1, VPIGM-4860; (**8, 9**) *Polytrichoides lineatus* Hermann, 1974, S4-4-F2-5, 8.9 × 129.3, EF-T29-4, VPIGM-4880, same specimen at different levels, showing bundled filaments.

Formation (Hawkins et al., 2017; Liu and Moczydłowska, 2019; Liu et al., 2021). Thus, the two biozones cannot be used in the sense of range biozone, and the concept of acme biozone is difficult to apply here because abundance data are not always available and also because of arbitrary nature of defining an acme biozone. The problem is further complicated by the general lack of acritarchs at the member II-III transition (barren interval) that hosts the negative $\delta^{13}C$ excursion EN2 and separates the two vaguely defined acme biozones.

In a recent attempt to clarify the acritarch biostratigraphy of the Doushantuo Formation, Liu and Moczydłowska (2019) proposed four assemblage zones, in ascending order: (a) *Appendisphaera grandis-Weissiella grandistella-Tianzhushania spinosa* Assemblage Zone, (b) *Tanarium tuberosum-Schizofusa zangwenlongii* Assemblage Zone, (c) *Tanarium conoideum-Cavaspina basiconica* Assemblage Zone, and (d) *Tanarium pycnacanthum-Ceratosphaeridium glaberosum* Assemblage Zone. The lower boundary of each assemblage zone is defined by the first joint appearance of the eponymous species (plural), although the upper boundary of the fourth assemblage zone has not been defined. The first three assemblage zones occur in member II of the Doushantuo Formation, and together they are roughly equivalent to the *Tianzhushania spinosa* biozones recognized by earlier authors. The fourth assemblage zone, which is separated from the third assemblage zone by EN2 and a barren interval, occurs in member III of the Doushantuo Formation and is roughly equivalent to the *T. conoideum-H. scaberfacium-H. anozos* biozone of previous authors.

One challenge in the application of these assemblage zones is that several eponymous species appear to have very long stratigraphic ranges. For example, if the Semri Group of the lower Vindhyan Supergroup in the Chambal Valley of eastern Rajasthan (India) is proven to be Paleo-/Mesoproterozoic (see Hughes, 2017, for further discussion), then at least five of the nine eponymous species (*Appendisphaera grandis*; *Cavaspina basiconica*; *Ceratosphaeridium glaberosum* Grey, 2005; *Tanarium conoideum*; and *T. tuberosum*) and the *Tanarium conoideum-Cavaspina basiconica* Assemblage Zone of Liu and Moczydłowska (2019) would extend to the Paleo-/Mesoproterozoic because these species have all been reported from the Semri Group (Prasad and Asher, 2016). The same can also be said of several eponymous species (*Ceratosphaeridium glaberosum*; *Gyalosphaeridium pulchrum* Zang in Zang and Walter, 1992; *Schizofusa risoria* Grey, 2005; and *Tanarium conoideum*) of the Australian acanthomorph assemblage zones established by Grey (2005). This problem highlights the importance of an independent assessment of the depositional age of the Semri Group in the Chambal Valley, as well as a critical re-examination of the Semri acanthomorphs. Additionally, the long stratigraphic ranges of certain eponymous taxa (e.g., *Appendisphaera grandis*, *Cavaspina basiconica*, *Ceratosphaeridium glaberosum*, and *Tanarium conoideum*) is apparent because of their potential presence in upper Ediacaran–lower Cambrian strata (Ouyang et al., 2017; Anderson et al., 2019; Grazhdankin et al., 2020) (see also Golubkova et al., 2015, although Vorob'Eva et al., 2009, assigned a middle Ediacaran age to the Keltma acanthomorph assemblage in the Timan Ridges of Baltica).

An additional challenge is related to the fact that the assemblage zones of Liu and Moczydłowska (2019) are each defined at the base by the joint first appearance of multiple eponymous species. If only one of the eponymous species is found and it happens to be a long-ranging taxon, it does not necessarily indicate a correlation with an assemblage zone bearing its name because this species can occur considerably below or above, particularly when the eponymous species (plural) that are used in combination to define the assemblage zone have drastically different first appearances. This problem can be exacerbated by stratigraphic condensation and cryptic unconformities, which may be the case in parts of the Doushantuo Formation (Liu and Moczydłowska, 2019).

On the other hand, Ouyang et al. (2021) have demonstrated that some eponymous species of Liu and Moczydłowska's (2019) assemblage zones do have consistent first appearance data in member II of the Doushantuo Formation in the Yangtze Gorges area. For example, *Tianzhushania spinosa*, *Appendisphaera grandis*, and *Weissiella brevis* tend to first appear near the base of member II of the Doushantuo Formation. Thus, barring the unresolved issue related to the age of the Semri Group, it is possible that the eponymous species chosen to define an assemblage zone may actually have first appearance data close to each other. If so, the presence of a single eponymous species is still useful biostratigraphic information, even if it may range up-section to a younger assemblage zone. In other words, the presence of a single eponymous species may be taken as a maximum age estimate as defined by the assemblage zone bearing its name. It is under this assumption that a biostratigraphic correlation between the Lesser Himalaya and the Yangtze Gorges area is made (Fig. 34).

The biostratigraphic correlation between the Lesser Himalaya and the Yangtze Gorges area is built on the common occurrence of numerous acritarch species, including several zonal taxa (Fig. 34). The presence of *Tianzhushania spinosa* and *T. polysiphonia* in the Infra-Krol Formation (Joshi and Tiwari, 2016) and the apparent absence of taxa indicative of the *Tanarium tuberosum-Schizofusa zangwenlongii* Assemblage Zone (Table 1), as well as the stratigraphic proximity between the Infra-Krol Formation and the basal Ediacaran cap dolostone, indicate a correlation with the *Appendisphaera grandis-Weissiella grandistella-Tianzhushania spinosa* Assemblage Zone in the Yangtze Gorges area. The presence of *Schizofusa zangwenlongii* in the Krol A Formation (this paper) invites a correlation with the *Tanarium tuberosum-Schizofusa zangwenlongii* Assemblage

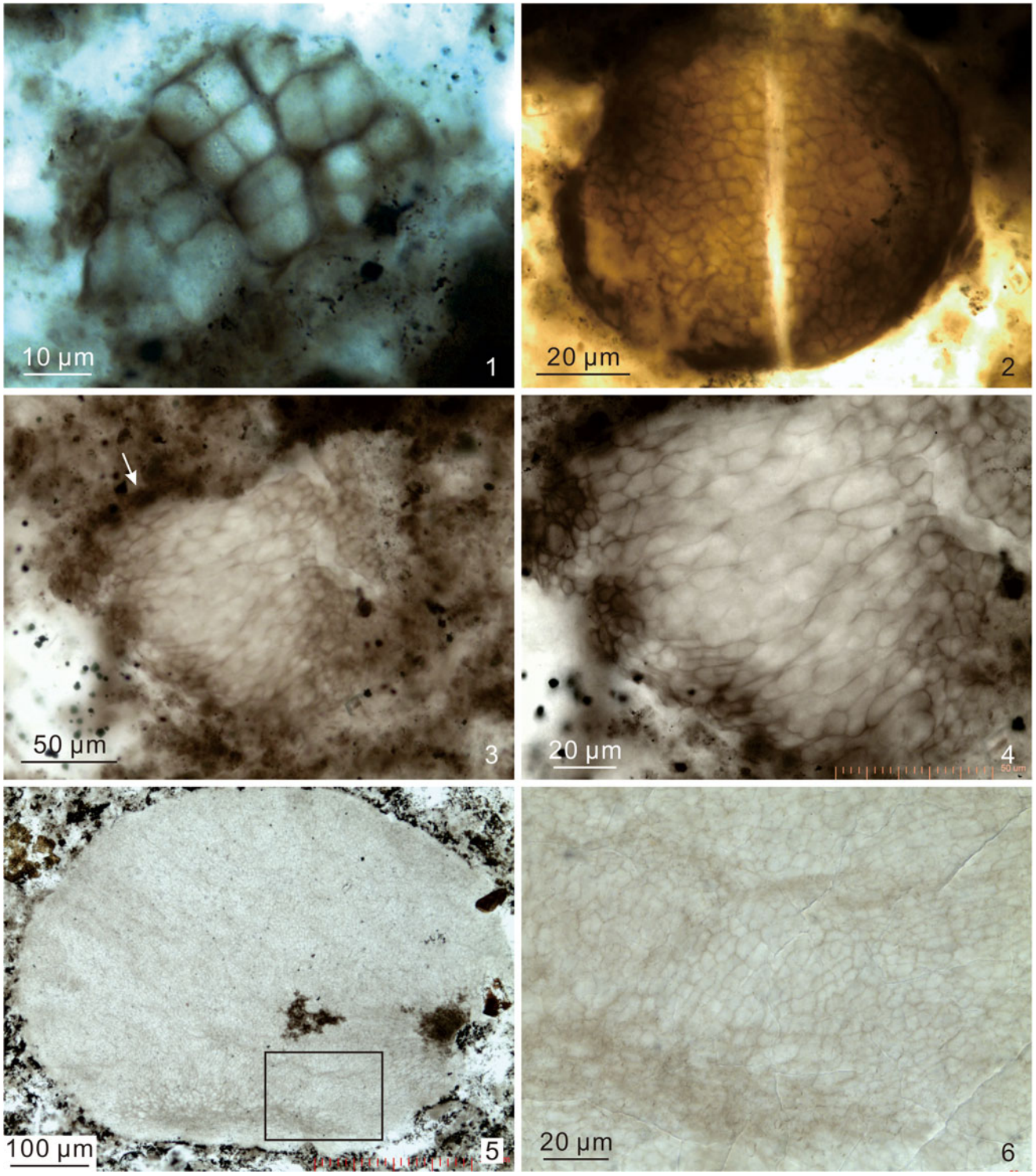

Figure 33. Multicellular algae. (**1**) *Sarcinophycus radiatus* Xiao and Knoll, 1999, DH-14-52.6-B, 13.6 × 120.5, EF-O20-2, VPIGM-4828; (**2**) *Wengania minuta* Xiao, 2004, S4-4-F2-13-A, 11.8 × 127.0, EF-Q26-4, VPIGM-4908; (**3, 4**) *Thallophycoides phloeatus* Zhang and Yuan, 1992, DH-14-68.0-A-2, 7.3 × 112.0, EF-V12, VPIGM-4863, arrow in (**3**) marks area magnified in (**4**); (**5, 6**) *Wengania exquisita* Zhang et al., 1998, S4-4-F2-5, 24.1 × 102.7, EF-D3-3, VPIGM-4879, rectangle in (**5**) marks area magnified in (**6**).

Zone or higher. Considering that *Schizofusa zangwenlongii* is actually more common in Doushantuo strata above the *Tanarium tuberosum-Schizofusa zangwenlongii* Assemblage Zone (Liu and Moczydłowska, 2019), that *Tanarium* cf. *T. conoideum* from the Krol A Formation (Fig. 26) may actually be *T. conoideum*, and that the negative $\delta^{13}C$ excursion in the lower Krol A Formation is correlated with EN2 in uppermost member II of the Doushantuo Formation, the Krol A assemblage is more likely

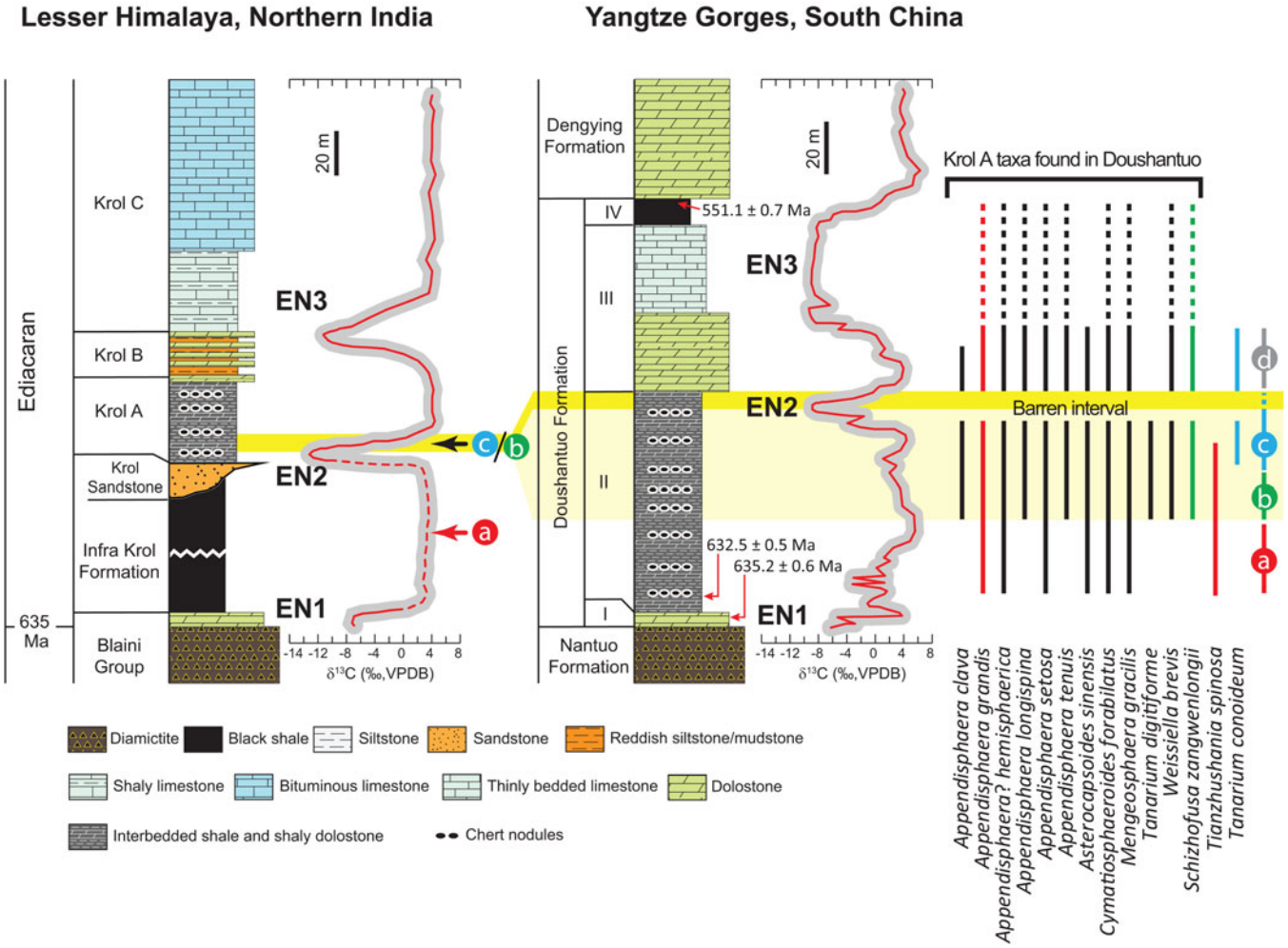

Figure 34. Integrated $\delta^{13}C$ chemostratigraphic and acritarch biostratigraphic correlation between Lesser Himalaya (northern India) and Yangtze Gorges area (South China). The $\delta^{13}C$ curve of Lesser Himalaya is summarized from Kaufman et al. (2006) and Etienne et al. (2011; cap dolostone data), supplemented by new data from this study (Fig. 3.2; Table 2). Note that the thickness of the Infra-Krol Formation is not fully drawn because no carbonate $\delta^{13}C$ data are available (dashed curve). The $\delta^{13}C$ curve of the Yangtze Gorges area is summarized from Jiang et al. (2007) and McFadden et al. (2008). Zircon U-Pb ages of the Doushantuo Formation are from Condon et al. (2005). Black and red arrows mark approximate stratigraphic horizons of, respectively, Krol A microfossils reported in this paper and the occurrence of *Tianzhushania spinosa* and *T. polysiphonia* in the Infra-Krol Formation reported by Joshi and Tiwari (2016). Solid vertical lines show approximate stratigraphic range of selected acritarch taxa in the Doushantuo Formation (see occurrence information in Systematic Paleontology; Liu et al., 2014a; Liu and Moczydłowska, 2019). It is uncertain whether acanthomorphs from Liujing in Guizhou Province (Shang et al., 2019) belong to member II (based on biostratigraphic correlation advocated in this paper) or upper member III to member IV of the Doushantuo Formation (based on lithostratigraphic correlation); the latter scenario is represented in the dashed vertical lines. Important zonal taxa are color coded according to the four acritarch assemblage zones recognized in the Yangtze Gorges area of South China (Liu and Moczydłowska, 2019): (a) *Appendisphaera grandis-Weissiella grandistella-Tianzhushania spinosa* Assemblage Zone; (b) *Tanarium tuberosum-Schizofusa zangwenlongii* Assemblage Zone; (c) *Tanarium conoideum-Cavaspina basiconica* Assemblage Zone; (d) *Tanarium pycnacanthum-Ceratosphaeridium glaberosum* Assemblage Zone. Note that all Krol A acritarch species, except new and open-nomenclature taxa, are also present in the Doushantuo Formation. Light yellow band, which includes the dark yellow band, represents permissive correlation between the fossiliferous lower Krol A Formation and the upper member II of the Doushantuo Formation in the Yangtze Gorges area based on biostratigraphic data. Dark yellow band denotes preferred correlation based on integrative chemo- and biostratigraphic data. See text for details.

correlated with the *Tanarium conoideum-Cavaspina basiconica* Assemblage Zone. Insofar as the Krol A assemblage is associated with the rising arm of a negative $\delta^{13}C$ excursion that is equivalent to EN2, it also fills a gap represented by a barren interval in the Yangtze Gorges area (Liu and Moczydłowska, 2019), where direct association of acanthomorphs and EN2 has not been documented due to the lack of fossiliferous chert nodules in this interval (McFadden et al., 2009). This correlation predicts that the second and fourth assemblage zones (i.e., the *Tanarium tuberosum-Schizofusa zangwenlongii* and *Tanarium pycnacanthum-Ceratosphaeridium glaberosum* assemblage zones) should be recorded, respectively, below and above the chert nodule interval of the lower Krol A Formation sampled in this study. The presence of an unconformity at the base of the Krol Sandstone compromises our effort to test this prediction, but an exploration of the upper Krol A and Krol B formations is warranted to search for microfossils indicative of the *Tanarium pycnacanthum-Ceratosphaeridium glaberosum* Assemblage Zone.

Whereas the Krol A Formation in the Lesser Himalaya and the lower Doushantuo Formation in the Yangtze Gorges show notable similarity in acritarch presence data, which facilitates biostratigraphic correlation, we would also like to point out some perceived differences in taxonomic abundance. We note

that the Krol A acritarch assemblage is characterized by the abundance of acanthomorphs with short and thin processes (e.g., *Appendisphaera clava*, *A. tenuis*, *Cymatiosphaeroides forabilatus*; Fig. 28), as well as the scarcity of acanthomorphs with large and long processes (e.g., various species of *Tanarium*, *Weissiella*, and *Sinosphaera* Zhang et al., 1998). As noted by Shukla and Tiwari (2014, p. 215) the "absence of *Tanarium*, the marker acritarch taxon of the upper Doushantuo assemblage in the Krol Group, is very peculiar." That the Krol A assemblage is likely correlated with one of the assemblage zones in the lower rather than the upper Doushantuo Formation may partially explain this peculiarity, but even the lower Doushantuo Formation (member II) in the Yangtze Gorges area contains abundant acanthomorphs with large and long processes (Liu and Moczydłowska, 2019; Ouyang et al., 2021). Different sampling intensities between the two regions are unlikely to have preferentially biased against acanthomorphs with large and long processes relative to those with short and thin processes. For the same reason, taphonomic bias is an unlikely explanation for this difference either, considering that both the Krol A assemblage in the Solan area and the Doushantuo acritarchs in the Yangtze Gorges area are taphonomically similar.

Paleoenvironmental and paleogeographic factors also may have played important roles in dictating taxonomic similarities and differences among acanthomorph assemblages in South China and northern India. As commented earlier in the paper, the overall taxonomic similarities and our ability to correlate Ediacaran acanthomorph assemblages between South China and northern India is facilitated by their paleogeographic proximity. However, there are more nuances. To elaborate, it is instructive to compare and contrast the Krol A assemblage against Doushantuo acritarchs from Liujing and Weng'an in Guizhou Province. The Liujing and Weng'an assemblages are paleogeographically close (~100 km apart; Fig. 35), but taphonomically and environmentally different; Liujing fossils are silicified in chert nodules in shales and argillaceous dolostones, whereas Weng'an fossils are phosphatized in intraclastic phosphorites. Like the Krol A assemblage, the Liujing assemblage is numerically dominated by acanthomorphs with short and thin processes, particularly *Cymatiosphaeroides forabilatus* (accounting for 48.7% of acanthomorph abundance) and *Mengeosphaera membranifera* Shang et al., 2019 (accounting for 21.3% of acanthomorph abundance), the latter species of which is similar to *Mengeosphaera gracilis* except the presence of an outer membrane. In contrast, qualitative data from Weng'an show that acanthomorphs with large processes (e.g., *Mengeosphaera chadianensis*) seem to be the most common taxa (Xiao et al., 2014). The zonal microfossils, including *Appendisphaera grandis*, *Cavaspina basiconica*, *Schizofusa zangwenlongii*, *Tanarium conoideum*, *Tanarium tuberosum*, and *Weissiella grandistella*, are present in the Liujing assemblage (Shang et al., 2019), whereas *Appendisphaera grandis*, *Cavaspina basiconica*, *Tanarium conoideum*, *Tanarium tuberosum*, *Tianzhushania spinosa*, and *Weissiella brevis* have been found in Weng'an (Xiao et al., 2014). These fossils indicate that the Liujing and Weng'an assemblages are unlikely correlated with the *Tanarium pycnacanthum-Ceratosphaeridium glaberosum* Assemblage Zone in the Yangtze Gorges area, but are probably part of the *Tanarium conoideum-Cavaspina basiconica* Assemblage Zone. If so, then the Krol A, Liujing, and Weng'an assemblages are broadly correlated to the same assemblage zone.

Thus, as revealed by the abundance data, the similarity between the Krol A and Liujing assemblages, as well as the difference between the Krol A and Weng'an assemblages, can be considered in a paleoenvironmental, taphonomic, and paleogeographic context. Whereas both Liujing and Weng'an are equally close to Krol A (Fig. 35), the former is additionally similar to the Krol A in taphonomy and paleoenvironment. We note that there is currently no independent chronostratigraphic data to constrain the age of the Liujing assemblage, so correlation of the Liujing assemblage with the *Tanarium conoideum-Cavaspina basiconica* Assemblage Zone awaits corroboration with additional data. Indeed, the fossiliferous units (beds 4 and 5) at Liujing are somewhat similar in lithostratigraphy to upper member III and member IV of the Doushantuo Formation in the Yangtze Gorges area (the reason for the dashed vertical lines in Fig. 34). Alternatively, the fossiliferous units at Liujing may be equivalent to member II of the Doushantuo Formation and strata equivalent to members III-IV may be missing at Liujing (as is the case in the eastern Huangling anticline of the Yangtze Gorges area, where upper member III and member IV are missing; Xiao et al., 2017; Zhou et al., 2017). If this is the case, then all dashed vertical lines in Figure 34 should be removed. A chemostratigraphic test of these two correlations requires $\delta^{13}C$ data from the Liujing section, which are currently unavailable. Nonetheless, the general statement stands that paleogeography, paleoenvironments, and taphonomy should be considered when carrying out Ediacaran biostratigraphic correlation using acanthomorphs.

If, as discussed above, the Liujing and Krol assemblages are correlated to the *Tanarium conoideum-Cavaspina basiconica* Assemblage Zone, their similarity in taxonomic presence and abundance is not unexpected, given their paleogeographic location (Fig. 35). Nine of the 12 biostratigraphically significant species from Krol A are also present at Liujing (see dashed vertical lines in Fig. 34), in addition, *Tanarium conoideum* may be present in both assemblages (see taxonomic discussion in *Tanarium* cf. *T. conoideum*). More importantly, both assemblages are numerically dominated by acanthomorphs with thin processes (e.g., *Appendisphaera grandis*, *A.*? *hemisphaerica*, *A. longispina*, *A. setosa*, *A. tenuis*, *Cymatiosphaeroides forabilatus*, and *Mengeosphaera gracilis*). From a paleogeographic viewpoint, this similarity makes perfect sense. According to several paleogeographic reconstructions (Jiang et al., 2003a; Qi et al., 2018; Merdith et al., 2021), the Lesser Himalaya was either directly facing or immediately juxtaposing the southwestern side of the Yangtze block. In these paleogeographic configurations, the Liujing section was paleogeographically closer to the Lesser Himalaya than the Yangtze Gorges area was to the Lesser Himalaya during the Ediacaran Period (Fig. 35). Hence, even though the Krol assemblage is generally similar to lower Doushantuo acritarchs in South China, it is particularly similar to the Liujing assemblage in both presence and abundance data. This similarity is related to their biostratigraphic equivalence, taphonomic comparability, and paleogeographic proximity.

The integrated bio- and chemostratigraphic correlation between the Krol A and Doushantuo Formation illustrates the

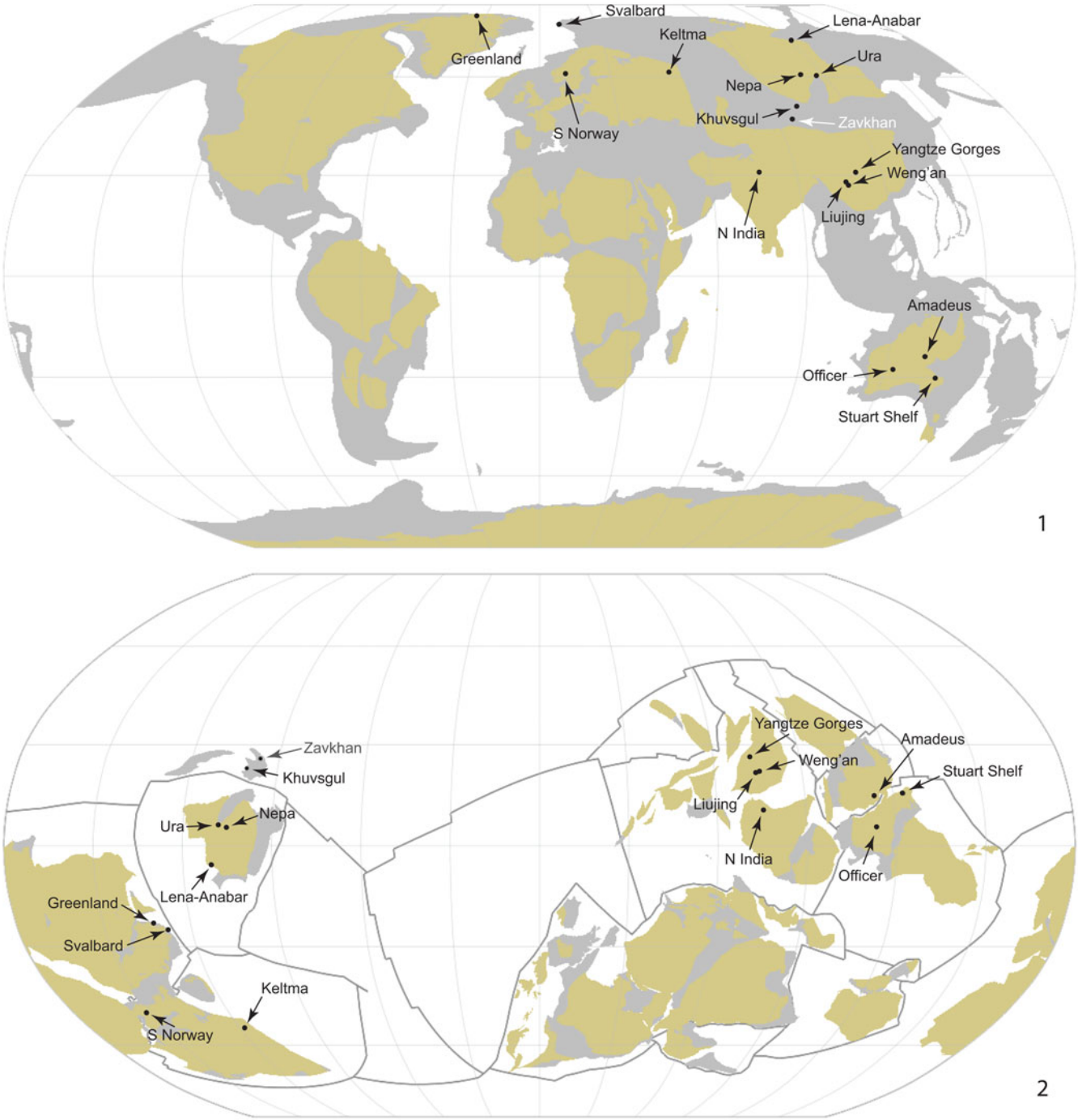

Figure 35. Representative localities from Ediacaran basins where acanthomorphs have been reported. Also included are terminal Ediacaran to early Cambrian assemblages from the Lena-Anabar Basin (Grazhdankin et al., 2020) and the Khuvsgul Basin (Anderson et al., 2017, 2019). Ediacaran acanthomorphs were reported from the Zavkhan material (Ragozina et al., 2016), but the published illustrations are not convincing. (**1**) Localities on a modern geographic map. The scarcity of Ediacaran acanthomorphs in the western hemisphere is likely due to poor sampling intensity. (**2**) Localities on a ca. 600 Ma paleogeographic map (Merdith et al., 2021). The paleogeographic location of Svalbard is uncertain, but it probably was close to Greenland (Gasser, 2013). Note that Ediacaran acanthomorphs are concentrated in low latitudes and the possibility of two paleobiogeographic provinces (Gondwana vs. Laurentia-Baltica-Siberia). Also note the paleogeographic proximity between Lesser Himalaya and South China (particularly Liujing and Weng'an). Maps were generated using the software gplate.

promise of Ediacaran acritarchs as important biostratigraphic tools for global correlation. The natural next step is to apply the same integrative approach to correlate Ediacaran strata in east Gondwana (South China, India, and South Australia) and beyond. With a solid chronostratigraphic framework, we can also begin to explore possible signs of paleobiogeographic differentiation of Ediacaran acanthomorphs. For example, according to the paleogeographic reconstruction of Merdith et al. (2021), Ediacaran acanthomorphs seem to be concentrated in low paleolatitudes. It is also tempting to recognize a

Tianzhushania paleobiogeographic province in part of east Gondwana, as indicated by the occurrence of this genus in northern India and South China (Liu et al., 2014a; Xiao et al., 2014; Joshi and Tiwari, 2016). As a side note, specimens published as ?*Trachyhystrichosphaera* sp. from the Scotia Group in Svalbard are somewhat similar to *Tianzhushania polysiphonia* in its clustered distribution of cylindrical processes, but do not seem to preserve other key features of the genus *Tianzhushania* (i.e., a multilaminate layer surrounding the vesicle wall and an outer membrane supported by the cylindrical processes), so their identification as *T. polysiphonia* remains to be confirmed. The speculation of a *Tianzhushania* paleobiogeographic province warrants further investigation with biostratigraphic, taphonomic, and paleoenvironmental controls. Nonetheless, we are confident that the growing data of Ediacaran acritarchs will soon illuminate a key component of Ediacaran paleobiogeography, which thus far has been derived mainly from macrofossils (Waggoner, 1999; Boag et al., 2016).

Conclusions

This study offers an instructive example of inter-basinal correlation of early Ediacaran strata between the Lesser Himalaya and the Yangtze Gorges area using integrative bio- and chemostratigraphic data, and the results are encouraging. Based on the common occurrence of *Tianzhushania spinosa* and *T. polysiphonia*, the Infra-Krol Formation in the Lesser Himalaya is correlated with the *Appendisphaera grandis-Weissiella grandistella-Tianzhushania spinosa* Assemblage Zone of the lower Doushantuo Formation in the Yangtze Gorges area. The Krol A Formation in the Lesser Himalaya contains over a dozen acanthomorph species, including two new species—*Cavaspina tiwariae* Xiao n. sp. and *Dictyotidium grazhdankinii* Xiao n. sp.—as well as numerous sphaeromorphs, filaments, coccoids, and multicellular algae. Many of these fossils, including all but the new and open-nomenclature acanthomorph taxa, are also present in the Doushantuo Formation. These microfossils indicate a biostratigraphic correlation with the *Tanarium tuberosum-Schizofusa zangwenlongii* Assemblage Zone or *Tanarium conoideum-Cavaspina basiconica* Assemblage Zone of the lower Doushantuo Formation in the Yangtze Gorges area. The prominent negative $\delta^{13}C$ excursion in association with the Krol A microfossils is correlated with the negative $\delta^{13}C$ excursion EN2 in the uppermost member II of the Doushantuo Formation in the Yangtze Gorge area, thus favoring a biostratigraphic correlation between the Krol A assemblage and the *Tanarium conoideum-Cavaspina basiconica* Assemblage Zone. The Krol A data thus indicate that the "barren interval" in the Yangtze Gorges area results from a taphonomic bias due to the lack of chert nodules and may be part of the *Tanarium conoideum-Cavaspina basiconica* Assemblage Zone. When placed in a paleogeographic context, Ediacaran acanthomorphs from northern India, South China, and elsewhere seem to be concentrated in, if not restricted to, low paleolatitudes, with tantalizing evidence for paleobiogeographic differentiation.

The Ediacaran stratigraphic correlation between the Lesser Himalaya and the Yangtze Gorges area is definitely aided by their similarity in lithostratigraphy, taphonomy, and paleogeography, but it also demonstrates the feasibility of global correlation of Ediacaran strata using integrative data. With a refined and tested chronostratigraphic framework, it is possible to assess Ediacaran evolutionary dynamics, paleobiogeographic patterns, and environmental changes at a temporal resolution that was previously unattainable.

Acknowledgments

The research was funded by the US National Science Foundation (EAR-1124062 and EAR-2021207 to SX, EAR-1124545 to GJ, and EAR-1124303 to NCH), the National Natural Science Foundation of China (41902004 to QY and 41672027 to CZ), China Postdoctoral Science Foundation (2021M692980 to QY), and Indian University Grants Commission Basic Scientific Research Program (20-1/2012 and 20-8-12/2012 to BPS). We thank X. Shang, S. Willman, and an anonymous reviewer for constructive comments that helped improve this paper. This paper is a contribution to IGCP668.

References

Acharyya, S.K., Raha, P.K., Das, D.P., Moitra, A.K., Shukla, M., and Bansal, R., 1989, Late Proterozoic microbiota from the Infrakrol rocks from Nainital synform, Kumaon Himalaya: Indian Journal of Geology, v. 61, p. 137–147.

Agić, H., Moczydłowska, M., and Yin, L.-M., 2015, Affinity, life cycle, and intracellular complexity of organic-walled microfossils from the Mesoproterozoic of Shanxi, China: Journal of Paleontology, v. 89, p. 28–50.

Allison, C.W., and Awramik, S.M., 1989, Organic-walled microfossils from earliest Cambrian or latest Proterozoic Tindir Group rocks, northwest Canada: Precambrian Research, v. 43, p. 253–294.

Anbarasu, K., 2001, Acritarchs from Mesoproterozoic Chitrakoot Formation, Semri Group, Chitrakoot Area, Central India: Journal of Geological Society of India, v. 57, p. 179–183.

Anderson, R.P., Macdonald, F.A., Jones, D.S., McMahon, S., and Briggs, D.E.G., 2017, Doushantuo-type microfossils from latest Ediacaran phosphorites of northern Mongolia: Geology, v. 45, p. 1079–1082.

Anderson, R.P., McMahon, S., Macdonald, F.A., Jones, D.S., and Briggs, D.E.G., 2019, Palaeobiology of latest Ediacaran phosphorites from the upper Khesen Formation, Khuvsgul Group, northern Mongolia: Journal of Systematic Palaeontology, v. 17, p. 501–532.

Anttila, E.S.C., and Macdonald, F.A., 2020, Cryogenian to early Cambrian evolution of the phosphorite-bearing Khovsgol basin, Mongolia: Geological Society of America Abstracts with Programs, v. 52(6). https://doi.org/10.1130/abs/2020AM-359065.

Anttila, E., Macdonald, F., and Bold, U., 2021, Stratigraphy of the Khuvsgul Group, Mongolia: Mongolian Geoscientist, v. 26, p. 2–15. https://doi.org/10.5564/mgs.v26i52.1516.

Auden, J.B., 1934, The geology of the Krol belt: Geological Survey of India Record, v. 71, p. 357–454.

Bhargava, O.N., Singh, B.P., Frank, W., and Tangri, S.K., 2021, Evolution of the Lesser Himalaya in space and time: Himalayan Geology, v. 42, p. 263–289.

Bhatt, D.K., 1991, The Precambrian-Cambrian transition interval in Himalaya with special reference to small shelly fossils—a review of current status of work: Journal of the Palaeontological Society of India, v. 36, p. 109–120.

Bhatt, D.K., Mamgain, A.K., and Misra, R.S., 1985, Small shelly fossils of early Cambrian (Tommotian) age from Chert-Phosphorite Member, Tal Formation, Mussoorie syncline, Lesser Himalaya, India and their chronostratigraphic evaluation: Journal of the Paleontological Society of India, v. 30, p. 92–102.

Bhattacharya, S.C., and Niyogi, D., 1971, Geological evolution of the Krol Belt in Simla Hills, H. P.: Himalayan Geology, v. 1, p. 178–212.

Boag, T., Darroch, S.A.F., and Laflamme, M., 2016, Ediacaran distributions in space and time: testing assemblage concepts of earliest macroscopic body fossils: Paleobiology, v. 42, p. 574–594.

Brasier, M., McLoughlin, N., Green, O., and Wacey, D., 2006, A fresh look at the fossil evidence for early Archaean cellular life: Philosophical Transactions of the Royal Society of London B: Biological Sciences, v. 361, p. 887–902.

Butterfield, N.J., Knoll, A.H., and Swett, K., 1994, Paleobiology of the Neoproterozoic Svanbergfjellet Formation, Spitsbergen: Fossils and Strata, v. 34, p. 1–84.

Cai, Y., Xiao, S., Li, G., and Hua, H., 2019, Diverse biomineralizing animals in the terminal Ediacaran Period herald the Cambrian Explosion: Geology, v. 47, p. 380–384.

Chen, M., and Liu, K., 1986, The geological significance of newly discovered microfossils from the upper Sinian (Doushantuo age) phosphorites: Scientia Geologica Sinica, v. 1, p. 46–53.

Cohen, P.A., Knoll, A.H., and Kodner, R.B., 2009, Large spinose microfossils in Ediacaran rocks as resting stages of early animals: Proceedings of the National Academy of Sciences of the United States of America, v. 106, p. 6519–6524.

Condon, D., Zhu, M., Bowring, S., Wang, W., Yang, A., and Jin, Y., 2005, U-Pb ages from the Neoproterozoic Doushantuo Formation, China: Science, v. 308, p. 95–98.

Eisenack, A., 1955, Chitinozoen, Hystrichosphären und andere Mikrofossilien aus dem *Beyrichia*-Kalk: Senckenbergiana Lethaea, v. 36, p. 157–188.

Eisenack, A., 1958, *Tasmanites* Newton 1875 und *Leiosphaeridia* n. gen. aus Gattungen der Hystrichosphaeridea: Palaeontographica Abteilung A, v. 110, p. 1–19.

Eisenack, A., Cramer, F.H., and Díez, C.R., 1979, Katalog der fossilen Dinoflagellaten, Hystrichospharen und verwandten Mikrofossilien. Band V: Acritarcha, Teil 3: Stuttgart, E. Schweizerbart'sche Verlagsbuchhandlung, 532 p.

Etienne, J.L., Allen, P.A., Guerroue, E.L., Heaman, L., Ghosh, S.K., and Islam, R., 2011, The Blaini Formation of the Lesser Himalaya, NW India, *in* Arnaud, E., Halverson, G. P., Shields-Zhou, G., eds., The Geological Record of Neoproterozoic Glaciations: Geological Society, London, Memoir 36, p. 347–355.

Evitt, W.R., 1963, A discussion and proposals concerning fossil dinoflagellates, hystrichospheres, and acritarchs: Proceedings of the National Academy of Sciences, USA, v. 49, p. 158–164; 298–302.

Fensome, R.A., Williams, G.L., Barss, M.S., Frerman, J.M., and Hill, J.M., 1990, Acritarchs and Fossil Prasinophytes: An Index to Genera, Species and Infraspecific Taxa: Salt Lake City, American Association of Stratigraphic Palynologists Foundation, 771 p.

Frank, W., Bhargava, O.N., Miller, C., and Banerjee, D.M., 2001, A review of the Proterozoic in the Himlaya and northern Indian shield: Journal of Asian Earth Sciences, Special Abstract Issue, 16th Himalayan-Karakoram-Tibet Workshop, Austria, v. 19 (3A), p. 18.

Gasser, D., 2013, The Caledonides of Greenland, Svalbard and other Arctic areas: status of research and open questions, *in* Corfu, F., Gasser, D., and Chew, D.M., eds., New Perspectives on the Caledonides of Scandinavia and Related Areas: Geological Society, London, Special Publications 390, p. 93–129.

Golubkova, E.Y., Raevskaya, E.G., and Kuznetsov, A.B., 2010, Lower Vendian microfossil assemblages of East Siberia: significance for solving regional stratigraphic problems: Stratigraphy and Geological Correlation, v. 18, p. 353–375.

Golubkova, Y.E., Zaitseva, T.S., Kuznetsov, A.B., Dovzhikova, E.G., and Maslov, A.V., 2015, Microfossils and Rb-Sr age of glauconite in the key section of the upper Proterozoic of the northeastern part of the Russian Plate (Keltmen-1 Borehole): Doklady Earth Sciences, v. 462, p. 547–551.

Grazhdankin, D., Nagovitsin, K., Golubkova, E., Karlova, G., Kochnev, B., Rogov, V., and Marusin, V., 2020, Doushantuo-Pertatataka-type acanthomorphs and Ediacaran ecosystem stability: Geology, v. 48, p. 708–712.

Grey, K., 2005, Ediacaran palynology of Australia: Memoirs of the Association of Australasian Palaeontologists, v. 31, p. 1–439.

Hawkins, A.D., Xiao, S., Jiang, G., Wang, X., and Shi, X., 2017, New biostratigraphic and chemostratigraphic data from the Ediacaran Doushantuo Formation in intra-shelf and upper slope facies of the Yangtze platform: implications for biozonation of acanthomorphic acritarchs in South China: Precambrian Research, v. 300, p. 28–39.

Hermann, T.N., 1974, Findings of mass accumulations of trichomes in the Riphean, *in* Timofeev, B.V., ed., Proterozoic and Paleozoic Microfossils of the USSR: Moscow, Nauka, p. 6–10.

Hofmann, M., Linnemann, U., Rai, V., Becker, S., Gärtner, A., and Sagawe, A., 2011, The India and South China cratons at the margin of Rodinia: synchronous Neoproterozoic magmatism revealed by LA-ICP-MS zircon analyses: Lithos, v. 123, p. 176–187.

Hughes, N.C., 2017, Biostratigraphical dating conundrums in the Cambrian and earlier stratigraphy of the Indian subcontinent: The Palaeobotanist, v. 66, p. 1–15.

Hughes, N.C., Peng, S., Bhargava, O.N., Ahluwalia, A.D., Walia, S., Myrow, P.M., and Parcha, S.K., 2005, Cambrian biostratigraphy of the Tal Group, Lesser Himalaya, India, and early Tsanglangpuan (late early Cambrian) trilobites from the Nigali Dhar syncline: Geological Magazine, v. 142, p. 57–80.

Hughes, N.C., Myrow, P.M., McKenzie, N.R., Xiao, S., Banerjee, D.M., Stockli, D.F., and Tang, Q., 2015, Age and implications of the phosphatic Birmania Formation, Rajasthan, India: Precambrian Research, v. 267, p. 164–173.

Jain, A.K., Banerjee, D.M., and Kale, V.S., 2020, Tectonics of the Indian Subcontinent: Cham, Switzerland, Springer Nature, 576 p.

Jankauskas, T.V., Mikhailova, N.S., and Hermann, T.N., 1989, Mikrofossilii Dokembriya SSSR [Precambrian Microfossils of the USSR]: Leningrad, Nauka, 190 p.

Jiang, G., Christie-Blick, N., Kaufman, A.J., Banerjee, D.M., and Rai, V., 2002, Sequence stratigraphy of the Neoproterozoic Infra Krol Formation and Krol Group, Lesser Himalaya, India: Journal of Sedimentary Research, v. 72, p. 524–542.

Jiang, G., Sohl, L.E., and Christie-Blick, N., 2003a, Neoproterozoic stratigraphic comparison of the Lesser Himalaya (India) and Yangtze block (South China): paleogeographic implications: Geology, v. 31, p. 917–920.

Jiang, G., Christie-Blick, N., Kaufman, A.J., Banerjee, D.M., and Rai, V., 2003b, Carbonate platform growth and cyclicity at a terminal Proterozoic passive margin, Infra Krol Formation and Krol Group, Lesser Himalaya, India: Sedimentology, v. 50, p. 921–952.

Jiang, G., Kaufman, A.J., Christie-Blick, N., Zhang, S., and Wu, H., 2007, Carbon isotope variability across the Ediacaran Yangtze platform in South China: implications for a large surface-to-deep ocean $\delta^{13}C$ gradient: Earth and Planetary Science Letters, v. 261, p. 303–320.

Joshi, H., and Tiwari, M., 2016, *Tianzhushania spinosa* and other large acanthomorphic acritarchs of Ediacaran Period from the Infrakrol Formation, Lesser Himalaya, India: Precambrian Research, v. 286, p. 325–336.

Kaufman, A.J., Jiang, G., Christie-Blick, N., Banerjee, D.M., and Rai, V., 2006, Stable isotope record of the terminal Neoproterozoic Krol platform in the Lesser Himalayas of northern India: Precambrian Research, v. 147, p. 156–185.

Knoll, A.H., 1984, Microbiotas of the late Precambrian Hunnberg Formation, Nordaustlandet, Svalbard: Journal of Paleontology, v. 58, p. 131–162.

Knoll, A.H., 1992, Microfossils in metasedimentary cherts of the Scotia Group, Prins Karls Forland, western Svalbard: Palaeontology, v. 35, p. 751–774.

Knoll, A.H., Swett, K., and Mark, J., 1991, Paleobiology of a Neoproterozoic tidal flat/lagoonal complex: the Draken Conglomerate Formation, Spitsbergen: Journal of Paleontology, v. 65, p. 531–570.

Knoll, A.H., Grotzinger, J.P., Kaufman, A.J., and Kolosov, P., 1995, Integrated approaches to terminal Proterozoic stratigraphy: an example from the Olenek Uplift, northeastern Siberia: Precambrian Research, v. 73, p. 251–270.

Kolosova, S.P., 1991, Pozdnedokembriyskie shipovatie mikrofossilii vostoka sibirkoy platformi [Late Precambrian acanthomorphic acritarchs from the eastern Siberian Platform]: Algologiya [Algologia], v. 1, p. 53–59.

Kumar, G., and Rai, V., 1992, Organic-walled microfossils from the bedded black chert of the Krol Formation (Vendian), Solan area, Himachal-Pradesh, India: Journal of the Geological Society of India, v. 39, p. 229–234.

Liu, H., Qi, S.L., Fan, J.L., Guo, W., Pei, M.S., Huang, D.J., Cheng, L., Bian, M., Liu, L., Zhao, Y.X., and Zhang, J., 2021, An acritarch assemblage from the lower Ediacaran Doushantuo Formation in Changyang, Hubei Province: Journal of Stratigraphy, v. 15, p. 19–28.

Liu, P., and Moczydłowska, M., 2019, Ediacaran microfossils from the Doushantuo Formation chert nodules in the Yangtze Gorges area, South China, and new biozones: Fossils and Strata, v. 65, p. 1–172.

Liu, P., Yin, C., Gao, L., Tang, F., and Chen, S., 2009, New material of microfossils from the Ediacaran Doushantuo Formation in the Zhangcunping area, Yichang, Hubei Province and its zircon SHRIMP U-Pb age: Chinese Science Bulletin, v. 54, p. 1058–1064.

Liu, P., Yin, C., Chen, S., Tang, F., and Gao, L., 2013, The biostratigraphic succession of acanthomorphic acritarchs of the Ediacaran Doushantuo Formation in the Yangtze Gorges area, South China and its biostratigraphic correlation with Australia: Precambrian Research, v. 225, p. 29–43.

Liu, P., Xiao, S., Yin, C., Chen, S., Zhou, C., and Li, M., 2014a, Ediacaran acanthomorphic acritarchs and other microfossils from chert nodules of the upper Doushantuo Formation in the Yangtze Gorges area, South China: Journal of Paleontology, v. 88 (S72), p. 1–139.

Liu, P., Chen, S., Zhu, M., Li, M., Yin, C., and Shang, X., 2014b, High-resolution biostratigraphic and chemostratigraphic data from the Chenjiayuanzi section of the Doushantuo Formation in the Yangtze Gorges area, South China: implication for subdivision and global correlation of the Ediacaran System: Precambrian Research, v. 249, p. 199–214.

McFadden, K.A., Huang, J., Chu, X., Jiang, G., Kaufman, A.J., Zhou, C., Yuan, X., and Xiao, S., 2008, Pulsed oxidation and biological evolution in the Ediacaran Doushantuo Formation: Proceedings of the National Academy of Sciences, v. 105, p. 3197–3202.

McFadden, K.A., Xiao, S., Zhou, C., and Kowalewski, M., 2009, Quantitative evaluation of the biostratigraphic distribution of acanthomorphic acritarchs in the Ediacaran Doushantuo Formation in the Yangtze Gorges area, South China: Precambrian Research, v. 173, p. 170–190.

McKenzie, N.R., Hughes, N.C., Myrow, P.M., Xiao, S., and Sharma, M., 2011, Correlation of Precambrian–Cambrian sedimentary successions across northern India and the utility of isotopic signatures of Himalayan lithotectonic zones: Earth and Planetary Science Letters, v. 312, p. 471–483.

Merdith, A.S., Williams, S.E., Collins, A.S., Tetley, M.G., Mulder, J.A., Blades, M.L., Young, A., Armistead, S.E., Cannon, J., Zahirovic, S., and Müller, R.D., 2021, Extending full-plate tectonic models into deep time: linking the Neoproterozoic and the Phanerozoic: Earth-Science Reviews, v. 214, 103477. https://doi.org/10.1016/j.earscirev.2020.103477.

Moczydłowska, M., 2005, Taxonomic review of some Ediacaran acritarchs from the Siberian Platform: Precambrian Research, v. 136, p. 283–307.

Moczydłowska, M., and Nagovitsin, K.E., 2012, Ediacaran radiation of organic-walled microbiota recorded in the Ura Formation, Patom Uplift, East Siberia: Precambrian Research, v. 198–199, p. 1–24.

Moczydłowska, M., Vidal, G., and Rudavskaya, V.A., 1993, Neoproterozoic (Vendian) phytoplankton from the Siberian Platform, Yakutia: Palaeontology, v. 36, p. 495–521.

Muscente, A.D., Hawkins, A.D., and Xiao, S., 2015, Fossil preservation through phosphatization and silicification in the Ediacaran Doushantuo Formation (South China): a comparative synthesis: Palaeogeography Palaeoclimatology Palaeoecology, v. 434, p. 46–62.

Muscente, A.D., Bykova, N., Boag, T.H., Buatois, L.A., Mángano, M.G., Eleish, A., Prabhu, A., Pan, F., Meyer, M.B., Schiffbauer, J.D., Fox, P., Hazen, R.M., and Knoll, A.H., 2019, Ediacaran biozones identified with network analysis provide evidence for pulsed extinctions of early complex life: Nature Communications, v. 10, 911. https://doi.org/10.1038/s41467-019-08837-3.

Nagovitsin, K.E., Faizullin, M.S., and Yakshin, M.S., 2004, New forms of Baikalian acanthomorphytes from the Ura Formation of the Patom Uplift, East Siberia: Geologiya e Geofisika, v. 45, p. 7–19.

Naumova, S.N., 1949, Spory nizhnego kembriya (Spores from the lower Cambrian): Izvestiya Akademii Nauk SSSR, Seriya Geologicheskaya, v. 1949 (4), p. 49–56.

Oehler, J.H., and Schopf, J.W., 1971, Artificial microfossils: experimental studies of permineralization of blue-green algae in silica: Science, v. 174, p. 1229–1231.

Ouyang, Q., Zhou, C., Guan, C., and Wang, W., 2015, New microfossils from the Ediacaran Doushantuo Formation in the Yangtze Gorges area, South China, and their biostratigraphic implications: Acta Palaeontologica Sinica, v. 54, p. 207–229.

Ouyang, Q., Guan, C., Zhou, C., and Xiao, S., 2017, Acanthomorphic acritarchs of the Doushantuo Formation from an upper slope section in northwestern Hunan Province, South China, with implications for early Ediacaran biostratigraphy: Precambrian Research, v. 298, p. 512–529.

Ouyang, Q., Zhou, C., Xiao, S., Chen, Z., and Shao, Y., 2019, Acanthomorphic acritarchs from the Ediacaran Doushantuo Formation at Zhangcunping in South China, with implications for the evolution of early Ediacaran eukaryotes: Precambrian Research, v. 320, p. 171–192.

Ouyang, Q., Zhou, C., Xiao, S., Guan, C., Chen, Z., Yuan, X., and Sun, Y., 2021, Distribution of Ediacaran acanthomorphic acritarchs in the lower Doushantuo Formation of the Yangtze Gorges area, South China: evolutionary and stratigraphic implications: Precambrian Research, v. 353, 106005. https://www.doi.org/10.1016/j.precamres.2020.106005.

Prasad, B., and Asher, R., 2016, Record of Ediacaran complex acanthomorphic acritarchs from the lower Vindhyan succession of the Chambal Valley (East Rajasthan), India and their biostratigraphic significance: Journal of the Palaeontological Society of India, v. 61, p. 29–62.

Prasad, B., and Asher, R., 2021, Vindhyans of the Chambal Valley: Ediacaran complex acanthomorphs and associated acritarchs evidence for an Infra-Cambrian sedimentary basin in south-eastern Rajasthan, India: Journal of the Palaeontological Society of India, v. 66, p. 113–140.

Qi, L., Xu, Y., Cawood, P.A., and Du, Y., 2018, Reconstructing Cryogenian to Ediacaran successions and paleogeography of the South China Block: Precambrian Research, v. 314, p. 452–467.

Ragozina, A.L., Dorjnamjaa, D., Serezhnikova, E.A., Zaitseva, L.V., and Enkhbaatar, B., 2016, Association of macro- and microfossils in the Vendian (Ediacaran) postglacial successions in western Mongolia: Stratigraphy and Geological Correlation, v. 24, p. 242–251.

Rasmussen, B., Bose, P.K., Sarkar, S., Banerjee, S., Fletcher, I.R., and McNaughton, N.J., 2002, 1.6 Ga U-Pb zircon age for the Chorhat Sandstone, lower Vindhyan, India: Possible implications for early evolution of animals: Geology, v. 30, p. 103–106.

Ray, J.S., Martin, M.W., Veizer, J., and Bowring, S.A., 2002, U-Pb zircon dating and Sr isotope systematics of the Vindhyan Supergroup, India: Geology, v. 30, p. 131–134.

Reitlinger, E.A., 1959, Atlas of Microscopic Organic Remains and Problematica of Ancient Deposits of Siberia [in Russian]: Moscow, Academiya Nauk SSSR, 62 p.

Rozanov, A.Y., Missarzhevskii, V.V., Volkova, N.A., Voronova, L.C., Krylov, I.N., Keller, B.M., Korolyuk, I.K., Lendzion, K., Michniak, R., Pykhova, N.G., and Sidarov, A.D., 1969, The Tommotian Stage and the Cambrian Lower Boundary Problem: New Delhi, Amerind Publishing Company (1981 translation), 359 p.

Schopf, J.W., 1968, Microflora of the Bitter Springs Formation, late Precambrian, central Australia: Journal of Paleontology, v. 42, p. 651–688.

Schopf, J.W., and Blacic, J.M., 1971, New microorganisms from the Bitter Springs Formation (late Precambrian) of the north-central Amadeus Basin, Australia: Journal of Paleontology, v. 45, p. 925–960.

Sergeev, V.N., Knoll, A.H., and Vorob'Eva, N.G., 2011, Ediacaran microfossils from the Ura Formation, Baikal-Patom Uplift, Siberia: taxonomy and biostratigraphic significance: Journal of Paleontology, v. 85, p. 987–1011.

Shang, X., and Liu, P., 2020, Acritarchs from the Ediacaran Doushantuo Formation at the Tianping section in Zhangjiajie area of Hunan Province, South China and their biostratigraphic significance: Journal of Stratigraphy, v. 44, p. 150–162.

Shang, X., Moczydłowska, M., Liu, P., and Liu, L., 2018, Organic composition and diagenetic mineralization of microfossils in the Ediacaran Doushantuo chert nodule by Raman and petrographic analyses: Precambrian Research, v. 314, p. 145–159.

Shang, X., Liu, P., and Moczydłowska, M., 2019, Acritarchs from the Doushantuo Formation at Liujing section in Songlin area of Guizhou Province, South China: Implications for early–middle Ediacaran biostratigraphy: Precambrian Research, v. 334, 105453. https://doi.org/10.1016/j.precamres.2019.105453.

Shanker, R., Kumar, G., Mathur, V.K., and Johsi, A., 1993, Stratigraphy of Blaini, Infra Krol and Tal succession, Krol Belt, Lesser Himalaya: Indian Journal of Petroleum Geology, v. 2, p. 99–136.

Shanker, R., Mathur, V.K., and Kumar, G., 1997, Additional Ediacaran biota from the Krol Group, Lesser Himalaya, India and their significance: Geoscience Journal, v. 18, p. 79–91.

Sharma, M., Kumar, S., Tiwari, M., Shukla, Y., Pandey, S.K., Srivastava, P., and Banerjee, S., 2012, Palaeobiological constraints and the Precambrian biosphere: Indian evidence: Proceedings of Indian National Science Academy, v. 78, p. 407–422.

Sharma, M., Tiwari, M., Ahmad, S., Shukla, R., Shukla, B., Singh, V.K., Pandey, S., Ansari, A., Shukla, Y., and Kumar, S., 2016, Palaeobiology of Indian Proterozoic and early Cambrian successions: recent developments: Proceedings of Indian National Science Academy, v. 82, p. 559–579.

Sharma, M., Shukla, Y., and Sergeev, V.N., 2021, Microfossils from the Krol 'A' of the Lesser Himalaya, India: additional supporting data for its early Ediacaran age: Palaeoworld, v. 30, p. 610–626.

Shukla, R., and Tiwari, M., 2014, Ediacaran acanthomorphic acritarchs from the Outer Krol Belt, Lesser Himalaya, India: their significance for global correlation: Palaeoworld, v. 23, p. 209–224.

Shukla, M., Babu, R., Mathur, V.K., and Srivastava, D.K., 2005a, Microbial remains from the Chambaghat Formation, Krol Group, Himachal Lesser Himalaya, India and their significance: Current Science, v. 88, p. 1223–1225.

Shukla, M., Babu, R., Mathur, V.K., and Srivastava, D.K., 2005b, Additional terminal Proterozoic organic-walled microfossils from the Infra-Krol Formation, Nainital Syncline, Lesser Himalaya, Uttaranchal: Journal of the Geological Society of India, v. 65, p. 197–210.

Shukla, M., Mathur, V.K., Babu, R., and Srivastava, D.K., 2008, Ediacaran microbiota from the Baliana and Krol groups, Lesser Himalaya, India: The Palaeobotanist, v. 57, p. 359–378.

Singh, A., and Rai, V., 2013, Thallophytic algae from the Krol Formation (Ediacaran Period), Lesser Himalaya, India: Journal of the Palaeontological Society of India, v. 58, p. 251–258.

Singh, I.B., and Rai, V., 1983, Fauna and biogenic structures in Krol-Tal succession (Vendian–early Cambrian), Lesser Himalaya and a biostratigraphic and palaeontological significance: Journal of the Paleontological Society of India, v. 28, p. 67–90.

Singh, V.K., and Sharma, M., 2014, Morphologically complex organic-walled microfossils (OWM) from the late Palaeoproterozoic–early Mesoproterozoic Chitrakut Formation, Vindhyan Supergroup, central India and their implications on the antiquity of eukaryotes: Journal of the Palaeontological Society of India, v. 59, p. 89–102.

Spjeldnaes, N., 1963, A new fossil (*Papillomembrana* sp.) from the upper Precambrian of Norway: Nature, v. 200, p. 63–64.

Spjeldnaes, N., 1967, Fossils from pebbles of the Biskopåsen Formation in southern Norway: Bulletin, Norges Geologiske Undersokelse, v. 251, p. 53–82.

Staplin, F.L., 1961, Reef-controlled distribution of Devonian microplankton in Alberta: Palaeontology, v. 4, p. 392–424.

Tarhan, L.G., Hughes, N.C., Myrow, P.M., Bhargava, O.N., Ahluwalia, A.D., and Kudryavtsev, A.B., 2014, Precambrian-Cambrian boundary interval occurrence and form of the enigmatic tubular body fossil *Shaanxilithes ningqiangensis* from the Lesser Himalaya of India: Palaeontology, v. 57, p. 283–298.

Tian, L., Song, H., Ye, Q., Hu, J., An, Z., Zhao, X., Bottjer, D., and Tong, J., 2020, Recurrent anoxia recorded in shallow marine facies at Zhangcunping (western Hubei, China) throughout the Ediacaran to earliest Cambrian: Precambrian Research, v. 340, 105617. https://doi.org/10.1016/j.precamres.2020.105617.

Timofeev, B.V., 1966, Mircropaleophytological Investigations of Ancient Formations: Moscow, Nauka, 147 p.

Timofeev, B.V., Hermann, T.N., and Mikhailova, N.S., 1976, Microphytofossils of the Precambrian, Cambrian and Ordovician: Leningrad, Nauka, 106 p.

Tiwari, M., 1999, Organic-walled microfossils from the Chert-phosphorite Member, Tal Formation, Precambrian-Cambrian boundary, India: Precambrian Research, v. 97, p. 99–113.

Tiwari, M., and Azmi, R.J., 1992, Late Proterozoic organic-walled microfossils from the Infrakrol of Solan, Himchal Lesser Himalaya: an additional age constraint in the Krol Belt succession: Palaeobotanist, v. 39, p. 387–394.

Tiwari, M., and Knoll, A.H., 1994, Large acanthomorphic acritarchs from the Infrakrol Formation of the Lesser Himalaya and their stratigraphic significance: Journal of Himalayan Geology, v. 5, p. 193–201.

Tiwari, M., and Pant, C.C., 2004, Neoproterozoic silicified microfossils in Infrakrol Formation of Lesser Himalaya, India: Himalayan Geology, v. 25, p. 1–21.

Turland, N.J., Wiersema, J.H., Barrie, F.R., Greuter, W., Hawksworth, D.L., Herendeen, P.S., Knapp, S., Kusber, W.-H., Li, D.-Z., Marhold, K., May, T.W., McNeill, J., Monro, A.M., Prado, J., Price, M.J., and Smith, G.F., eds., 2018, International Code of Nomenclature for Algae, Fungi, and Plants (Shenzhen Code) Adopted by the Nineteenth International Botanical Congress Shenzhen, China, July 2017. Regnum Vegetabile 159: Glashütten, Germany, Koeltz Botanical Books.

Veis, A.F., Vorob'Eva, N.G., and Golubkova, E.Y., 2006, The early Vendian microfossils first found in the Russian Plate: taxonomic composition and biostratigraphic significance: Stratigraphy and Geological Correlation, v. 14, p. 368–385.

Venkatachala, B.S., Shukla, M., Bansal, R., and Acharyya, S.K., 1990, Upper Proterozoic microfossils from the Infra Krol sediments, Nainital synform, Kumaon Himalaya, India: Palaeobotanist, v. 38, p. 29–38.

Vidal, G., 1990, Giant acanthomorph acritarchs from the upper Proterozoic in southern Norway: Palaeontology, v. 33, p. 287–298.

Vidal, G., and Ford, T.D., 1985, Microbiotas from the late Proterozoic Chuar Group (northern Arizona) and Uinta Mountain Group (Utah) and their chronostratigraphic implications: Precambrian Research, v. 28, p. 349–389.

Vorob'Eva, N.G., and Petrov, P.Y., 2020, Microbiota of the Barakun Formation and biostratigraphic characteristics of the Dal'nyaya Taiga Group: early Vendian of the Ura Uplift (Eastern Siberia): Stratigraphy and Geological Correlation, v. 28, p. 365–380.

Vorob'Eva, N.G., Sergeev, V.N., and Semikhatov, M.A., 2006, Unique lower Vendian Kel'tma microbiota, Timan ridge: new evidence for the paleontological essence and global significance of the Vendian System: Doklady Earth Sciences, v. 410, p. 1038–1043.

Vorob'Eva, N.G., Sergeev, V.N., and Chumakov, N.M., 2008, New finds of early Vendian microfossils in the Ura Formation: revision of the Patom Supergroup Age, middle Siberia: Doklady Earth Sciences, v. 419A, p. 411–416.

Vorob'Eva, N.G., Sergeev, V.N., and Knoll, A.H., 2009, Neoproterozoic microfossils from the northeastern margin of the East European Platform: Journal of Paleontology, v. 83, p. 161–196.

Voronova, L.G., and Missarzhevsky, V.V., 1969, Nakhodki vodoroslej i trubok chervej v pogranichnykh sloyakh kembriya i dokembriya na severe Sibirskoj platformy. [Finds of algae and worm tubes in the Precambrian-Cambrian boundary beds of the northern part of the Siberian Platform]: Doklady AN SSSR, v. 184, p. 207–210. [In Russian]

Waggoner, B., 1999, Biogeographic analyses of the Ediacara biota; a conflict with paleotectonic reconstructions: Paleobiology, v. 25, p. 440–458.

Waggoner, B., 2003, The Ediacaran biotas in space and time: Integrative and Comparative Biology, v. 43, p. 104–113.

Webb, A.A.G., Yin, A., Harrison, T.M., Célérier, J., Gehrels, G.E., Manning, C.E., and Grove, M., 2011, Cenozoic tectonic history of the Himachal Himalaya (northwestern India) and its constraints on the formation mechanism of the Himalayan orogen: Geosphere, v. 7, p. 1013–1061.

Wetzel, O., 1933, Die in organische Substanz erhaltenen Mikrofossilien des baltischen Kreide-Feuersteins: Palaeontographica, v. 78, p. 1–110.

Wetzel, W., 1952, Beitrag zur Kenntnis des dan-zeitlichen Meeresplanktons: Geologisches Jahrbuch, v. 66, p. 391–402.

Willman, S., and Moczydłowska, M., 2008, Ediacaran acritarch biota from the Giles 1 drillhole, Officer Basin, Australia, and its potential for biostratigraphic correlation: Precambrian Research, v. 162, p. 498–530.

Willman, S., and Moczydłowska, M., 2011, Acritarchs in the Ediacaran of Australia—local or global significance? Evidence from the Lake Maurice West 1 drillcore: Review of Palaeobotany and Palynology, v. 166, p. 12–28.

Willman, S., Peel, J.S., Ineson, J.R., Schovsbo, N.H., Rugen, E.J., and Frei, R., 2021, Ediacaran Doushantuo-type biota discovered in Laurentia: Communications Biology, v. 3, 647. https://doi.org/10.1038/s42003-020-01381-7.

Xiao, S., 2004a, Neoproterozoic glaciations and the fossil record, *in* Jenkins, G.S., McMenamin, M., Sohl, L.E., and McKay, C.P., eds., The Extreme Proterozoic: Geology, Geochemistry, and Climate: Washington, DC, American Geophysical Union (AGU), p. 199–214.

Xiao, S., 2004b, New multicellular algal fossils and acritarchs in Doushantuo chert nodules (Neoproterozoic, Yangtze Gorges, South China): Journal of Paleontology, v. 78, p. 393–401.

Xiao, S., and Knoll, A.H., 1999, Fossil preservation in the Neoproterozoic Doushantuo phosphorite Lagerstätte, South China: Lethaia, v. 32, p. 219–240.

Xiao, S., and Knoll, A.H., 2000, Phosphatized animal embryos from the Neoproterozoic Doushantuo Formation at Weng'an, Guizhou, South China: Journal of Paleontology, v. 74, p. 767–788.

Xiao, S., and Narbonne, G.M., 2020, The Ediacaran Period, *in* Gradstein, F.M., Ogg, J.G., Schmitz, M.D., and Ogg, G.M., eds., Geologic Time Scale 2020 (Volume 1): Oxford, Elsevier, p. 521–561.

Xiao, S., and Tang, Q., 2022, Part B, Volume 2, Chapter 7: Microfossils of prokaryotes (Bacteria and Archaea): research history, taphonomy, and paleobiology: Treatise Online, no. 160. https://journals.ku.edu/treatiseonline/article/view/16311.

Xiao, S., Knoll, A.H., Kaufman, A.J., Yin, L., and Zhang, Y., 1997, Neoproterozoic fossils in Mesoproterozoic rocks? Chemostratigraphic resolution of a biostratigraphic conundrum from the North China Platform: Precambrian Research, v. 84, p. 197–220.

Xiao, S., Knoll, A.H., Yuan, X., and Pueschel, C.M., 2004, Phosphatized multicellular algae in the Neoproterozoic Doushantuo Formation, China, and the early evolution of florideophyte red algae: American Journal of Botany, v. 91, p. 214–227.

Xiao, S., McFadden, K.A., Peek, S., Kaufman, A.J., Zhou, C., Jiang, G., and Hu, J., 2012, Integrated chemostratigraphy of the Doushantuo Formation at the northern Xiaofenghe section (Yangtze Gorges, South China) and its implication for Ediacaran stratigraphic correlation and ocean redox models: Precambrian Research, v. 192–95, p. 125–141.

Xiao, S., Zhou, C., Liu, P., Wang, D., and Yuan, X., 2014, Phosphatized acanthomorphic acritarchs and related microfossils from the Ediacaran Doushantuo Formation at Weng'an (South China) and their implications for biostratigraphic correlation: Journal of Paleontology, v. 88, p. 1–67.

Xiao, S., Narbonne, G.M., Zhou, C., Laflamme, M., Grazhdankin, D.V., Moczydłowska-Vidal, M., and Cui, H., 2016, Toward an Ediacaran time scale: problems, protocols, and prospects: Episodes, v. 39, p. 540–555.

Xiao, S., Bykova, N., Kovalick, A., and Gill, B.C., 2017, Stable carbon isotopes of sedimentary kerogens and carbonaceous macrofossils from the Ediacaran Miaohe Member in South China: Implications for stratigraphic correlation and sources of sedimentary organic carbon: Precambrian Research, v. 302, p. 171–179.

Xing, Y., and Liu, G., 1973, Sinian micropaleoflora in the Yan-Liao area and its geological significance: Acta Geologica Sinica, v. 1973, p. 1–31.

Xing, Y., Ding, Q., Luo, H., He, T., and Wang, Y., 1984, The Sinian-Cambrian boundary of China: Bulletin of the Institute of Geology, Chinese Academy of Geological Sciences, v. 10, p. 1–262.

Yan, Y., and Zhu, S., 1992, Discovery of acanthomorphic acritarchs from the Baicaoping Formation in Yongji, Shanxi and its geological significance: Acta Micropalaeontologica Sinica, v. 9, p. 267–282.

Yang, L., Pang, K., Chen, L., Zhong, Z., and Yang, F., 2020, New materials of microfossils from the Ediacaran Doushantuo Formation in the Baizhu phosphorite deposit, Baokang, Hubei Province: Acta Micropalaeontologica Sinica, v. 37, p. 1–20.

Ye, Q., Tong, J., An, Z., Tian, L., Zhao, X., and Zhu, S., 2015, Phosphatized fossil assemblage from the Ediacaran Doushantuo Formation in Zhangcunping area, Yichang, Hubei Province: Acta Palaeontologica Sinica, v. 54, p. 43–65.

Yin, C., and Gao, L., 1999, Microflora in Baicaoping Formation of Ruyang Group in southern margin of North China Platform and discussion: Professional Papers of Stratigraphy and Palaeontology, v. 27, p. 81–94.

Yin, C., and Liu, G., 1988, Micropaleofloras, *in* Zhao, Z., Xing, Y., Ding, Q., Liu, G., Zhao, Y., Zhang, S., Meng, X., Yin, C., Ning, B., and Han, P., eds., The Sinian System of Hubei: Wuhan, China University of Geosciences Press, p. 170–180.

Yin, C., Liu, Y., Gao, L., Wang, Z., Tang, F., and Liu, P., 2007, Phosphatized Biota in Early Sinian (Ediacaran)—Weng'an Biota and Its Environment: Beijing, Geological Publishing House, 132 p.

Yin, C., Liu, P., Chen, S., Tang, F., Gao, L., and Wang, Z., 2009, Acritarch biostratigraphic succession of the Ediacaran Doushantuo Formation in the Yangtze Gorges: Acta Palaeontologica Sinica, v. 48, p. 146–154.

Yin, L., 1987, Microbiotas of latest Precambrian sequences in China, *in* Nanjing Institute of Geology and Palaeontology Academica Sinica, ed., Stratigraphy and Palaeontology of Systemic Boundaries in China:

Precambrian-Cambrian Boundary (1): Nanjing, Nanjing University Press, p. 415–494.
Yin, L., and Li, Z., 1978, Precambrian microfloras of southwest China with reference to their stratigraphic significance: Memoir Nanjing Institute of Geology and Palaeontology, Academia Sinica, v. 10, p. 41–108.
Yin, L., Wang, D., Yuan, X., and Zhou, C., 2011, Diverse small spinose acritarchs from the Ediacaran Doushantuo Formation, South China: Palaeoworld, v. 20, p. 279–289.
Yuan, X., and Hofmann, H.J., 1998, New microfossils from the Neoproterozoic (Sinian) Doushantuo Formation, Weng'an, Guizhou Province, southwestern China: Alcheringa, v. 22, p. 189–222.
Yuan, X., Xiao, S., Yin, L., Knoll, A.H., Zhou, C., and Mu, X., 2002, Doushantuo Fossils: Life on the Eve of Animal Radiation: Hefei, China, China University of Science and Technology Press, 171 p.
Zang, W., and Walter, M.R., 1992, Late Proterozoic and Cambrian microfossils and biostratigraphy, Amadeus Basin, central Australia: The Association of Australasia Palaeontologists Memoir, v. 12, p. 1–132.
Zhang, Y., 1989, Multicellular thallophytes with differentiated tissues from late Proterozoic phosphate rocks of South China: Lethaia, v. 22, p. 113–132.
Zhang, Y., and Yuan, X., 1992, New data on multicellular thallophytes and fragments of cellular tissues from late Proterozoic phosphate rocks, South China: Lethaia, v. 25, p. 1–18.
Zhang, Y., Yin, L., Xiao, S., and Knoll, A.H., 1998, Permineralized fossils from the terminal Proterozoic Doushantuo Formation, South China: Journal of Paleontology, v. 72 (S50), p. 1–52.
Zhang, Z., 1986, New material of filamentous fossil cyanophytes from the Dushantuo Formation (late Sinian) in the eastern Yangtze Gorges: Scientia Geologica Sinica, v. 21, p. 30–37.
Zhou, C., Brasier, M.D., and Xue, Y., 2001, Three-dimensional phosphatic preservation of giant acritarchs from the terminal Proterozoic Doushantuo Formation in Guizhou and Hubei provinces, South China: Palaeontology, v. 44, p. 1157–1178.
Zhou, C., Chen, Z., and Xue, Y., 2002, New microfossils from the late Neoproterozoic Doushantuo Formation at Chaoyang phosphorite deposit in Jiangxi Province, South China: Acta Palaeontologica Sinica, v. 41, p. 178–192.
Zhou, C., Xie, G., McFadden, K., Xiao, S., and Yuan, X., 2007, The diversification and extinction of Doushantuo-Pertatataka acritarchs in South China: causes and biostratigraphic significance: Geological Journal, v. 42, p. 229–262.
Zhou, C., Xiao, S., Wang, W., Guan, C., Ouyang, Q., and Chen, Z., 2017, The stratigraphic complexity of the middle Ediacaran carbon isotopic record in the Yangtze Gorges area, South China, and its implications for the age and chemostratigraphic significance of the Shuram excursion: Precambrian Research, v. 288, p. 23–38.
Zhu, M., Zhuravlev, A.Y., Wood, R.A., Zhao, F., and Sukhov, S.S., 2017, A deep root for the Cambrian Explosion: implications of new bio- and chemostratigraphy from the Siberian Platform: Geology, v. 45, p. 459–462.

Accepted: 26 January 2022